Novel Intelligent Control Techniques in Solar-based Energy Harvesting Systems

By

Mahmoud Mohamed Eid

A Thesis Submitted in Partial Fulfillment

Of the Requirements for the Degree of Master of Applied Science

In

Electrical, Computer and Software Engineering

Faculty of Engineering and Applied Science,

University of Ontario Institute of Technology

Oshawa, Ontario, Canada

Abstract

The sun is considered a precious source of energy. Much research has been done to increase our usage from solar energy since it is a renewable source and, most importantly, it is free and green. However in order to use solar panels "photovoltaic", it is important that we are getting the maximum power from the solar panels, which is very difficult and depends on factors such as solar intensity, temperature and the load itself. This is why Maximum Power Point Tracking (MPPT) controller is necessary to ensure that maximum power is delivered to connect appliances. Many MPPT algorithms have been developed with different accuracies and limitations. In this thesis, a novel algorithm is developed, implemented and a comparison is done with other algorithms. The results from the proposed system show fast tracking algorithm with a very small error.

The new algorithm has been applied to a solar-based water pump, which is a very important application. Water pumping can be implemented in different ways. If electrical energy is used for water pumping, the cost can be very high for areas, such as the rural and remote areas, where there is no conventional power grids. Solar-based water pumps offers a much needed alternative solution, which is easy to install, environmentally friendly, and needs less energy.

A simple system consists of solar photovoltaic (PV) panels, DC controller, DC water pump, and a very efficient DC converter. In this thesis, a triple DC-DC converter has been developed. The purpose for the triple output DC-DC converter is to provide the power needed to power up and control the DC water pump which requires different voltage levels.

A complete solar photovoltaic system with our proposed MPPT algorithm and developed DC-DC converter has been implemented. Detailed simulations and analysis are provided as well as prototyping phase is successfully achieved and tested. A 10W prototype was built and experimental results are provided for the proof of concept and to show the merits of the proposed thesis work.

Acknowledgements

I owe a great many thanks to many people who helped me during this work. My deepest appreciation and gratitude goes to my supervisors, Dr. Mohamed Youssef and Dr. Ying Wang, for guiding and motivating me. As great supervisors, they are always trying to provide me with guidance and feedbacks about my performance. I'm truly honored by having them as teachers and supervisors.

I want to thank my family for their encouragement and patience, and for inspiring me to always strive towards high expectations and insist to achieve them. Their support gave me the faith to further my education and reach out new goals.

I would like to express my gratitude to the UOIT for the inspiring study environment that it provides.

CONTENTS

List of Tables

List of Figures

List of Abbreviations

AC	Alternating Current
ANFIS	Adaptive Neuro Fuzzy Inference System
BLDC	Brushless DC Motor
CMOS	Complementary Metal Oxide Semiconductor
D	Duty Cycle
DC	Direct Current
EPP	Estimate Perturb Perturb
FF	Fill Factor
MPPT	Maximum Power Point Tracking
MPP	Maximum Power Point
MOSFET	Metal Oxide Semiconductor Field Effect Transistor
PI	Proportional Integral
PID	Proportional Integral Derivative
PSIM	PowerSim Simulation Tool
PWM	Pulse Width Modulation
PV	Photovoltaic
P&O	Perturb and Observe
Rpm	Revolutions per Minute

Chapter 1: Introduction

1.1 Introduction and Motivation

Solar photovoltaic technology offers an environmental friendly source of electricity; long live the sunshine. Without pollution, or depletion of the natural resources, the world can harvest enormous amount of energy. Unfortunately, the photovoltaic (PV) system is somewhat costly and inefficient. We can decrease the cost by increasing the total power output from the solar panels or increasing the efficiency of any circuit connected to the solar panel. This can be done by using an efficient controller, which is accurate and provides speedy calculations to track the maximum power point of the solar cell.

The output power induced in the PV module depends on the solar insulation and temperature of the PV modules. Hence, any proposed calculation methodology should be tolerant and adaptive to these environmental effects. To date numerous maximum power point tracking (MPPT) methods have been proposed. They differ in many aspects such as complexity, accuracy, sensors required, cost or efficiency, and speed. Based on the control variable used, these methods can be categorized into perturb and observe method, open and short-circuit method, incremental conductance algorithm, fuzzy logic and artificial neural network. In this thesis, a novel methodology is presented to extract the maximum power of the PV cell. The method surpasses all the aforementioned techniques in both accuracy, speed of convergence and works well under different environmental conditions. The results of the proposed algorithm are compared with the incremental conductance algorithm as an example.

A single input triple output DC-DC converter is implemented using a coupled inductor. Many applications requires multi outputs with different voltage levels. This converter boosts the low-voltage input power source to a controllable DC high-voltage, middle-voltage output terminal, and a third output of low voltage useful for some applications. The controllable high voltage DC terminal can be used as an input for various applications, such as driving brushless DC motors (BLDC) in our case for driving the DC brushless motor used in the water pumping or powering the backbone of telecom system rack. The middle voltage output terminal can be used for charging battery modules. The low voltage can be used for individual low voltage control buses in the

aforementioned applications. The coupled-inductor based DC-DC converter provides cost effective, compact footprint, for different output voltages with different levels, and high step up ratio. PSIM simulations and design procedure are presented to show the merits of the proposed topology.

Water is important for our life. Water pumping can be implemented in different ways. If electrical energy is used for water pumping, the cost of electricity is an important factor since in some areas, for example rural and remote areas, the cost of electric energy can be very high. Knowing that the conventional power grids probably are not available in these areas, motor generators can be an alternative solution. However the problems with motor generators are that they are not cost effective due to fuel dependency, they are not environmentally friendly and also need frequent maintenance. Therefore there is a huge need for solutions which are cost effective, environmentally friendly, easy to install, available in rural and remote areas, and require low maintenance. Solar powered DC water pumps is such a potential solution. Solar DC water pumps are easy to install, reliable, and operates fully automatically. Typical system consists of solar PV panels, solar DC controller, DC water pump.

1.2 Scope of Work

This research focuses on designing and implementing an efficient algorithm for maximum power point tracking, and implementing the algorithm into a complete system in the solar based water pumps, which is a very important application, and designing a DC-DC converter of triple output, which is very useful for many applications in addition to being used in water pumping applications. Complete and detailed simulations and analysis are provided as well as experimental results.

1.3 Thesis Contributions

Contributions of this thesis can be summarized as the following.

- Development of novel Estimate Perturb Perturb (EPP)-based algorithm for maximum power point tracking (MPPT) PV applications. Both software implementation using PSIM and prototyping are successfully achieved and tested
- Development of novel single input triple output DC-DC converter.

- Implementation of the new algorithm and circuit into a complete system in the solar based water pumps.

Publications:

- M. Eid, M. Youssef and Y. Wang, "Single Input Triple Output DC-DC Converter for Automation Applications", *IEEE Proceedings of the International Conference of Energy and Telecommunications*, INTELEC October 2015 Japan.
- M. Eid, M. Youssef and Y. Wang, "A Novel Efficient EPP-Based Algorithm for MPPT PV Applications", *IEEE Proceedings of the International Conference of Energy and Telecommunications*, INTELEC October 2015 Japan
- M. Eid, M. Youssef, and Y. Wang, "Intelligent Control Techniques in Solar-Based Energy Harvesting System", to be submitted to the *IEEE Transactions of Sustainable Energy*.

1.4 Thesis Outline

In this thesis, a sufficient background in addition to the literature review is presented in chapter 2. In chapter 3, the proposed MPPT Algorithm is presented. The proposed DC-DC converter is analyzed with different modes of operations in chapter 4. Subsequently, in chapter 5, a complete system, integrating the proposed MPPT Algorithm and the proposed DC-DC converter, is shown with DC motor used in water pumping connected to the system. Next, simulation results using PSIM along with an overview on a system prototype with experimental results are shown in chapter 6. In the last chapter, chapter 7, conclusions and future work are discussed.

Chapter 2: Background and Literature Review

In the first half of this chapter, some fundamental notions of the solar cells nature and harvesting solutions, relevant to the research proposed here, are presented. The second half illustrates the different designs and algorithms for MPPT and simulations are provided to estimate the speed of tracking and accuracy of each algorithm. All simulations were done using PSIM.

2.1 Background

The power of sun, represented in sunlight, was used by the ancients to ignite fires to destroy enemy warships using "burning mirrors". Till the eighteenth century the main use of solar energy was for heating and lighting purposes. Europeans built solar heated greenhouses during eighteenth century. French scientists operated a steam engine using solar collectors. After that many versions of solar collectors were invented. The first solar operated selenium cell was invented in 1883 by Charles Fritts. Silicon solar cells was developed in 1954, following fundamental work done in 1940s by Russell Ohl. However, it was very high in cost (300$ per watt) [1].

Photovoltaic converts sunlight to electric energy and it depends on the photoelectric effect. Only absorbed light by solar cells is useful for generating power as there is part of the light reflected from the panel, which is not useful. Many designs were developed to make the surface of the solar panel absorb and not reflect light. This absorbed light excites the electrons in the PV cell atoms to become free electrons forming part of the electrical flow.

The basic structure of solar cells is a p-n Junction. Figure 2.1 shows the inner structure of solar cell after the structure is exposed to sunlight. Some electrons are excited in the n-layer and some holes of positive charges as well in the p-layer. Hence we have free charges ready to form current flow. The basic process consists of absorption of a photon, formation of electron-hole pair, charge separation, and charge transport to the anode (holes) and cathode (electrons), supplying a direct current for the load.

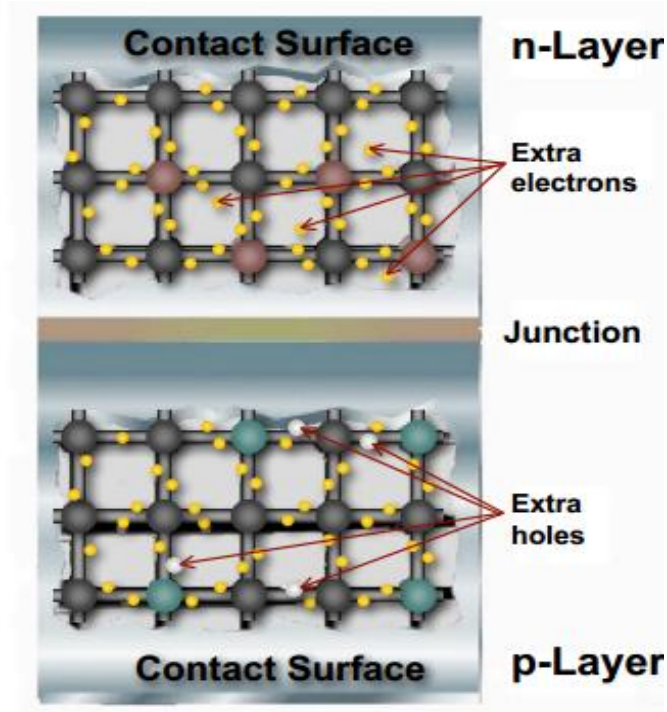

Figure 2.1: Photoelectric effect inside solar cell structure [2]

2.2 Solar Cell Modeling

Ideal solar cells can be modeled as a diode. The IV curve of a solar cell is a combination of the IV curve of the solar cell diode in the dark with the light-generated current (Lindholm, Fossum, & Burgess, 1979). The light causes the IV curve to shift down into the fourth quadrant where power is generated from the cell. The current in the cell can be calculated through equation (2.1) as [3]

$$I = I_0 \left[e^{\frac{qV}{nKT}} - 1 \right] - I_L \qquad (2.1)$$

where: I_L is the light generated current.

I_0: PV cell reverse saturation current (A)

q: electron in charge (C) (-1.602*10^{-19})

K: Boltzmann's constant (J/°k) (1.380*10^{-23})

n: ideality factor

T: PV cell Temperature in (°k)

Figure 2.2 shows the IV curve of the solar panel under different light intensity conditions.

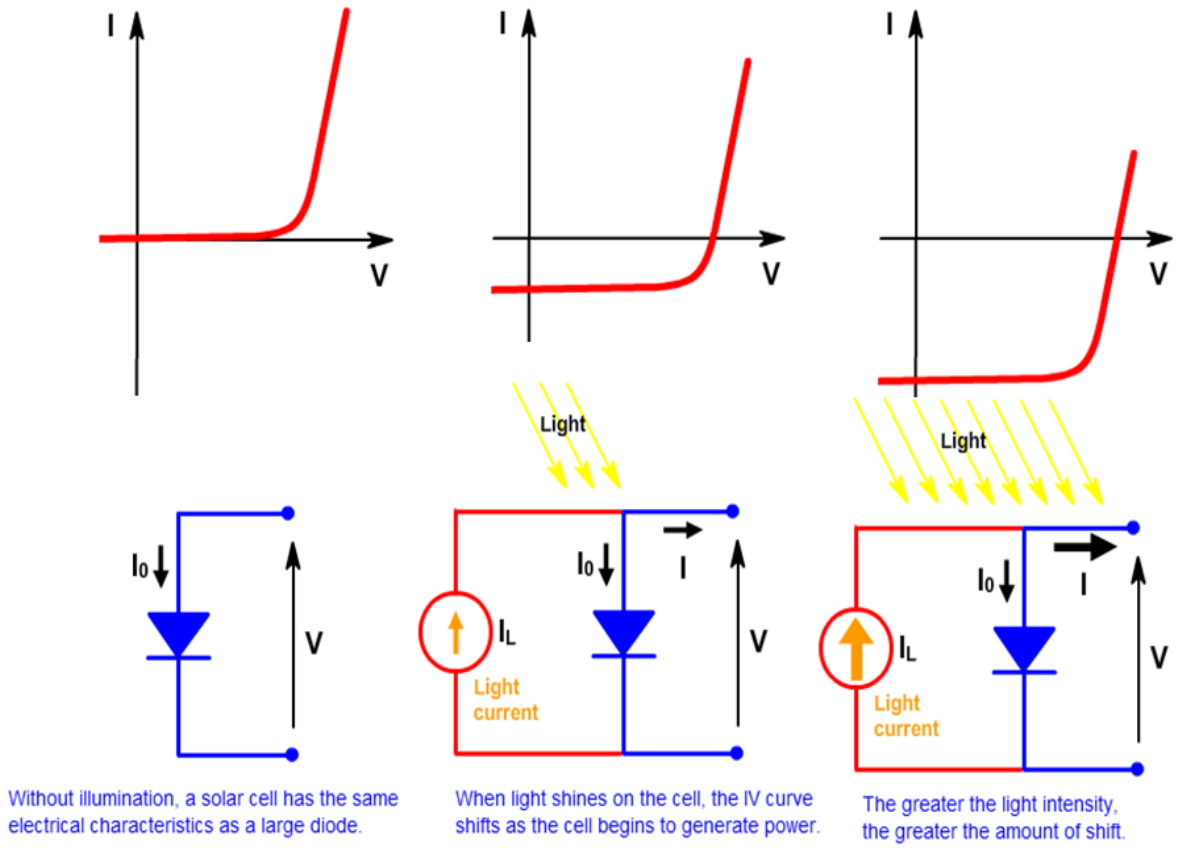

Figure 2.2: Ideal solar cell IV curve under different illumination conditions [2]

By increasing light intensity or illumination, the amount of light generated current increases. Since the cell is generating power, the convention is to invert the current as shown in Figure 2.3.

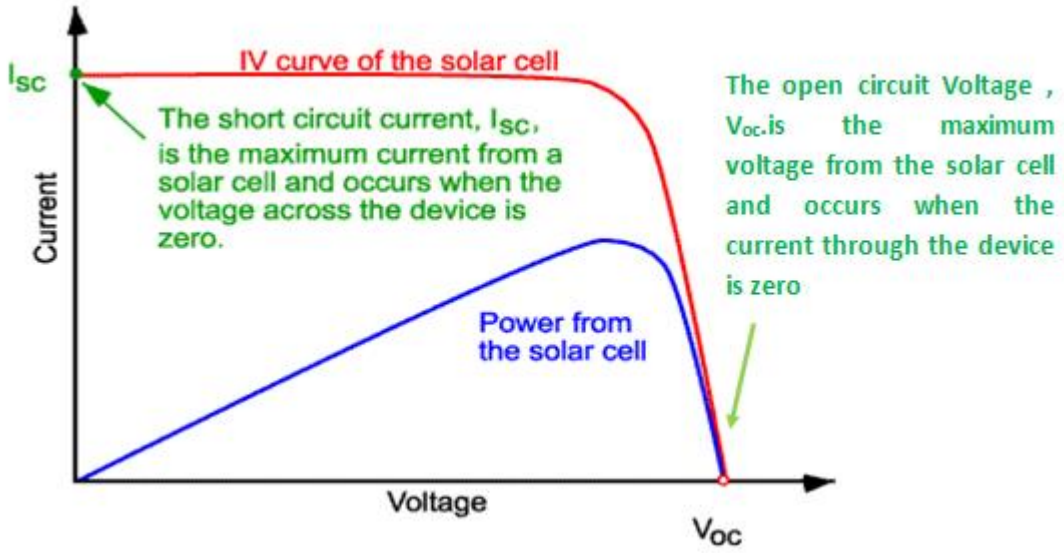

Figure 2.3: The IV curve for solar cells [3]

In Figure 2.3, I_{sc} is short circuit current, and V_{oc} is open circuit voltage.

The previous modeling assumes ideal operation. For better accuracy, other components should be taken into consideration during the circuit modeling, such as shunt and series resistance.

Shunt Resistance: Significant power loss exists due to the shunt resistance R_{SH}, which is caused by manufacturing defects. Low shunt resistance results in power loss in solar cells since it provides an equivalent parallel current path for the light-generated current. It decreases the amount of current flowing through the solar cell junction and thus directly decreases the voltage output from the solar cell. The effect of a shunt resistance is very obvious at low intensity, since there will be less light-generated current. The loss of this current to the shunt will be very obvious. In addition, at lower voltages when the effective resistance of the solar cell is high, the impact of shunt resistance is large.

Series Resistance: It has many probable causes such as movement of current through the emitter and base of the solar cell, the resistance due to the contact between the metal contact and the silicon, and the top and real metal contact resistance itself. The main effect of the series resistance is reducing the fill factor, and at very high values of the series resistance R_s it also reduces the short-circuit current. The fill factor "FF" in equation (2.2) as [2] is a measure of the "squareness" of the solar cell and is the area of the largest rectangle which will fit in the IV curve is defined as the ratio between the optimum power can be obtained from the solar cell to the product of the open circuit voltage and the short circuit current. Figure 2.4 shows the equivalent solar cell circuit after adding the resistance parasitics of the solar cell.

$$FF = \frac{P_{max}}{V_{oc} I_{sc}} \qquad (2.2)$$

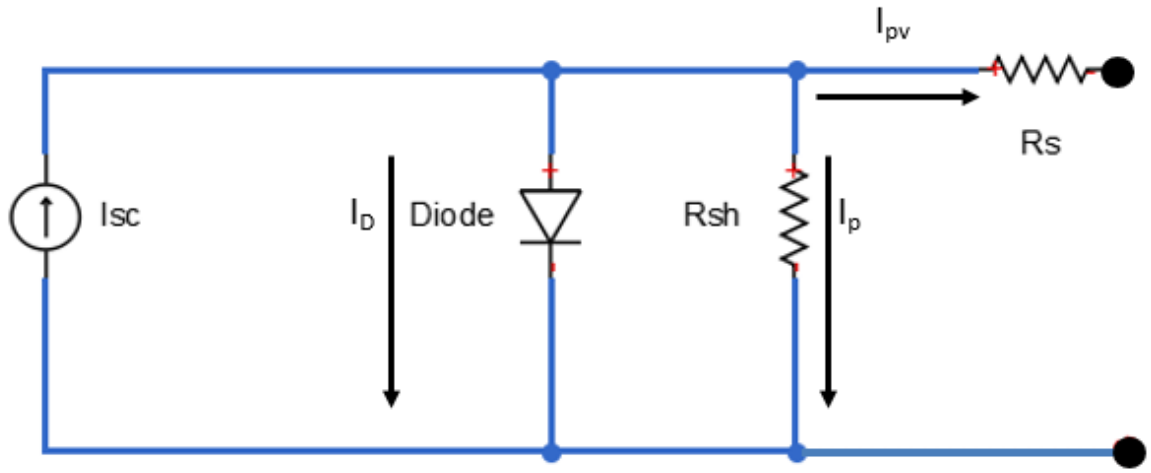

Figure 2.4: Single diode model solar cell equivalent circuit with series and shunt resistance

Output voltage is given by equation (2.3) as [3].

$$V_{PV} = \frac{\alpha N_S k T}{q} \ln\left[\frac{I_{sc} - I_{PV} + N_P I_0}{N_P I_0}\right] - \frac{N_S}{N_P} R_S I_{PV} \qquad (2.3)$$

The parameters in the output voltage are as follows:

α: Ideality factor

I_0: PV cell reverse saturation current (A)

I_{PV}: PV cell output current

I_{SC}: Short -circuit cell current

K: Boltzmann's constant (J/◦k)

N_P: Number of parallel strings

N_s: Number of series cells per string

q: Electron in charge (C)

R_s: Series resistance of PV cell

T : Temperature of the PV cell in (◦k)

I_D: Diode current.

I_P: Shunt current.

The ideality factor of the diode represents a measurement of how the diode equation follows the ideal diode.

As shown in Figure 2.5, if we connect two cells in series the total voltage will increase. If we connect them in parallel the total current increases. The connections depend on the application, whether it needs high current or high voltage.

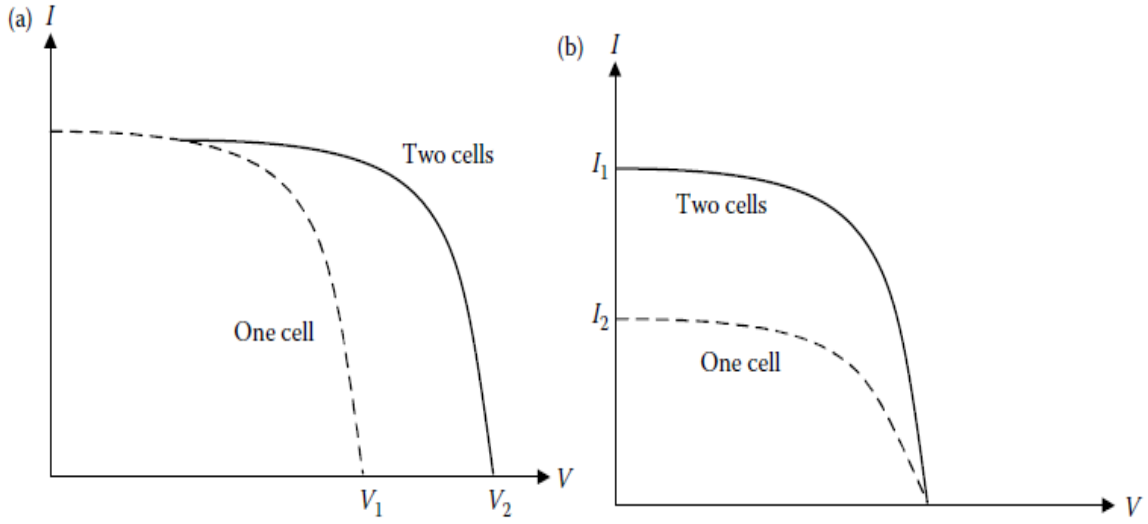

Figure 2.5: Series and parallel connections of solar cells [1]

(a) Series; (b) Parallel connection of identical cells

Characteristic Resistance: One important definition for this research is the characteristic resistance of the solar panel. The characteristic resistance of the solar cell is defined as the solar cell output resistance at the point of maximum power. In other word if the load connected to the solar panel equals the characteristic resistance of the solar cell, the maximum power is transferred and delivered to the load, and we can say that the solar cell is operating on the maximum power point.

Figure 2.6 shows the output resistance of solar cell in the IV curve and also shows the characteristic resistance.

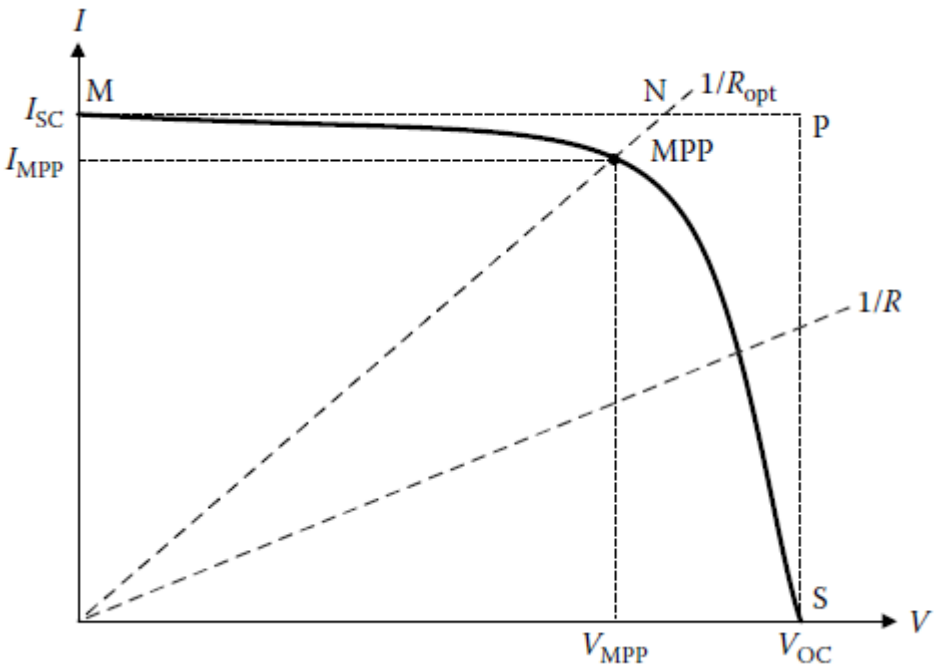

Figure 2.6: Characteristic resistance defination in the I-V curve [1]

The characteristic resistance of a solar cell is the inverse of the slope of the line intersecting the IV curve on I_M, V_M current and voltages respectively giving the maximum power transmission. The maximum power definition is given in equation (2.4).

$$P_{max} = I_{Mpp} * V_{Mpp} \qquad (2.4)$$

The power graph can be obtained by multiplying current and voltage values as shown in Figure 2.7.

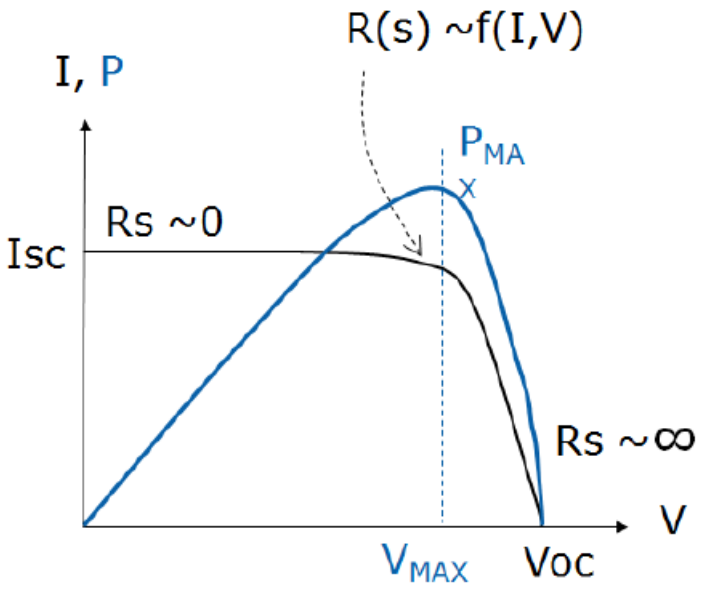

Figure 2.7: P-V curve for solar cells [2]

The power voltage curve starts with zero continue increasing till it reaches the maximum value at P_{MA} then decreases to zero again.

Assuming in order to receive the maximum power we succeeded to choose the load having the same resistance as the characteristic resistance of the solar panel, are we going to receive the maximum power? The answer will be yes, if the environmental conditions are constant, i.e. same temperature and light intensity and no shading effects. This means that the previous curves are for certain temperature and solar irradiance. If these parameters change, we are going to have another curve, i.e. V_M, I_M will be shifted, resulting in another characteristic impedance. If the load is matched at certain time, the maximum power is received. If any parameter, such as temperature or irradiance, changes, the load will no longer be matched and hence not receiving the maximum power.

Figure 2.8 shows the temperature effects on the I-V curve of the solar cells. As the temperature increases as the V_{oc} decreases, the point of the maximum power shifts to the left.

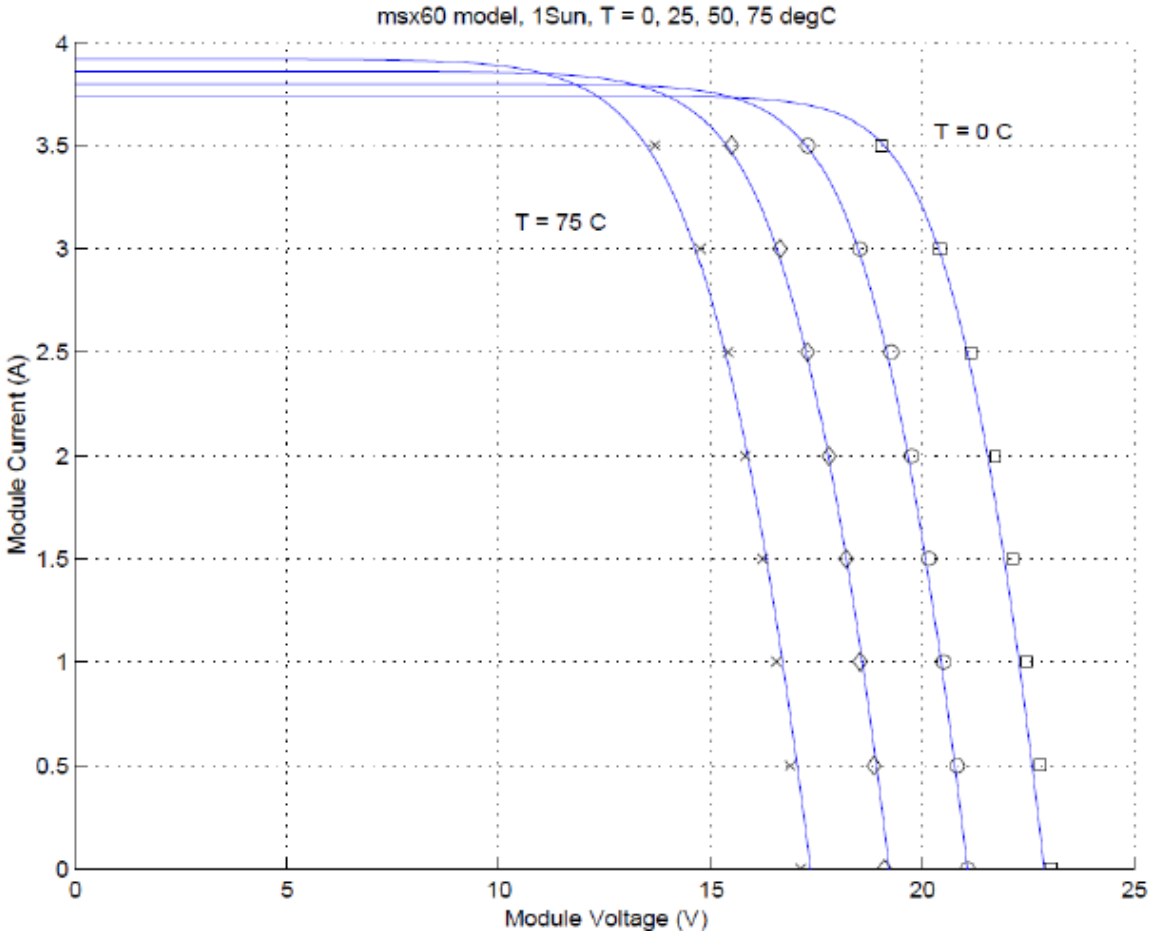

Figure 2.8: Temperature effect on the I-V curve [1]

Figure 2.9 shows the effect of solar irradiance changes on the solar cell. As the intensity increases and the value of the short circuit current, I_{sc}, increases, the curves shift up. It means the value of the point of the maximum power changes, which makes the process of tracking the point of maximum power challenging and an intelligent system is needed.

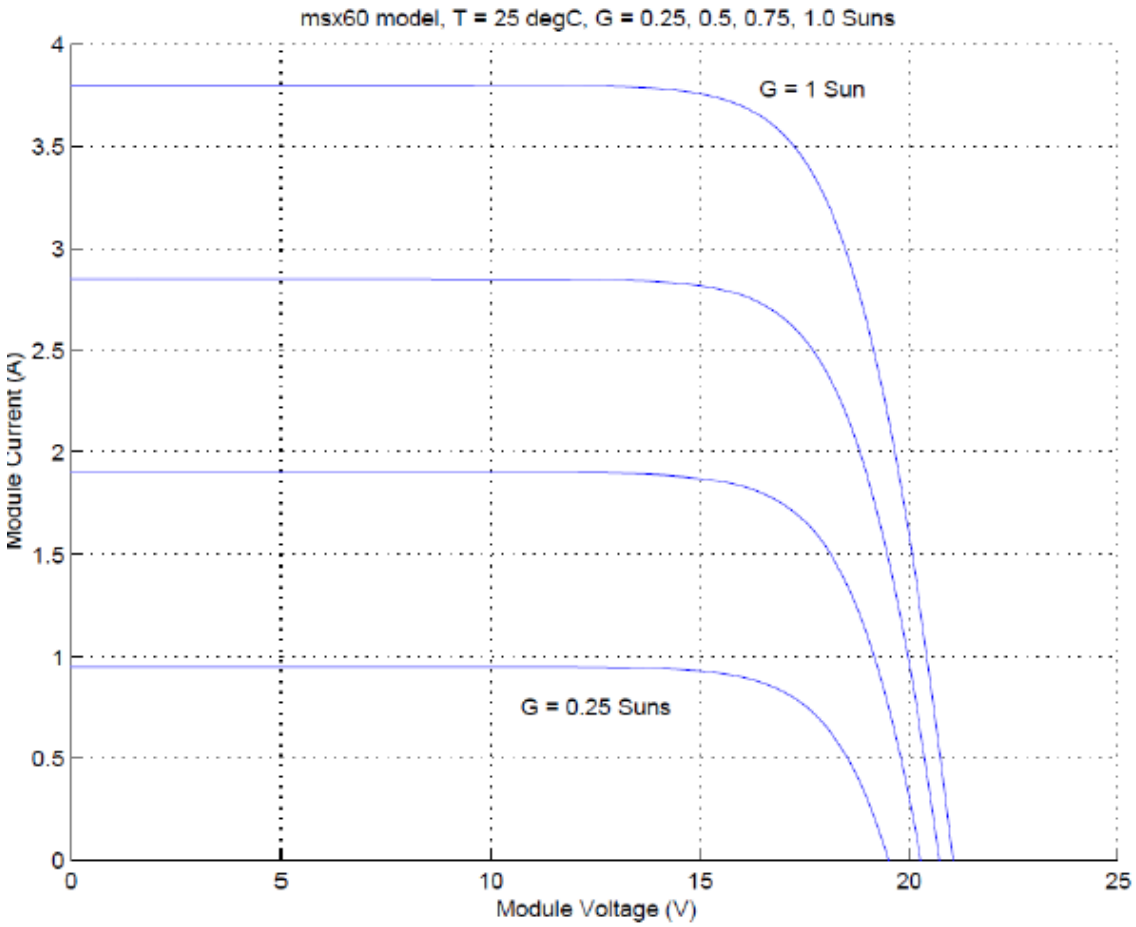

Figure 2.9: The effect of solar intensity on the I-V curve [1]

The light intensity on a solar cell is given a notation or value function of number of suns, where one sun is equivalent to 1 kW/m^2. Therefore a system with 8 kW/m^2 incident on the solar cell will be operating at eight suns.

2.3 Literature Review

The success of a PV application depends on the performance of the power electronics device used, i.e. whether it can extract the maximum power from the PV array connected. It is really important to develop a control system for maximum power point tacking to operate properly under different environmental conditions, and to develop a cost effective system with high performance to increase the market share of PV sources as a reliable source for electricity. Up till now much

research has been done on developing an appropriate algorithm for tracking the point of maximum power.

2.3.1 Existing MPPT Methods

Many algorithms have been developed to track the maximum power point, such as perturb and observe, open and short circuit method, incremental conductance, fuzzy logic, first order differential, and artificial neural network [4-51]. For comparison, we implemented some of the existing algorithms and analyzed the performance.

2.3.1.1 Perturb and Observe

Perturb and observe, also known as hill climbing or perturbation, is the most commonly used due to its simplicity and low cost. It works basically by trial and error and increases its step size in searching for the maximum in the IV curve of the solar cell as shown in Figure 2.10 until it reaches the maximum. It is typically done by perturbing the step and the observing the current and voltage to calculate the power and comparing the new values with the old values. If the new power value is higher, the algorithm is moving in the right direction. If the new value is lower, the algorithm changes the direction of perturbation since the old point is the maximum.

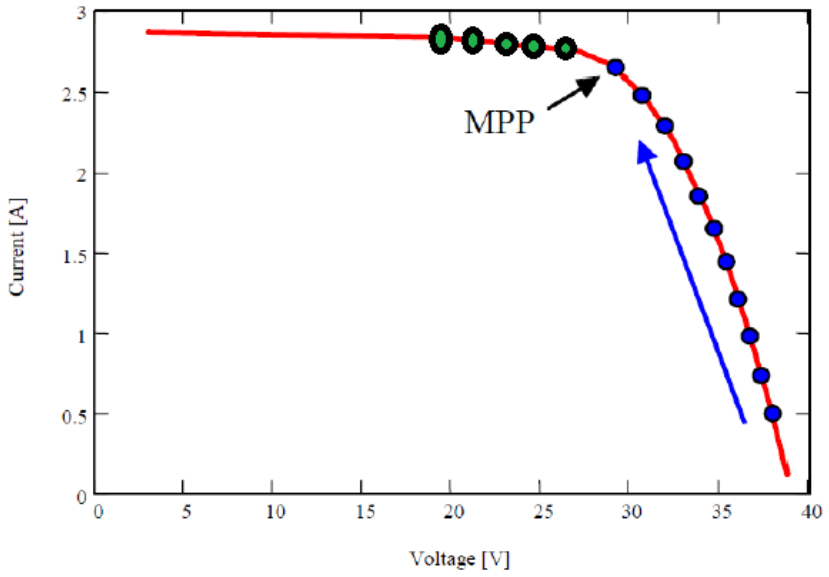

Figure 2.10: Perturb and observe process in the I-V curve [2]

Figure 2.11 shows the perturb and observe flowchart. In every time sample, the present power P(K) is calculated from the measured I(K) and V(K), the present current and voltage respectively. If the present power is larger than the old or previous measured power, the step delta will be in the same direction. Otherwise the step size is multiplied by negative one and the search direction becomes in the positive direction. The process is summarized also in Table 2.1.

Table 2.1. Perturbation Table based on Observation

Perturbation	**Change in Power**	**Next Perturbation**
Positive	Positive	Positive
Positive	Negative	Negative
Negative	Positive	Negative
Negative	Negative	Positive

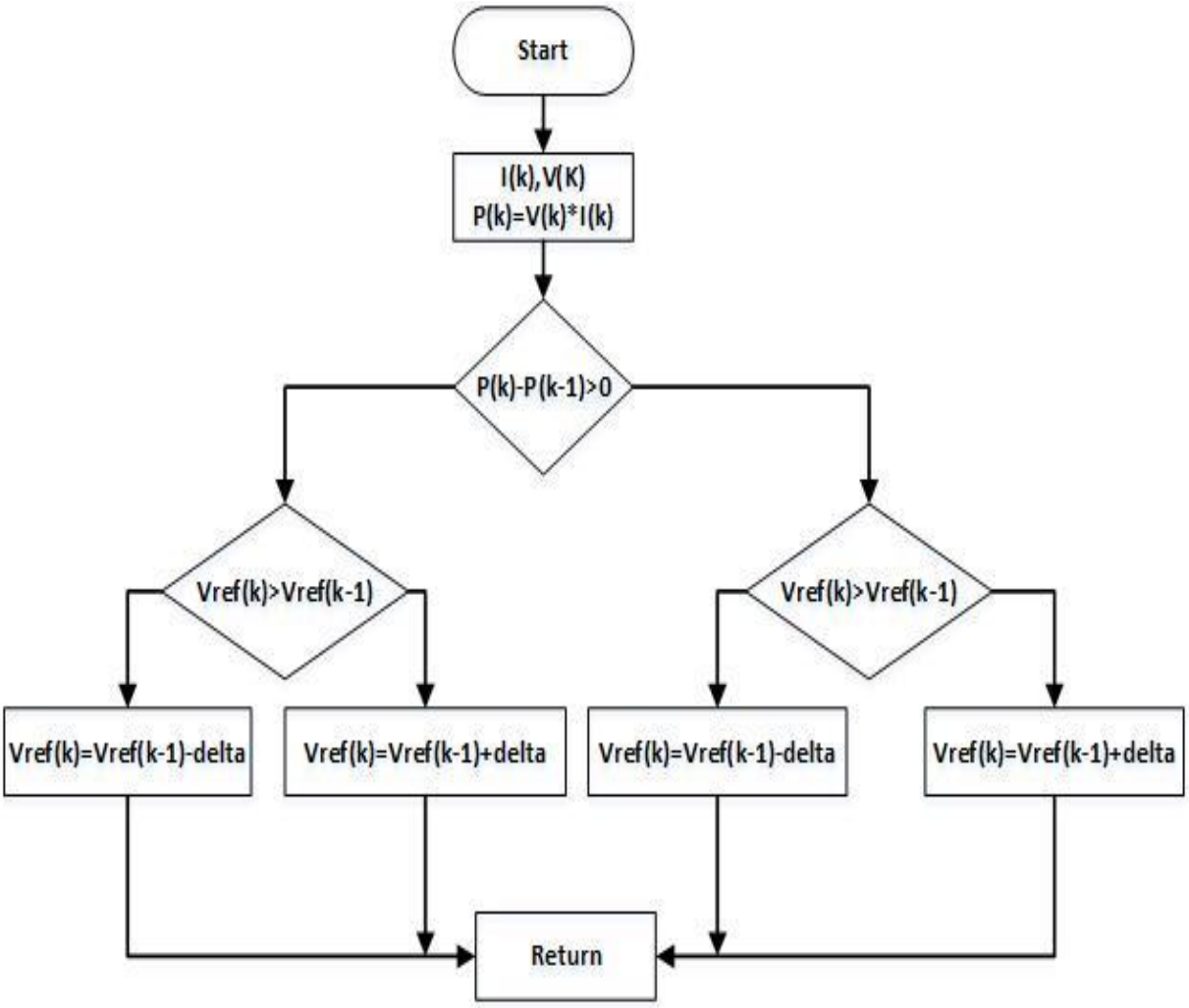

Figure 2.11: Perturb and observe algorithm flowchart

Simulations were done using PSIM to check the algorithm accuracy and how fast it is. As shown in Figure 2.12 and Figure 2.13, a comparison was done between the real power maximum, which is shown in red, and the power output obtained using the perturb and observe algorithm. It can be seen that the perturb and observe succeeded to track the maximum power but with some error as in Figure 2.12 and some delay as shown in Figure 2.13.

The perturb and observe algorithm has some drawbacks in steady state under constant environmental conditions. The system experiences fluctuations or oscillations around the point of maximum power. Moreover the perturb and observe algorithm may get confused during an environmental change, such as shading or any temperature changes.

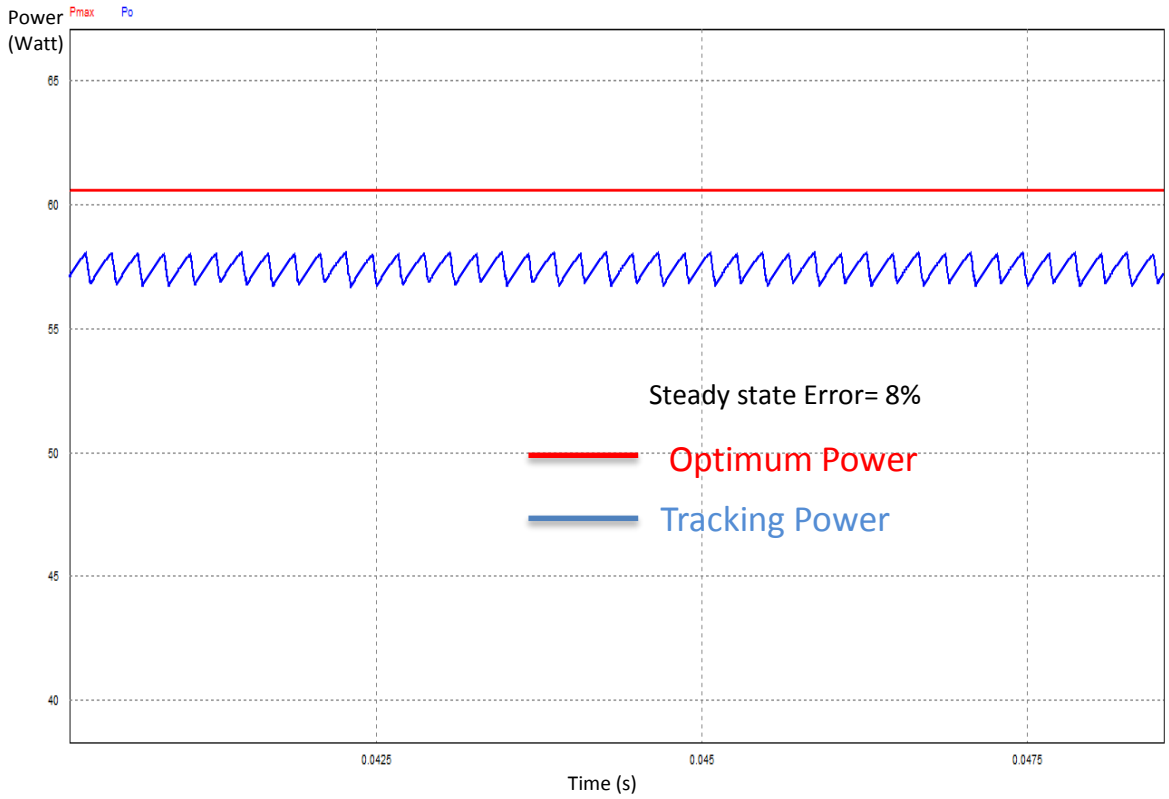

Figure 2.12: The optimum power versus power output using perturb and observe algorithm

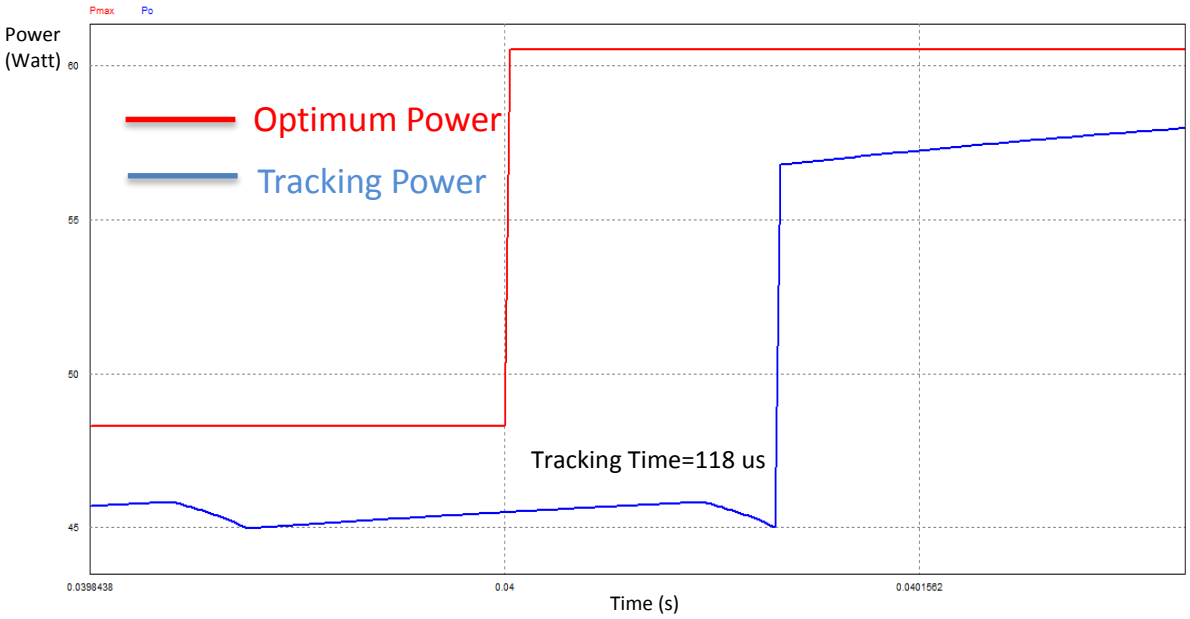

Figure 2.13: The MPPT tracking time for the perturb and observe algorithm

2.3.1.2 Incremental Conductance

Incremental conductance is based on sensing the voltage and the current of the PV array, and works by comparing the ratio of the derivative of conductance with the instantaneous conductance. When the instantaneous conductance equals the conductance of the PV, maximum power point is reached, and the fundamental equations are shown below [52].

$$\frac{dI}{dV} = -\frac{I}{V} \quad , at\ MPP \tag{2.1}$$

$$\frac{dI}{dV} > -\frac{I}{V} \quad , left\ of\ the\ MPP \tag{2.2}$$

$$\frac{dI}{dV} < -\frac{I}{V} \quad , right\ of\ the\ MPP \tag{2.3}$$

where I and V are the PV cells voltage and current, respectively. The left-hand side of the equations represents the incremental conductance of the PV module, and the right-hand side represents the instantaneous conductance. From (2.5)-(2.7), we can conclude that when the ratio of the change in the output conductance equals the negative output conductance, the solar array will operate at the MPP. It means by comparing the conductance each sample time, the MPPT will track the maximum power point of the PV module by sensing the voltage and current simultaneously.

The drawbacks of this techniques is that it can easily lose track of the MPP if any environmental changes happen, such as temperature rising. Another drawback is that there exists oscillations in the voltage and current around the MPP in the steady state, which is similar to the perturb and observe algorithm. Oscillations will occur if the step size of is not sufficiently small. It has some advantages, such as being reasonably faster in tracking than some other algorithms. The flowchart of this algorithm is shown in Figure 2.14. The algorithm starts its operation by getting the previous and present values for the current and voltage of the PV. And a comparison is carried out for the $\frac{dI}{dV}$ against $-\frac{I}{V}$. According to this comparison the duty cycle is adjusted to get the MPP of the PV.

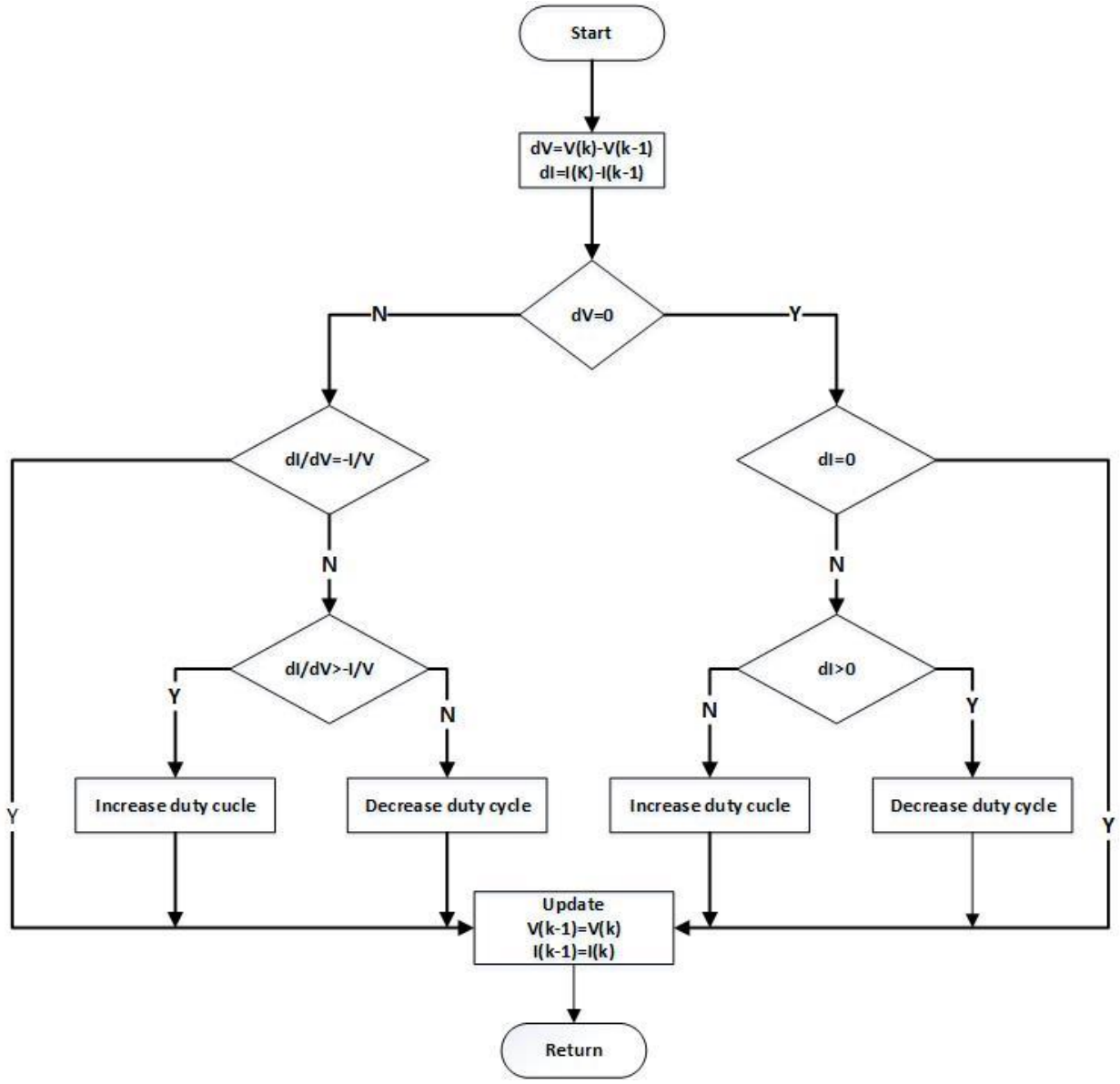

Figure 2.14: Incremental conductance algorithm flowchart

Simulations were done using the incremental conductance as part of the literature review using PSIM software and the results are shown in Figure 2.15 and Figure 2.16.

Figure 2.15 shows the maximum power versus the output power. As shown there are still some errors in tracking. But the results are much better than the perturb and observe algorithm.

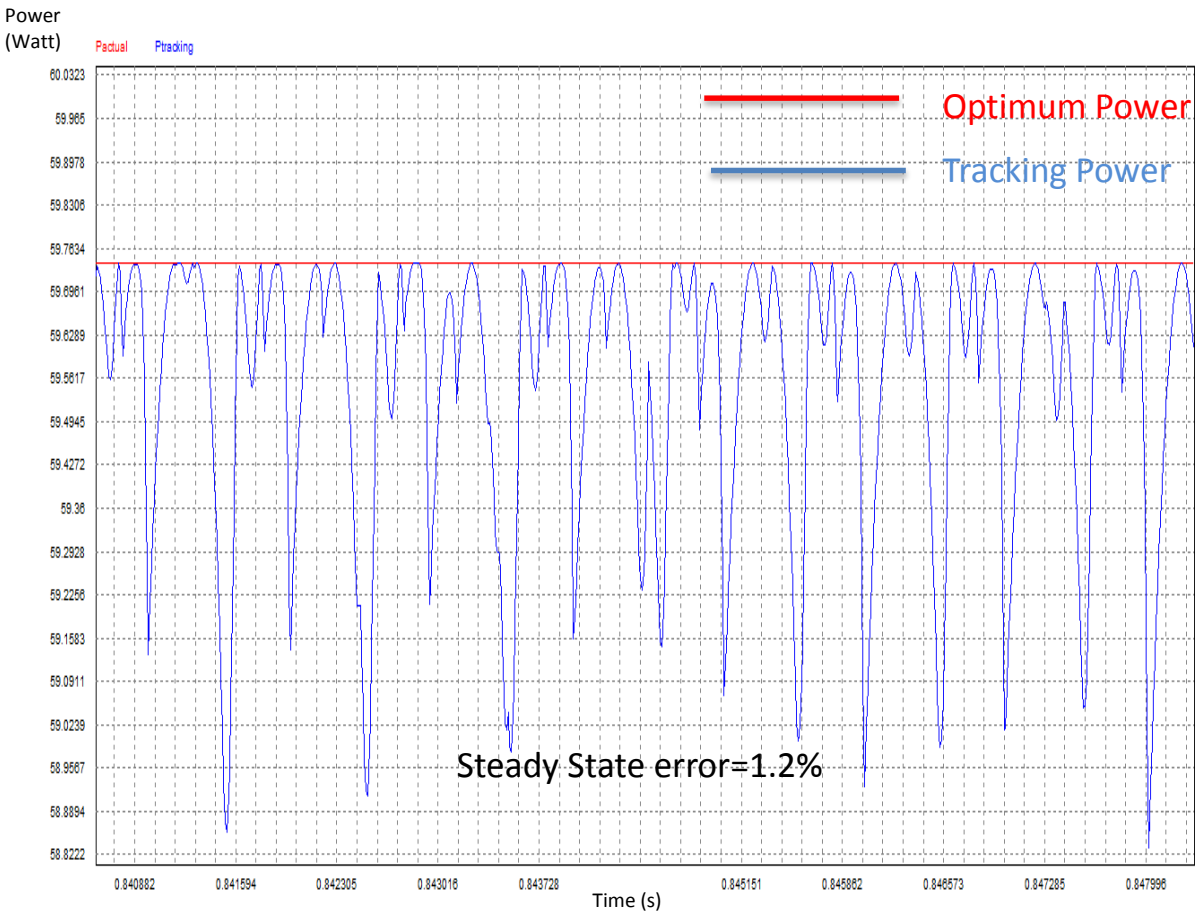

Figure 2.15: The optimum power versus power output using the incremental conductance algorithm

Figure 2.16 shows the tracking time for the incremental conductance. As can be seen it is much better than the perturb and observe algorithm having steady state error 1.2% compared to 8% in the perturb and observe and 10 us tracking time versus 118 us for the perturb and observe. The incremental conductance method shows better performance.

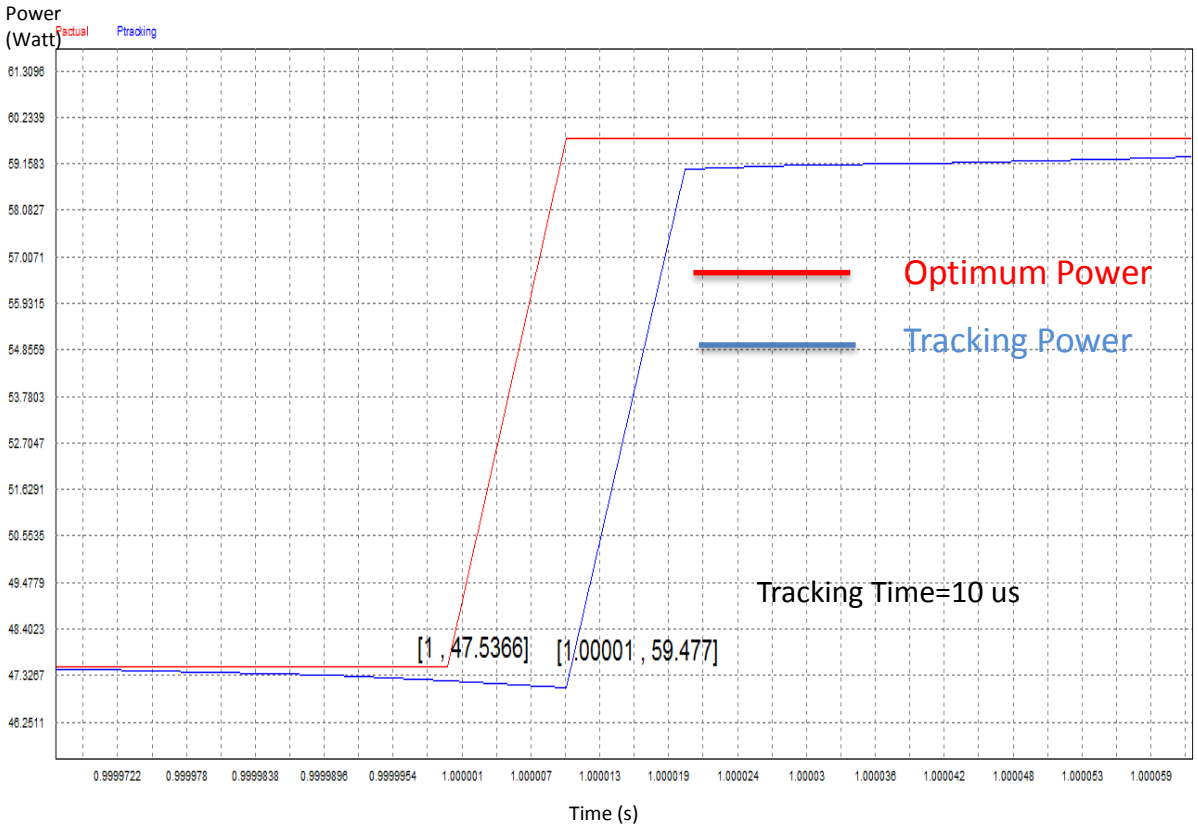

Figure 2.16: The MPPT tracking time for the incremental conductance algorithm

2.3.1.3 Open and Short Circuit Method

Open and short circuit method for MPPT is done by measuring the open circuit voltage and short circuit current on the real time, and estimating the maximum power point from a predefined PV current voltage curves. The advantage of this method is that it has fast response and does not cause oscillations. But it still has some disadvantages. For example, it does not always succeed to reach the point of maximum power as the predefined curves cannot give a perfect estimation for real time situations since the PV curve is nonlinear and depends on weather conditions.

2.3.1.4 First-Order Differential Method

Maximum power point tracking using first-order differential method is very simple and depends on measuring the current and voltages at each time sample and calculating $\frac{dP}{dV}$. When $\frac{dP}{dV} = 0$ it is the point of maximum power.

$$\frac{dP}{dV} = 0 \qquad (2.4)$$

$$\frac{d(V*I)}{dV} = 0 \qquad (2.5)$$

$$V * \frac{dI}{dV} + I = 0 \qquad (2.6)$$

We get

$$V * dI = I * dV \qquad (2.7)$$

Figure 2.17 shows the optimum power versus the output power using first order differential method simulations done using PSIM. The error is approximately 5 watts, which is quite large.

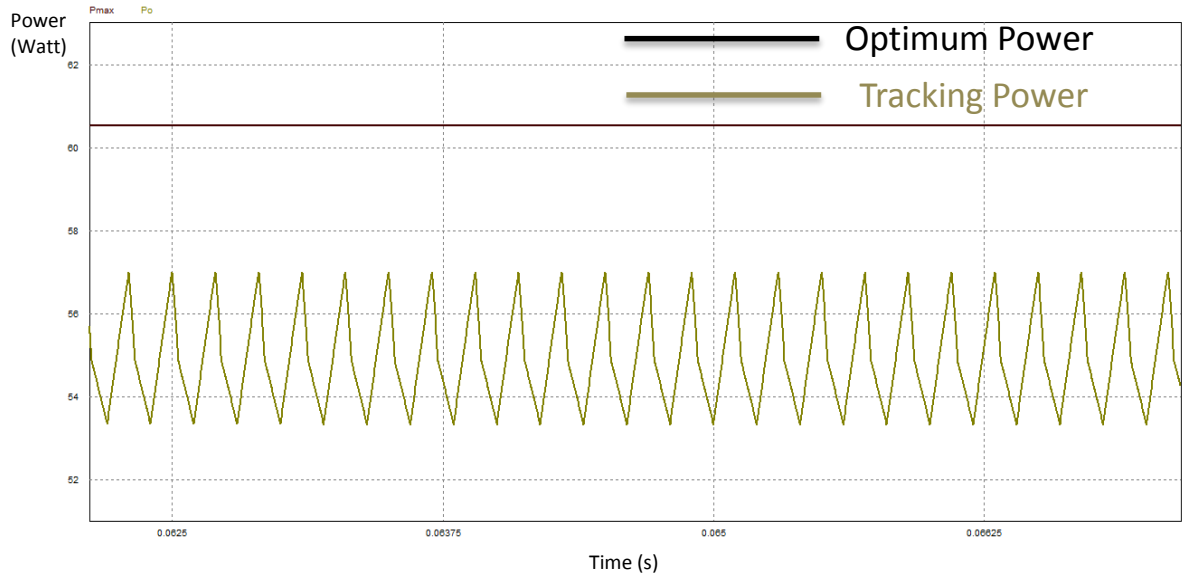

Figure 2.17: optimum power versus the output power using first order differential method

Figure 2.18 shows the time delay taken by the first order differential method to track the optimum power changes. As we can see it takes approximately 0.1 msec.

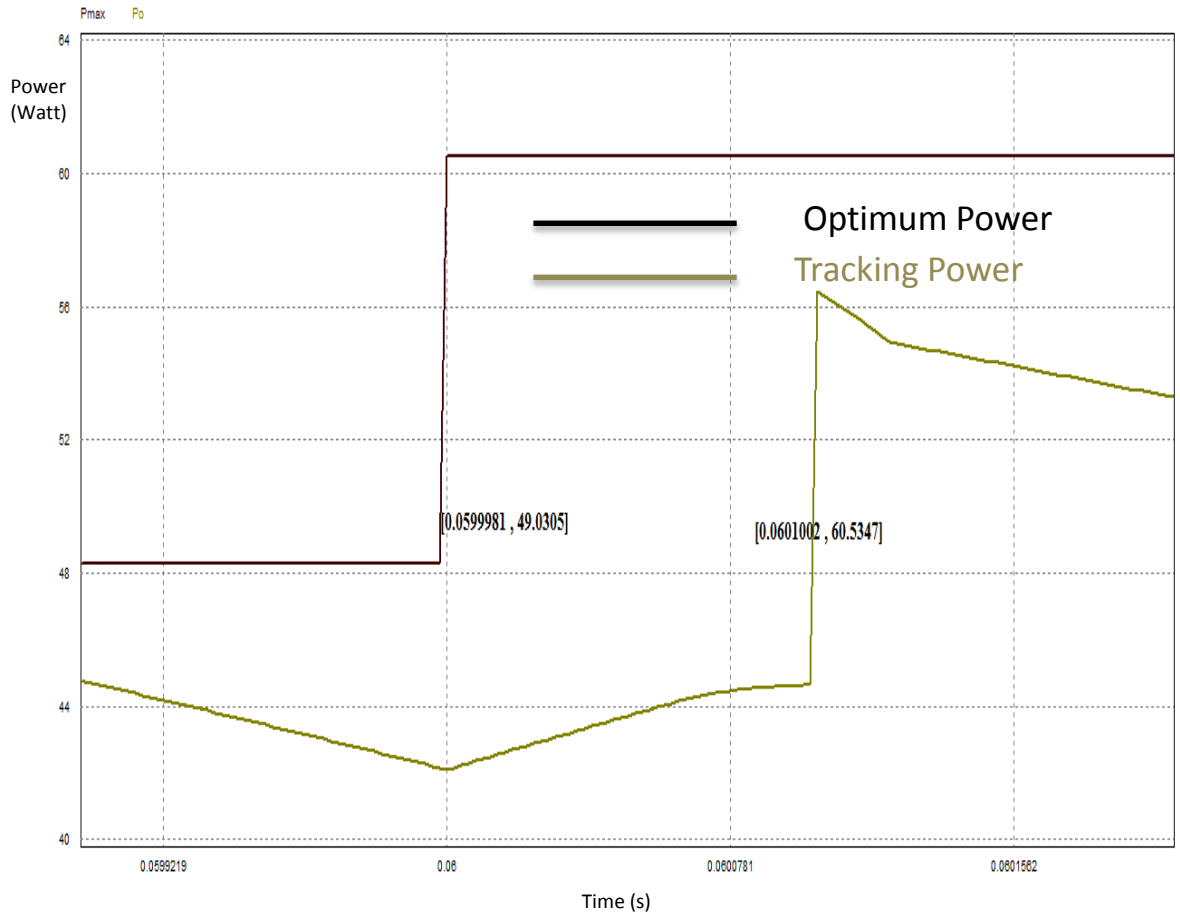

Figure 2.18: Tracking time using first order differential method

After simulating the previous existing maximum power point tracking methods, we can conclude that some of these methods work efficiently but only under certain environmental conditions, and others are not very accurate. In the next chapter a detailed analysis for the proposed algorithm is presented.

In the next section an important circuit is presented which is a basic component in MPPT algorithm implementation.

2.4 DC-DC Converters

DC-DC converter is an important electronic circuit, widely used in all kinds of applications. It converts the DC voltage from one level to another voltage level.

The boost converter is a step up DC-DC converter as shown in Figure 2.19. The relationship between the input and the output is a function of the duty cycle (D) used to control the switch [53]. This topology can be very easily converted to a buck converter by switching the position of the switch and the inductor. Power is transferred from input node to output node by the effect of periodic switching and then the loop filters block ripples appears on the output node.

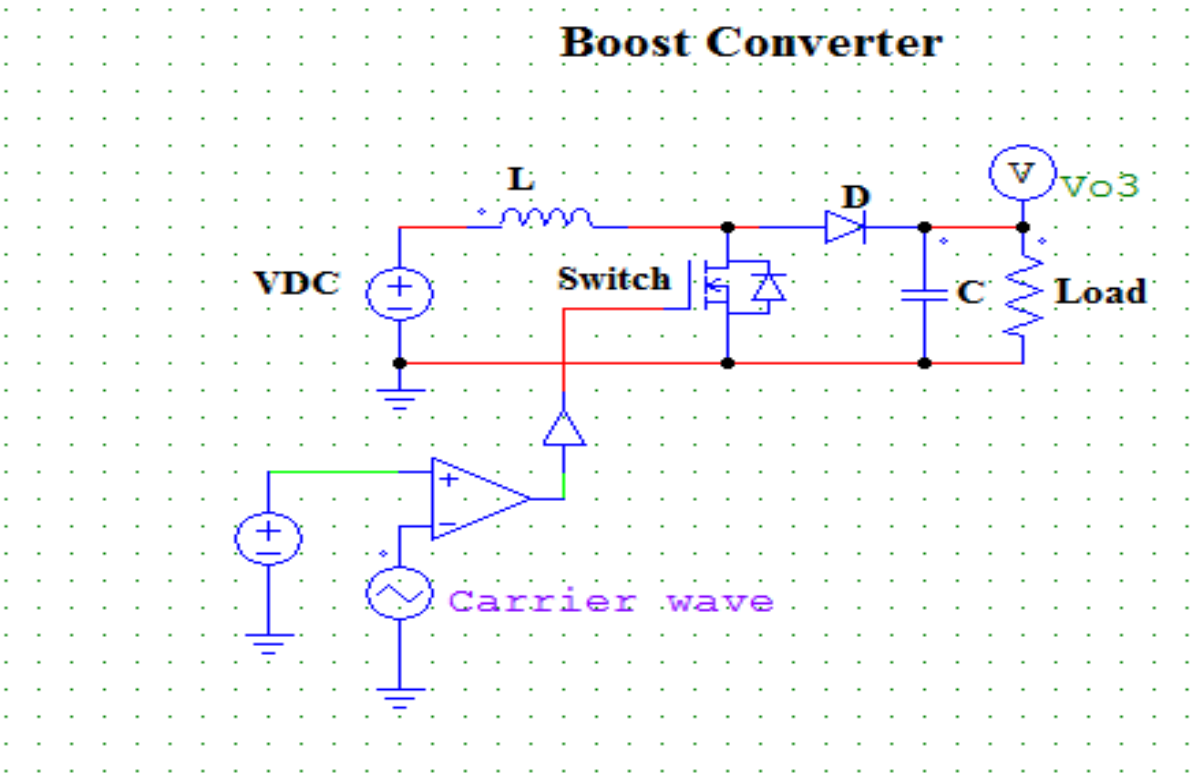

Figure 2.19: Basic boost converter circuit diagram

The following section is used to derive the important equations governing the boost DC-DC converter shown in Figure 2.19 to get the equation to show that the matching needed to receive the maximum power from the solar panel can be achieved using the previous circuit. The equations in this section as [53].

The Duty cycle D is given by $D = \frac{t_{on}}{T}$

t_{on}: is on time

T : is the signal period

$$V_{out} = V_{in} * \frac{1}{1-D} \quad (2.8)$$

$$I_{in} = I_{out} * \frac{1}{1-D} \quad (2.9)$$

The inductor ripple current is given by (2.10)

$$\Delta I = \frac{1}{L} V_{out} DT(1-D) \quad (2.10)$$

The average output power of the boost converter is given by (2.11).

$$I_{out} = I_{in}(1-D) = \frac{V_{out}}{R} \quad (2.11)$$

To calculate the inductor critical value to keep the circuit in continuous conduction mode we need set the minimum inductor current to zero.

$$I_{L,\min} = 0$$

We get

$$\mathrm{L_{crit}} = \frac{\mathrm{RT}}{2}(1-\mathrm{D})^2\mathrm{D} \quad (2.12)$$

For every converter we have some requirements on the output voltage ripple. For these requirements to be achieved, there are calculations for the output capacitor need to be done.

This is done by solving for the capacitor voltage at t=0, t=DT

Capacitor variations are given by (2.13).

$$\Delta V_C = V_C(0) - V_C(DT) = \frac{I_{out} DT}{C} \quad (2.13)$$

The ripple voltage is given by (2.14).

$$\frac{\Delta V_{out}}{V_{out}} = \frac{DT}{RC} = \frac{D}{RCf} \quad (2.14)$$

where

R: is the load resistance

f : is the switching frequency

$$C_{crit} = \frac{D}{Rf\left(\frac{\Delta V_{out}}{V_{out}}\right)} \tag{2.15}$$

Capacitance should be greater than or equal to C_{crit} to achieve the required output voltage ripple

Figure 2.20 shows the inductor current during the charging in DT period and discharging during the (1-D)T period of time.

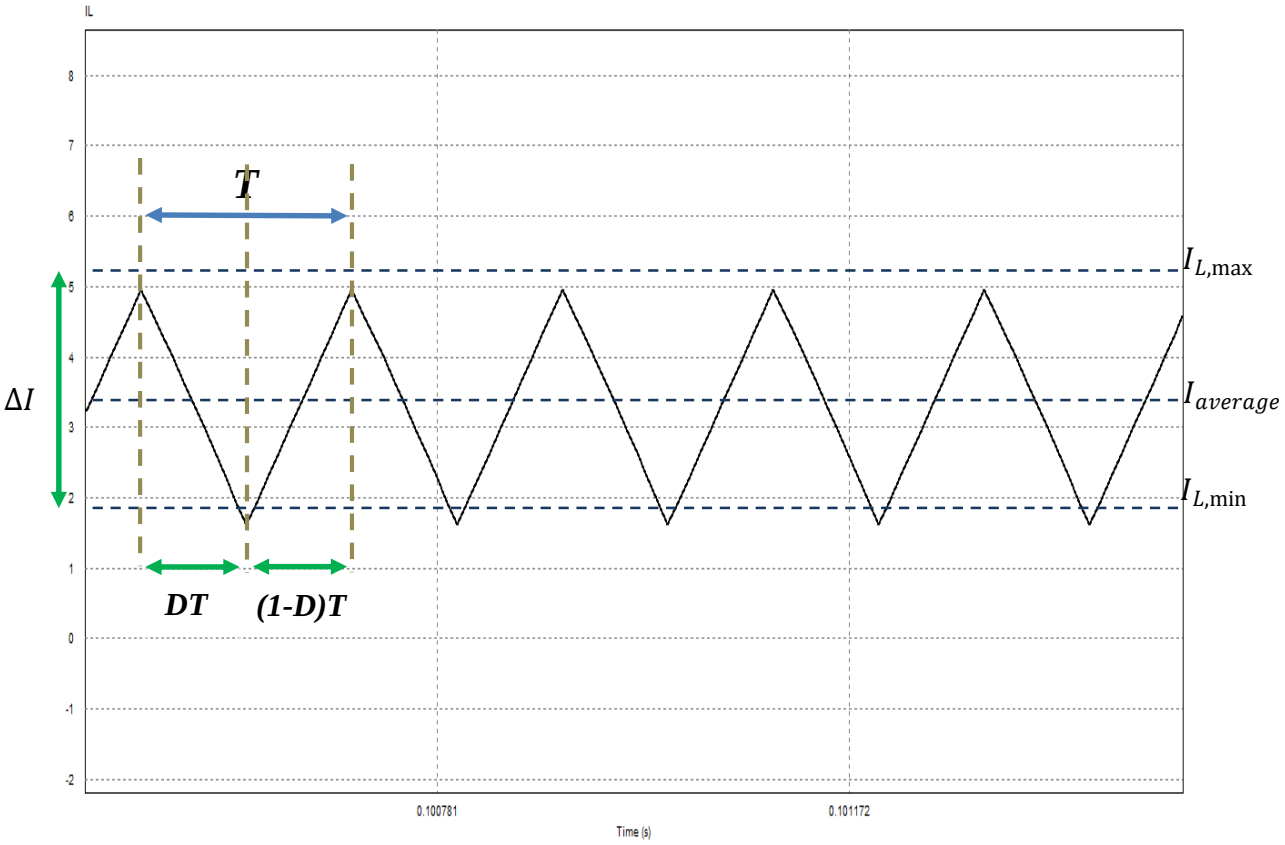

Figure 2.20: Inductor current

Figure 2.21 shows some important characteristic currents waveforms for the boost DC-DC converter. Figure 2.22 shows some important characteristic voltages waveforms for the boost DC-DC converter. These characteristic curves are very important during the design of any DC-DC converter since they show all stresses over most circuit components.

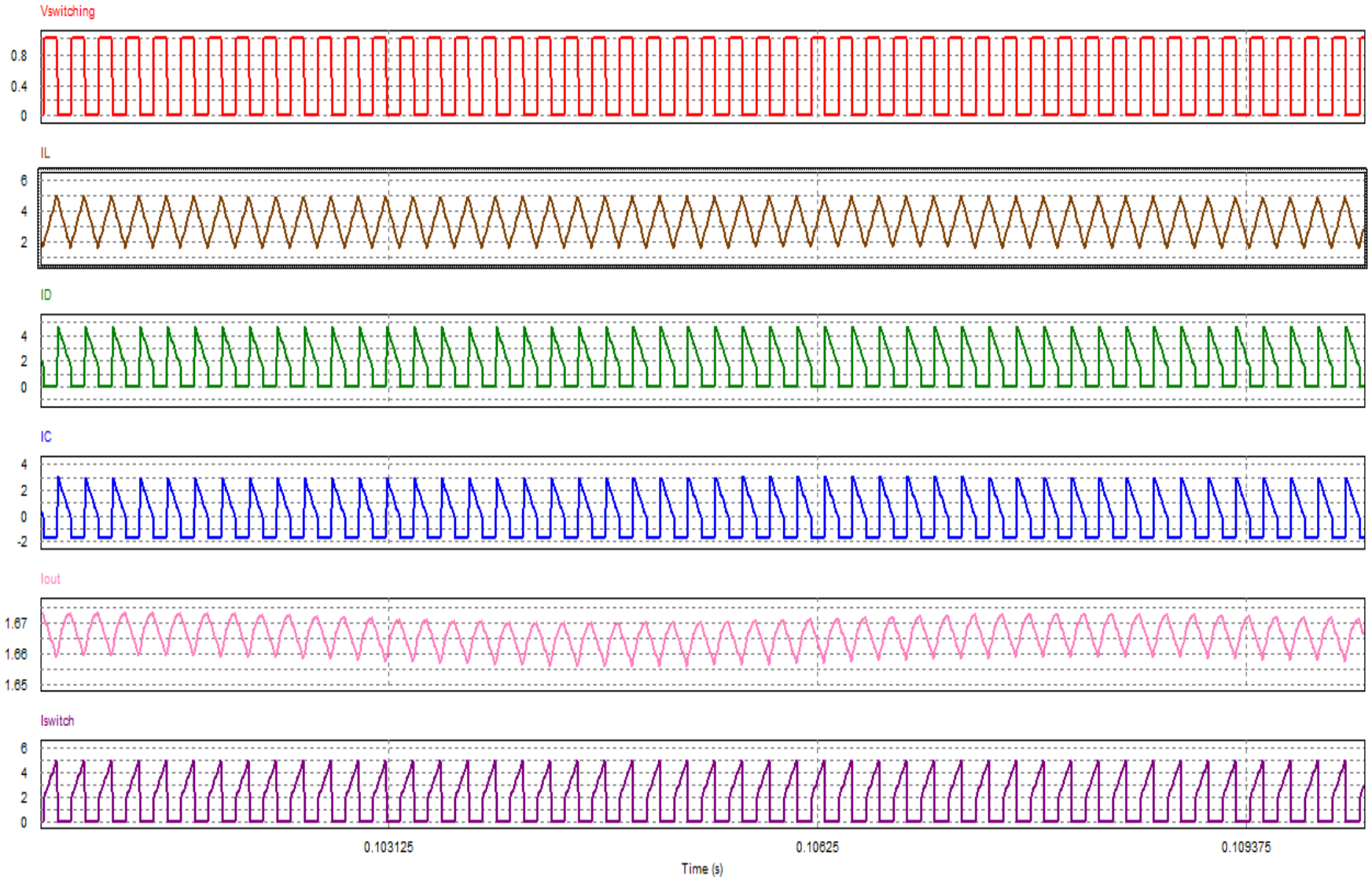

Figure 2.21: Boost converter currents characteristic curves

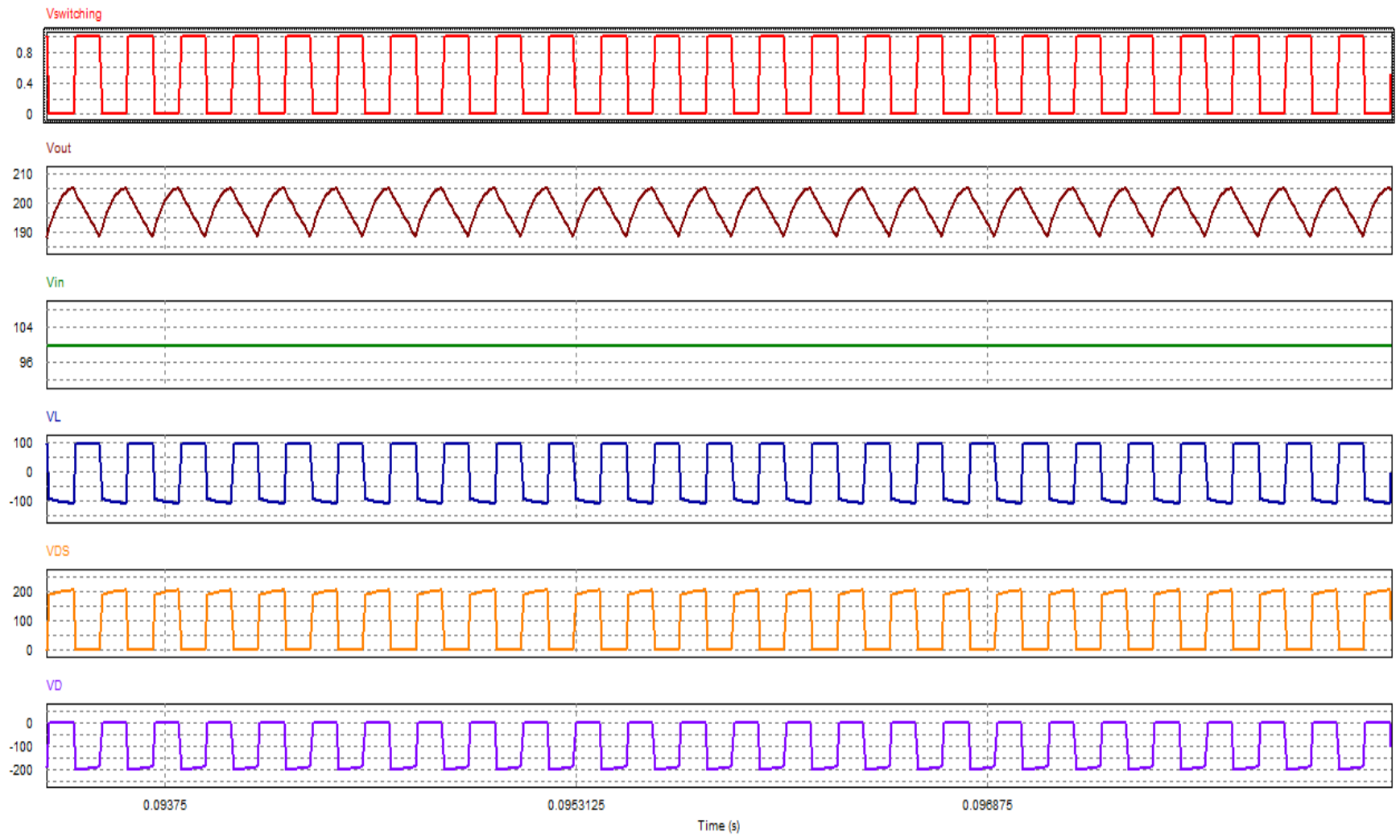

Figure 2.22: Boost converter voltages characteristic curves

$$R_{out} = R_{in} * \frac{1}{(1-D)^2} \qquad (2.16)$$

From equation (2.16) we find that the relationship between the input resistance and output resistance is a function of the duty cycle, which makes the boost converter work as a matching circuit. Hence we can use our MPPT algorithm to control the boost converter switching signal to match any load to our solar panel characteristic impedance, which is function of environmental conditions.

Chapter 3: A Novel Efficient EPP-Based Algorithm for MPPT

A new method for Maximum Power Point Tracking (MPPT) of the photovoltaic (PV) systems is presented, which uses a novel Estimate Perturb Perturb (EPP) Algorithm [44]. This algorithm is a modified version of the traditional perturb and observe algorithm as it uses one estimate process for every two perturbs in the searching for the maximum power point of the PV and during this process a variable perturbation step size is determined using a modified Newton- Raphson-method. This technique will cut down the online tracking time lapse to predict the next converter action almost without any delay. This novel method is mathematically presented and verified by a circuit simulation using PSIM. Simulation results will be given in chapter 6 to provide the proof of concept and merits of the proposed methodology. Great improvements have been demonstrated not only in the calculation speed but also in the accuracy of the MPPT methodology [54].

3.1 Introduction

The output power induced in the PV module depends on the solar insulation and temperature of the PV modules. Hence, the proposed calculation methodology should be tolerant and adaptive to these environmental effects.

To date numerous maximum power point (MPP) tracking methods have been proposed. They differ in many aspects such as complexity, accuracy, sensors required, cost or efficiency, and speed. Based on the control variable used, these methods can be categorized into perturb and observe method, open and short-circuit method, incremental conductance algorithm, fuzzy logic and artificial neural network. In this chapter, a novel methodology is presented to extract the maximum power of the PV cell. The method surpasses all the aforementioned techniques in both accuracy and speed of convergence. The results of the proposed algorithm are compared with the incremental conductance algorithm as an example.

The MPPT control is challenging in general as it totally depends on the sunshine condition, which is neither constant nor predictable and affects the amount of current and voltage of the PV

and accordingly the power and efficiency. That is the main reason behind the need for a new intelligent techniques developed specifically to overcome this problem.

A PV system for grid connected applications is commonly composed of five main components: a PV array to harvest solar energy to be converted to electric energy, DC-DC converter to convert the low voltage to higher dc voltage, a digital controller to control the converter operations with the MPPT algorithm implemented on it, an inverter to invert the DC voltage to an AC voltage suitable for home appliances, which is a single or three phase inverter, and an AC filter to absorb any current or voltage harmonics that could be generated by the inverter.

In order for any PV system to work efficiently, some technical requirements should be fulfilled, such as an optimal control that is intelligent enough to get the maximum power that could be generated from the PV under any operating environmental conditions, and a high performance to cost ratio to facilitate commercialization of the PV developed technologies, since the PV array has highly nonlinear characteristics and its performance is highly affected by the environmental conditions. It is technically challenging to develop a PV system to satisfy all of these requirements. However, we believe that the research community will be able to develop one solution soon. Our work is a small step toward the goal.

A block diagram for the photovoltaic power system is presented in Figure 3.1. The control algorithm is implemented in the MPPT control block. The system is composed of five main blocks that are considered the main core for the PV system for grid connected applications

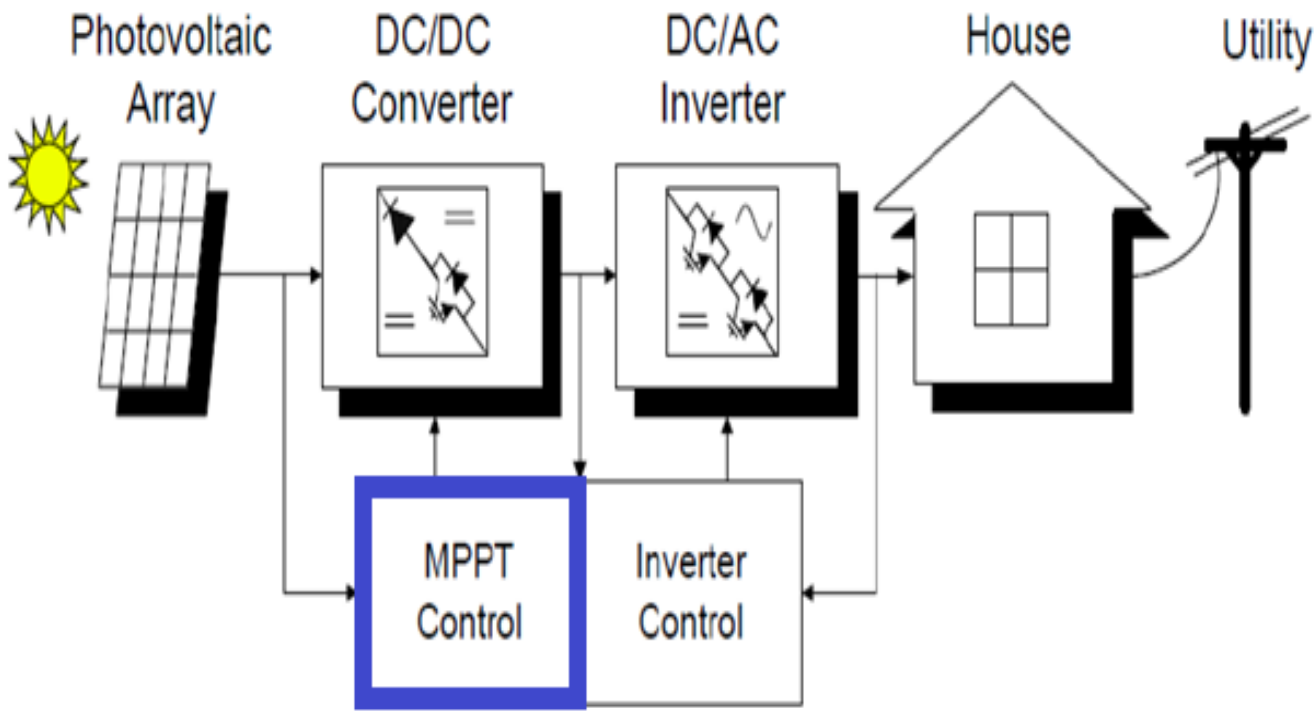

Figure 3.1: Block diagram of photovoltaic power system

3.2 Newton-Raphson Method Combined with EPP Algorithm

Compared to the traditional incremental conductance, the proposed method gives much better results regarding the tracking speed and accuracy, and it uses one estimation between every two perturbs. The flow chart describing this process is shown in Figure 3.2. In addition this method gives very good results for various shading effects and successfully tracks the power under conditions that the traditional incremental conductance algorithm may fail.

The algorithm consists of three modes, namely mode 0, mode 1, and mode 2. It starts at the beginning by mode 0, which is the estimation mode, and then goes to mode 1 after calculating the current power value based on the current and voltage measurements. Mode 1 and mode 2 are perturbation modes, on which a check is done as to go forward or backward in the perturbation. At every sample a new value for the step size is calculated according to the current and previous measurement, which makes the step size predictive.

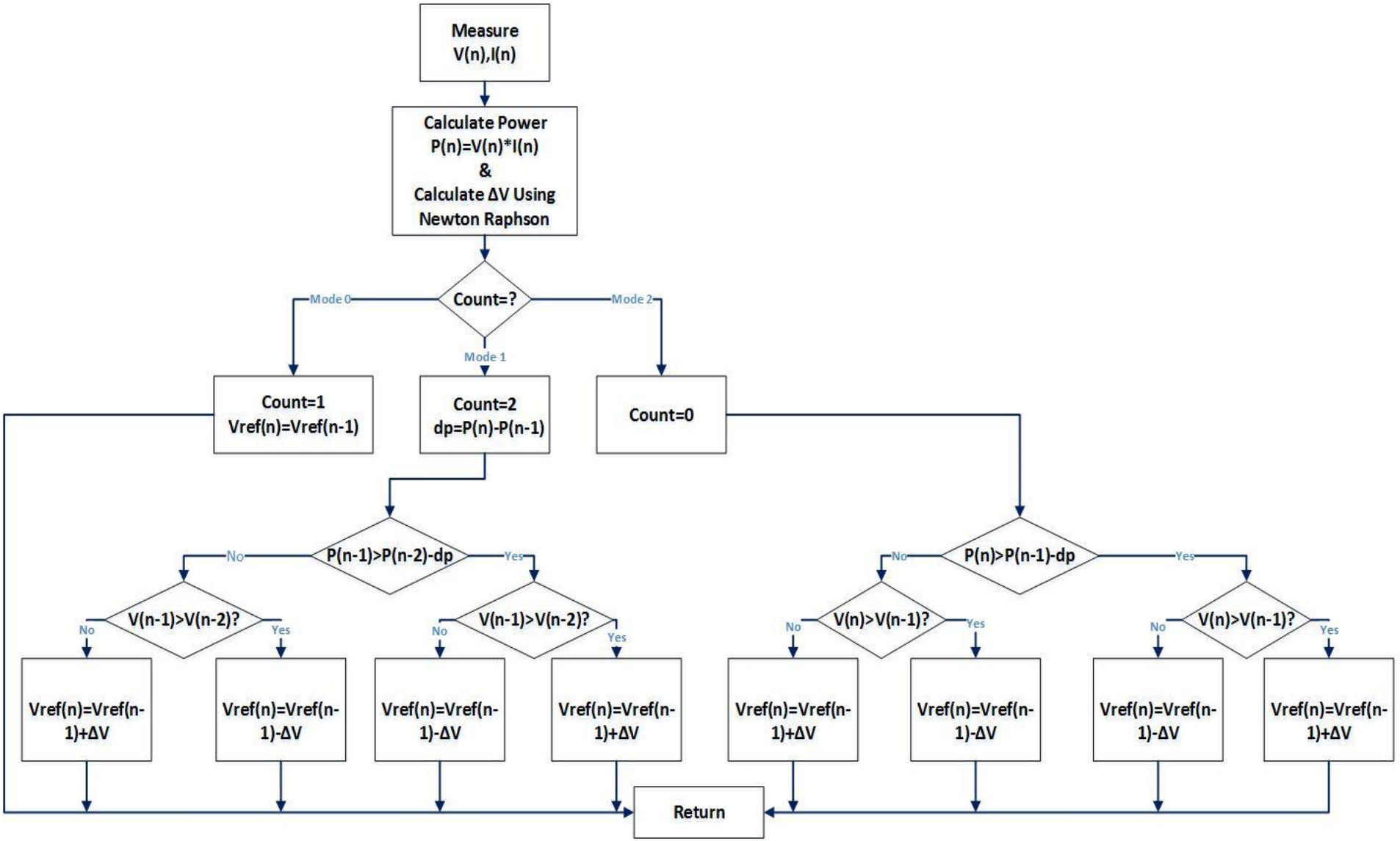

Figure 3.2: Flowchart for the MPPT proposed algorithm

The proposed algorithm uses EPP algorithm with a variable predictive perturbation step size ΔV, which makes the tracking speed better and the accuracy is very high. The step size is calculated using the Newton-Raphson Method [54]. It gives a predictive way to calculate an efficient step size that converges to the maximum power point very fast and with small error.

There is an optimum V_{pv} which maximizes the output power of the PV for every irradiation. To get the maximum power point, an optimal value of V_{pv} is immediately probed using EPP algorithm based on the following procedures: if an increment of V_{pv} causes an increase of P_{pv} in the former step, in the current step, the search for finding the optimal V_{pv} continues in the same direction. The opposite direction is followed otherwise. In this work, by using this combination of EPP algorithm and calculating the variable perturbation step using Newton-Raphson method, the resultant PV system is very efficient. The variable step technique operates according to Newton-Raphson method, and we can get a mathematical form for the step size from the following equations. Using Newton-Raphson to converge the solution the new solution in Newton-Raphson follows equation (3.1) [3].

$$X_{n+1} = X_n + \left(\frac{F(X_n)}{F'(X_n)}\right) \qquad (3.1)$$

where X_n is the initial values of X, $F(X_n)$ is the value of function at point X_n, and $F'(X_n)$ is the derivative of the function at point X_n. The function $F(X)$ can be written as below:

$$F(X) = \frac{dP}{dV} \qquad (3.2)$$

where P is the power measurement of the PV and V is the voltage. Equation (3.2) can be written as:

$$F(X_n) = \frac{P_n - P_{n-1}}{V_n - V_{n-1}} \quad = grad_n \qquad (3.3)$$

$$F'(X) = \frac{d^2P}{dV^2} \qquad (3.4)$$

where $F'(X_n)$ is the derivative of the function. We can rewrite equation (3.4) as shown below:

$$F'(X_n) = \frac{grad_n - grad_{n-1}}{V_n - V_{n-1}} \qquad (3.5)$$

Similarly from equation (3.1) we can assume the reference voltage $V_{ref}(n)$ is given by

$$V_{ref(n)} = V_{ref(n-1)} + \Delta V \qquad (3.6)$$

where $V_{ref}(n)$ is the voltage used then to control the duty cycle of the switch.

ΔV is the perturbation step. And from equations (3.2), (3.3), (3.5) we can get:

$$\Delta V = \frac{F(X_n)}{F'(X_n)} \qquad (3.7)$$

$$\Delta V = \frac{P_n - P_{n-1}}{grad_n - grad_{n-1}} \qquad (3.8)$$

Equation (3.8) is used to calculate the perturbation step size at each iteration. Using this variable step size, the maximum power point tracker converges to the maximum power value more rapidly and the power fluctuations decrease.

The simulation results for the proposed algorithm are presented in section 6.1, showing the detailed results, and sensitivity analysis to environmental effects is presented as well.

Chapter 4: Proposed Triple Output DC-DC Converter

This chapter presents the implementation of an efficient single input triple output DC-DC converter. A lot of applications require multiple outputs with different voltage levels. This converter boosts the low-voltage input power source to a controllable high-voltage DC bus and middle-voltage output terminals. The controllable high voltage DC terminal can be used as an input for various applications like driving brushless DC motors (BLDC) or powering the backbone of telecom system rack. Middle voltage output terminal can be used for charging battery modules and also can be used for individual low voltage control buses in the aforementioned applications. The proposed coupled-inductor based DC-DC converter provides cost effective, compact footprint, and high efficiency power conversion, for different output voltages with different levels and high step up ratio. PSIM simulations and design procedure will be presented to show the merits of the proposed topology [55].

4.1 Introduction

The proposed single input triple output DC-DC converter is implemented using coupled inductor and one power switch for different outputs with high step up ratio. Soft switching techniques are used to reduce the switching and conduction losses. Similar multi output DC-DC converters commonly use more than one power switch for each output [56-63] so the cost will be high if multi outputs are required. Many papers have presented single input multiple output DC-DC converters, implementing buck, boost and inverted output at the same time. However the big problem is that to implement one output at least three switches are needed, which is usually implemented for low output voltage and power applications and a hard switching is usually used in the implementation causing a lot of loss in the system. In [60] a DC-DC multi-output boost converter is presented, which is capable of dividing the power between outputs of different voltages. The issue in the design is that it uses more than two switches for every output. Moreover its control scheme is very difficult and the output loads cannot be supplied independently.

In the circuit presented in this chapter, one switch is required. This circuit is recommended for telecommunications and motor applications or any application requiring different DC voltage

levels. An interesting application for this converter is for automation applications, which will be presented in the next chapter.

4.2 Converter Design

The circuit diagram for the single input triple output DC-DC converter is shown in Figure 4.1. This circuit consists of six parts: a low-voltage side circuit, a clamping circuit, a two auxiliary circuits, a middle voltage circuit, and a high voltage circuit. The input is V_{fc} and the three outputs V_{o1}, V_{o2}, V_{o3} are the low voltage output, the middle voltage output, and the high voltage output, respectively. The main switch is expressed as s_1. L_{aux1} and L_{aux2} are the auxiliary inductors for the auxiliary circuits. L_p is the primary inductance of the coupled inductor, L_s is the inductance of the secondary circuit for the coupled inductor, L_{mp} is the magnetizing inductor, and the leakage inductor is L_{kp}. The turns ratio N and coupling coefficient K of this transformer "coupled inductor" are defined as:

$$N = \frac{N_2}{N_1} \tag{4.1}$$

$$K = \frac{L_{mp}}{L_{KP}+L_{mp}} \tag{4.2}$$

$$G_H = \frac{V_{o3}}{V_{fc}} = \frac{N+1}{1-D} \tag{4.3}$$

where N_1 and N_2 are the winding turns in the primary and secondary sides of the coupled inductor. G_H is the input to high voltage gain, D is the duty cycle of the modulated input signal of the switch, and V_{o3}, V_{fc}, are the high output and the input voltages respectively.

Figure 4.1 shows the converter circuit diagram with single input and three outputs.

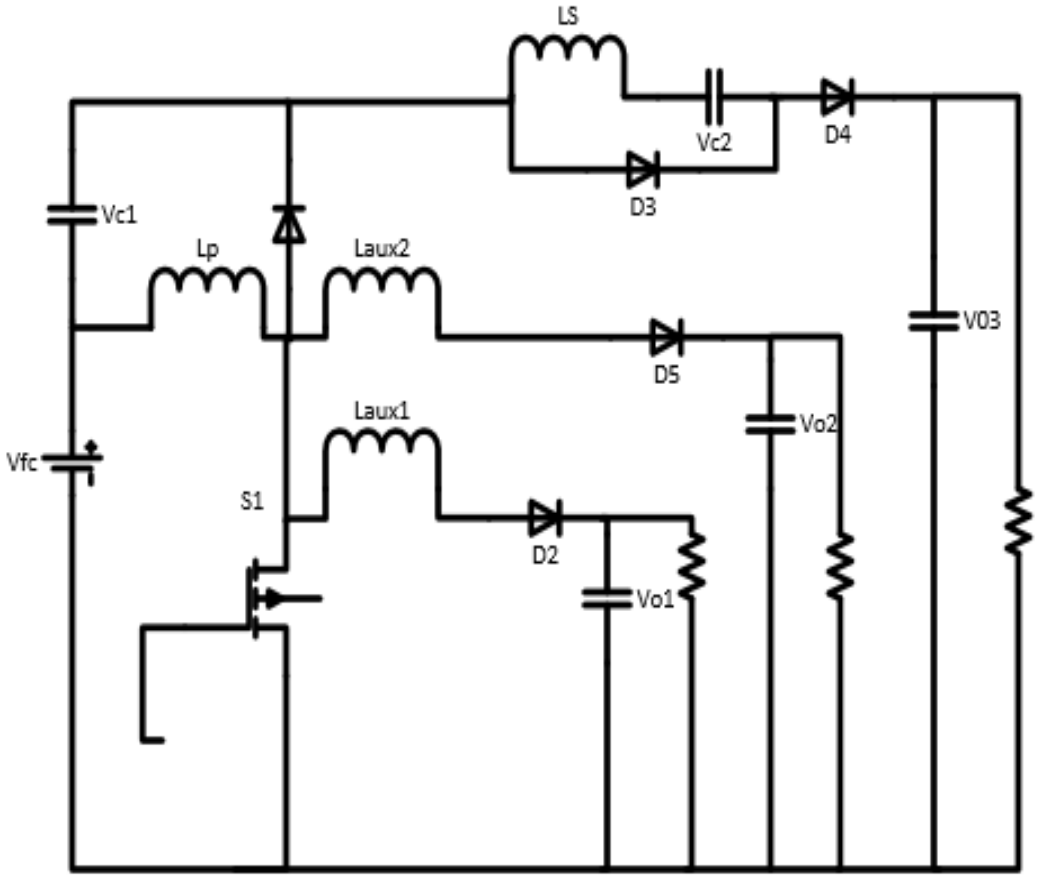

Figure 4.1: Converter circuit diagram

4.3 Modes of Operation

This circuit has six modes of operations as shown below.

Mode 1:

The circuit diagram of mode 1 is shown in Figure 4.2. At the beginning switch $S1$ is turned ON for a period of time and diode D4 is turned off since the voltage across the coupled inductor terminal is positive. The diode $D3$ turns ON. The secondary current of the coupled inductor i_{LS} charges to the capacitor $C2$. When the auxiliary inductor discharge the energy completely, at the end of the mode diode $D2$ turns OFF.

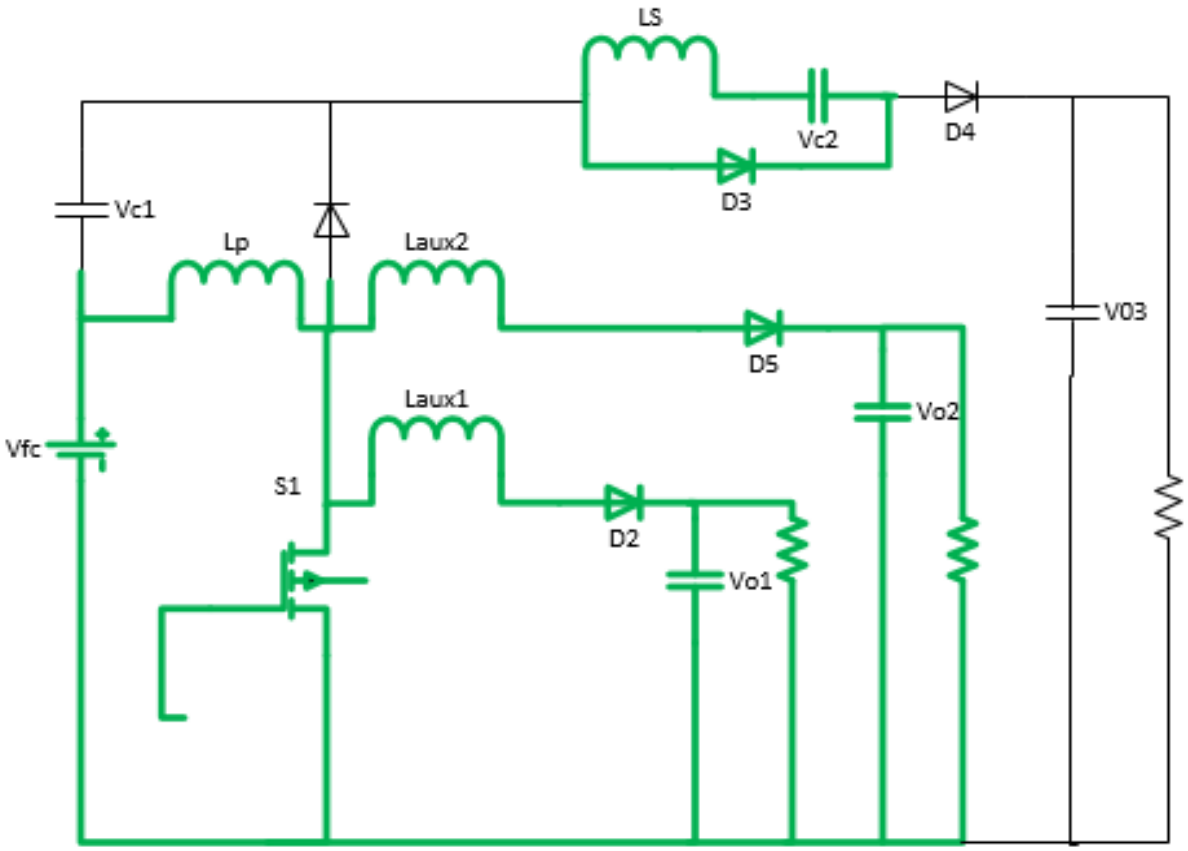

Figure 4.2: Mode 1

Mode 2:

The circuit diagram of mode 2 operation is shown in Figure 4.3. In this mode of operation the main switch $S1$ is still ON. The magnetizing current i_{lmp} increases gradually in linear way due to primary inductor charged by input power source. The middle voltage of capacitor $C2$ is also charged by secondary current i_{LS}through the diode $D3$. Both the voltages $Vlmp$ and VFC are equal in mode 1 and mode 2. The slopes of the leakage current of the coupled inductor $\frac{di_{LKP}}{dt}$ at both mode 1 and mode 2 are different due to the path of the auxiliary circuit. The auxiliary inductors release its charges completely, and at the end of mode 1 the diode $D2$ turns OFF. At the end of this mode diode $D3$ becomes reverse biased due to complete discharge of secondary side leakage current.

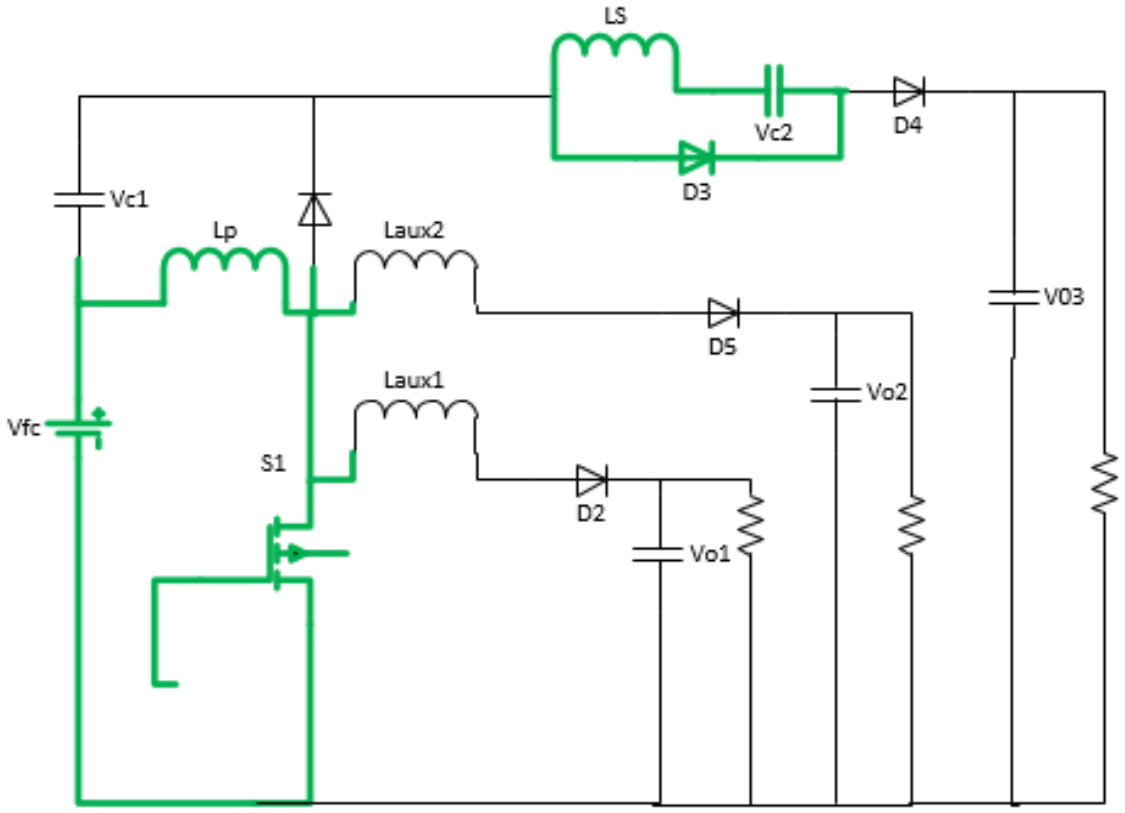

Figure 4.3: Mode 2

Mode 3:

The circuit diagram of mode 3 operation is shown in Figure 4.4. In this mode the main switch $S1$ is turned off. The coupled inductor secondary side leakage current charges capacitor C_2 through diode $D3$. When the voltage across the main switch S1 is greater than the voltage across capacitor $C1$, primary side leakage current is transmitted to auxiliary inductor $Laux$ and the diode $D2$ conducts along with the diode $D1$, which transmits the energy of the primary-side leakage inductor Lkp into the clamped capacitor $C1$. Auxiliary inductor supplies the power to load through diode $D2$. At the end of this mode diode $D3$ becomes reverse biased due to complete discharge of secondary side leakage current.

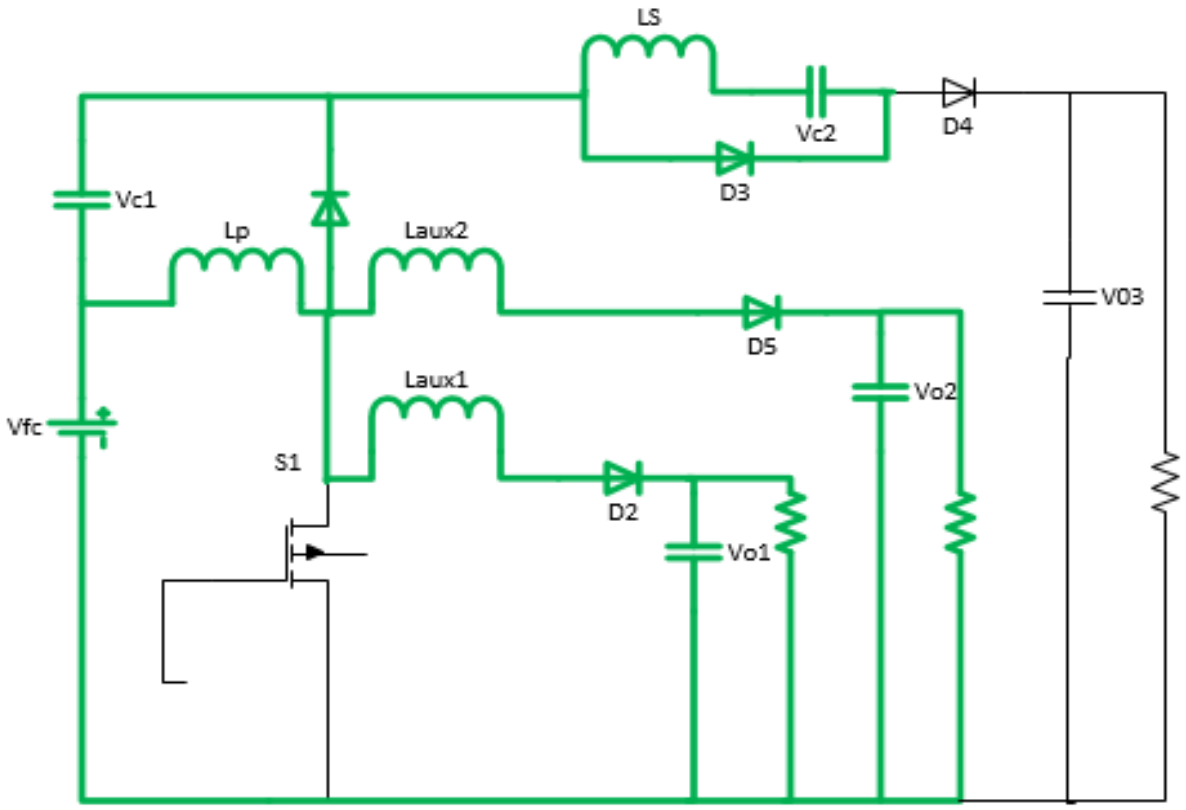

Figure 4.4: Mode 3

Mode 4:

The circuit diagram of mode 4 operation is shown in Figure 4.5. In this mode the main switch S1 is persistently turned OFF. When the coupled inductor primary side leakage energy released, the secondary current iLS of the coupled inductor is induced in reverse from the energy of the magnetizing inductor Lmp through ideal transformer, and diode D4 is conducting the energy to the high voltage side circuit. At the same time primary side leakage inductor is still releasing energy to auxiliary inductor. Hence, the diode D2 keeps conducting the auxiliary inductor current to output load at auxiliary circuit [64].

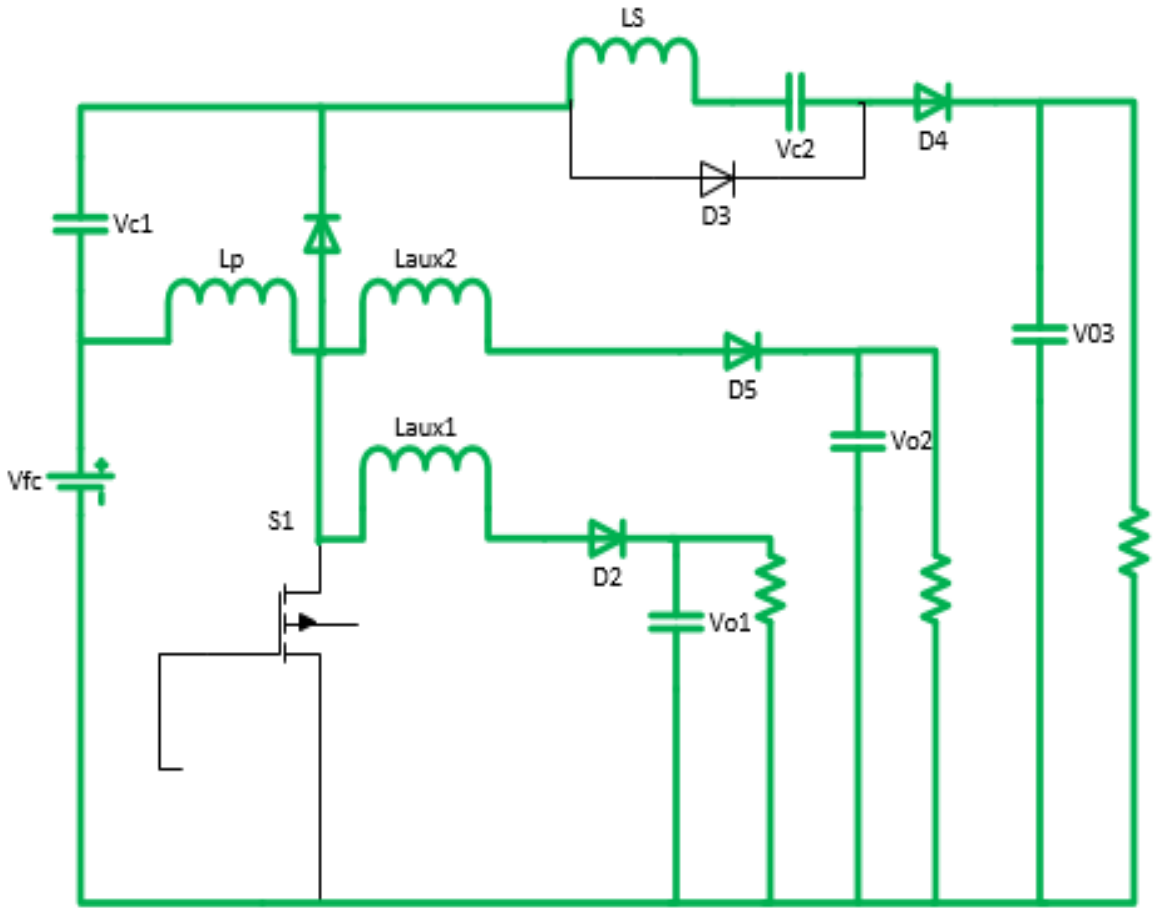

Figure 4.5: Mode 4

Mode 5:

The circuit diagram of mode 5 operation is shown in Figure 4.6. In this mode the main switch is still turn OFF. The primary leakage current is equal to the auxiliary inductor current [64] turning diode $D1$ is turns OFF. The input power source is connected in series with primary side of the coupled inductor and auxiliary inductors $Laux1$, $Laux2$, supplying power to output load through diode $D2$. At the same time, the input power source is connected in series with secondary side of the coupled inductor and middle voltage capacitor $C2$ releasing energy to high voltage side circuit through the diode $D4$.

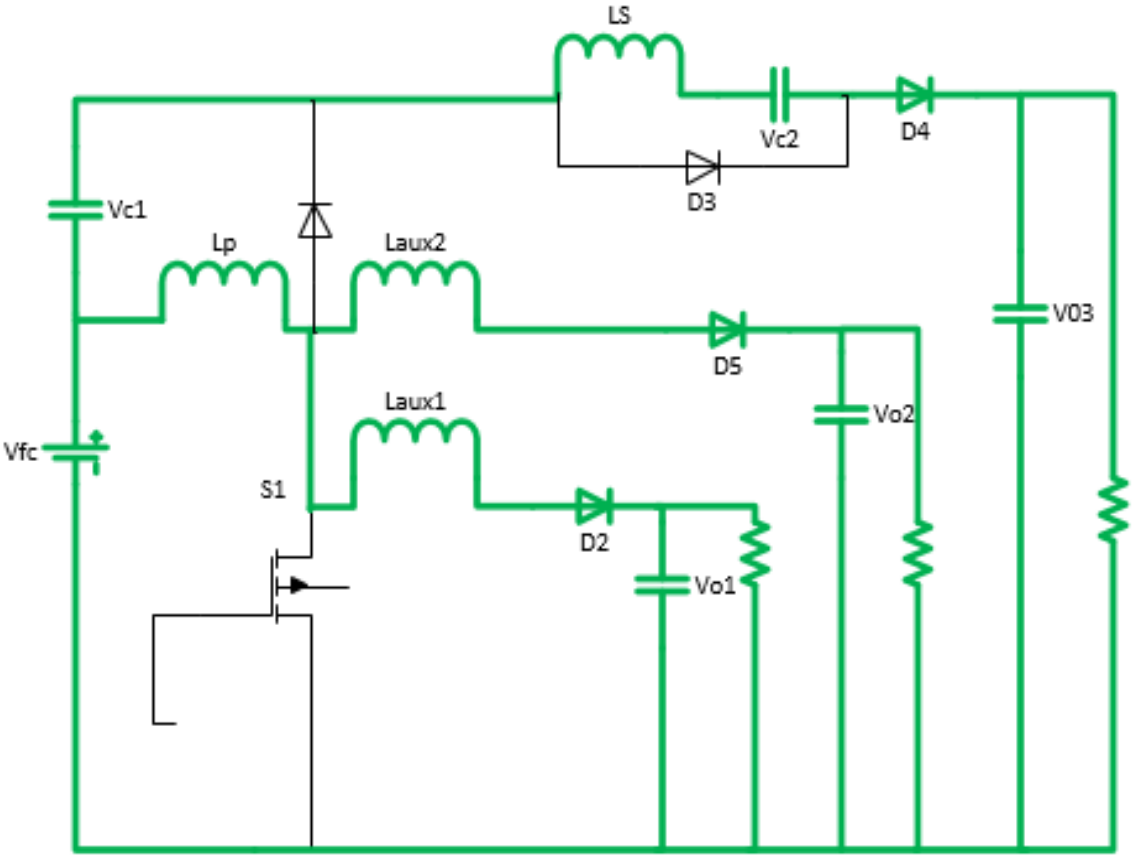

Figure 4.6: Mode 5

Mode 6:

The circuit diagram of mode 6 operation is shown in Figure 4.7. In this mode the main switch S1 is triggered. The input power source, capacitor $C1$, coupled inductor secondary side and middle voltage capacitor $C2$ are connected in series and the energy is released towards the high voltage side circuit through diode $D4$. Since diode $D1$ is a low voltage schottky diode, it will be cut off without a reverse-recovery current. Thus, the main switch is $S1$ is turned ON using ZCS condition and soft-switching which is helpful to reduce the switching loss. At the end of mode, the secondary current decays to zero. After that, next switching cycle is started and repeats the operation in the model.

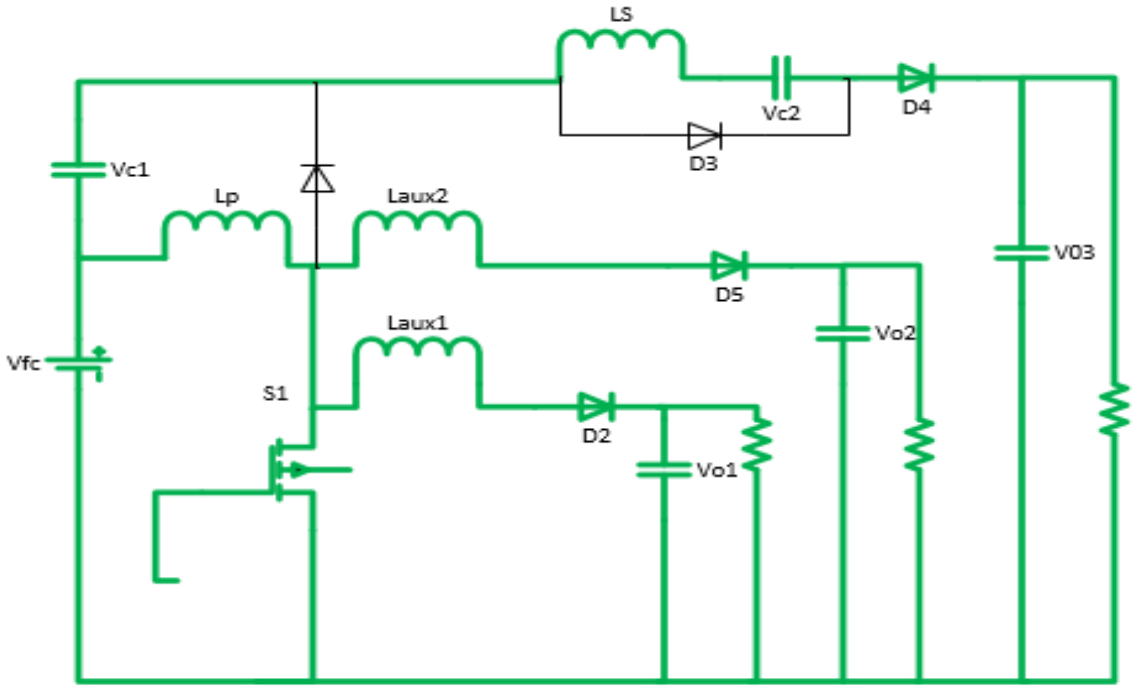

Figure 4.7: Mode 6

Figure 4.8 shows the closed loop circuit implemented using PSIM.

Detailed simulation results and sensitivity analysis for this DC-DC converter will be presented in section 6.2.

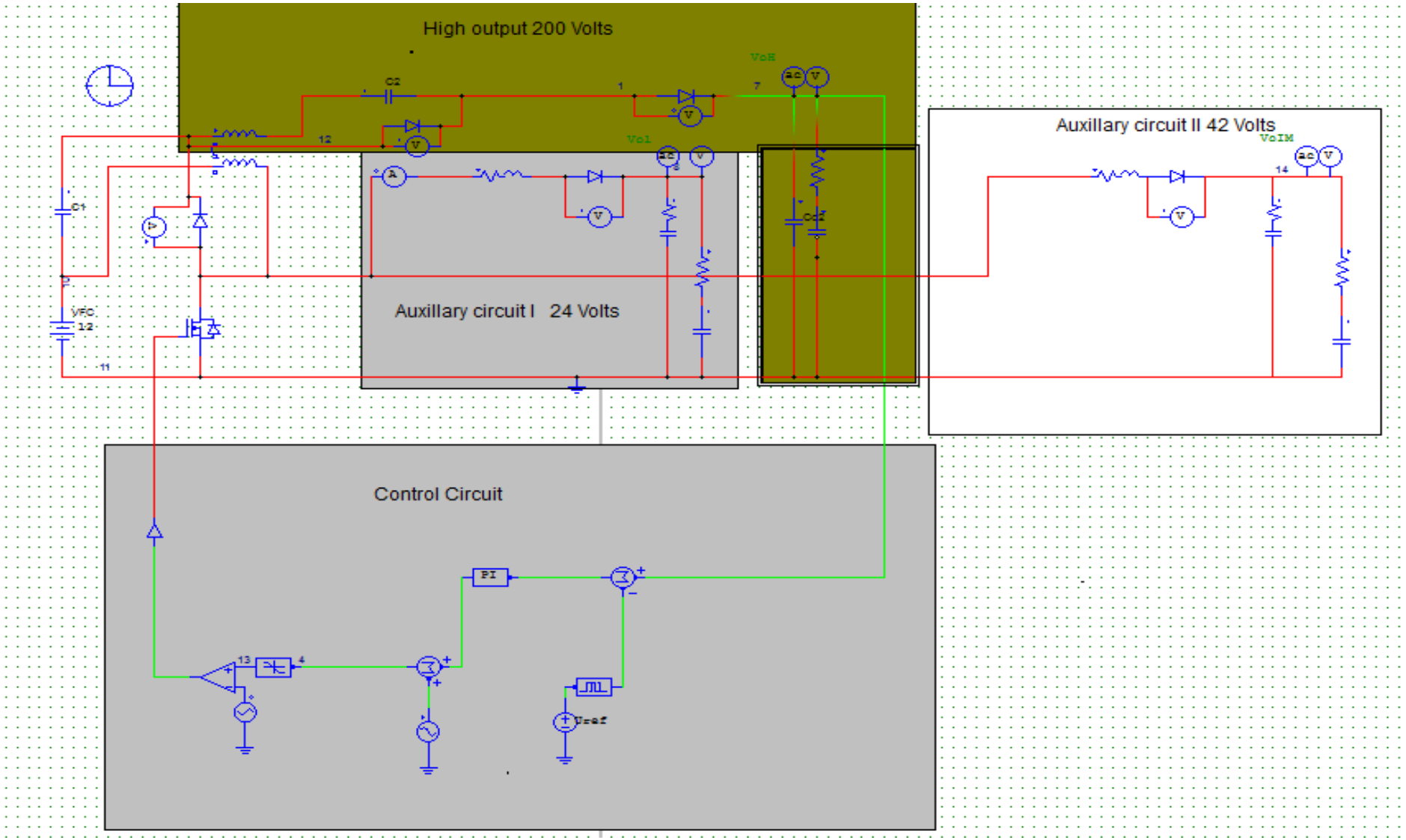

Figure 4.8: DC-DC closed loop circuit diagram

Chapter 5: Proposed Application Solar Based Water Pump

Water pumping is an important application, as we need water is all aspects of our lives. Comparing to electric or motor generator water pumping, solar powered DC water pumps offer many advantages, such as being low cost, environmentally friendly, easy to install, fully automatic and reliable.

5.1 System Block Diagram

A typical solar powered DC water pumping system consists of solar PV panels, solar DC controller, and DC water pump. A block diagram defining the complete system is shown in Figure 5.1.

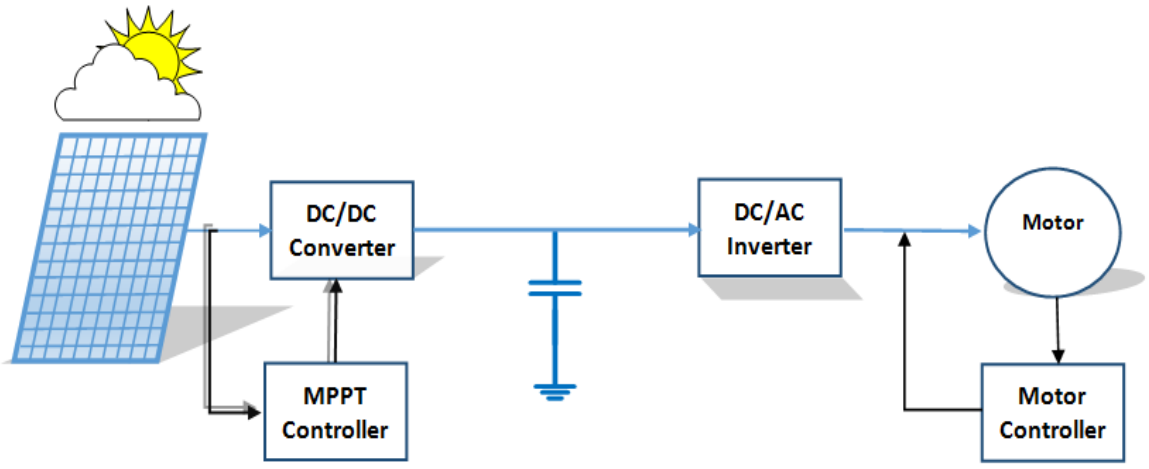

Figure 5.1: Block diagram for the complete system

Figure 5.2 shows the circuit diagram for the complete system including the solar panel with the proposed MPPT implemented, and the proposed DC-DC converter. The simulation results for this system is presented in section 6.3.

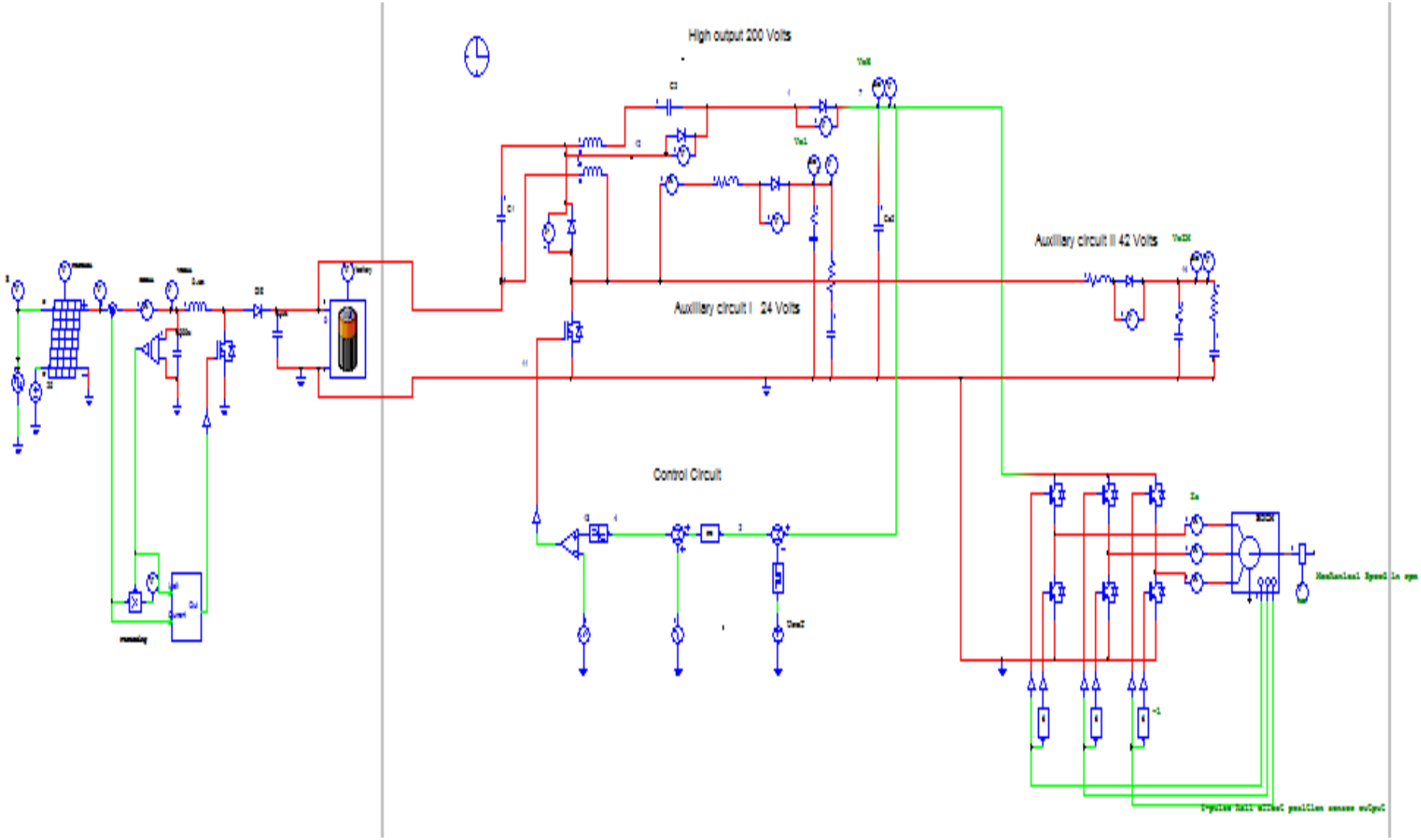

Figure 5.2: Complete system circuit diagram

Chapter 6: Results and Discussion

In this chapter, simulation results, with detailed sensitivity analysis, and experimental results are presented.

6.1 Proposed Algorithm Simulation Results

An implementation for the algorithm was done using PSIM software and the results are shown below. The circuit used in implementing the algorithm is shown in Figure 6.1.

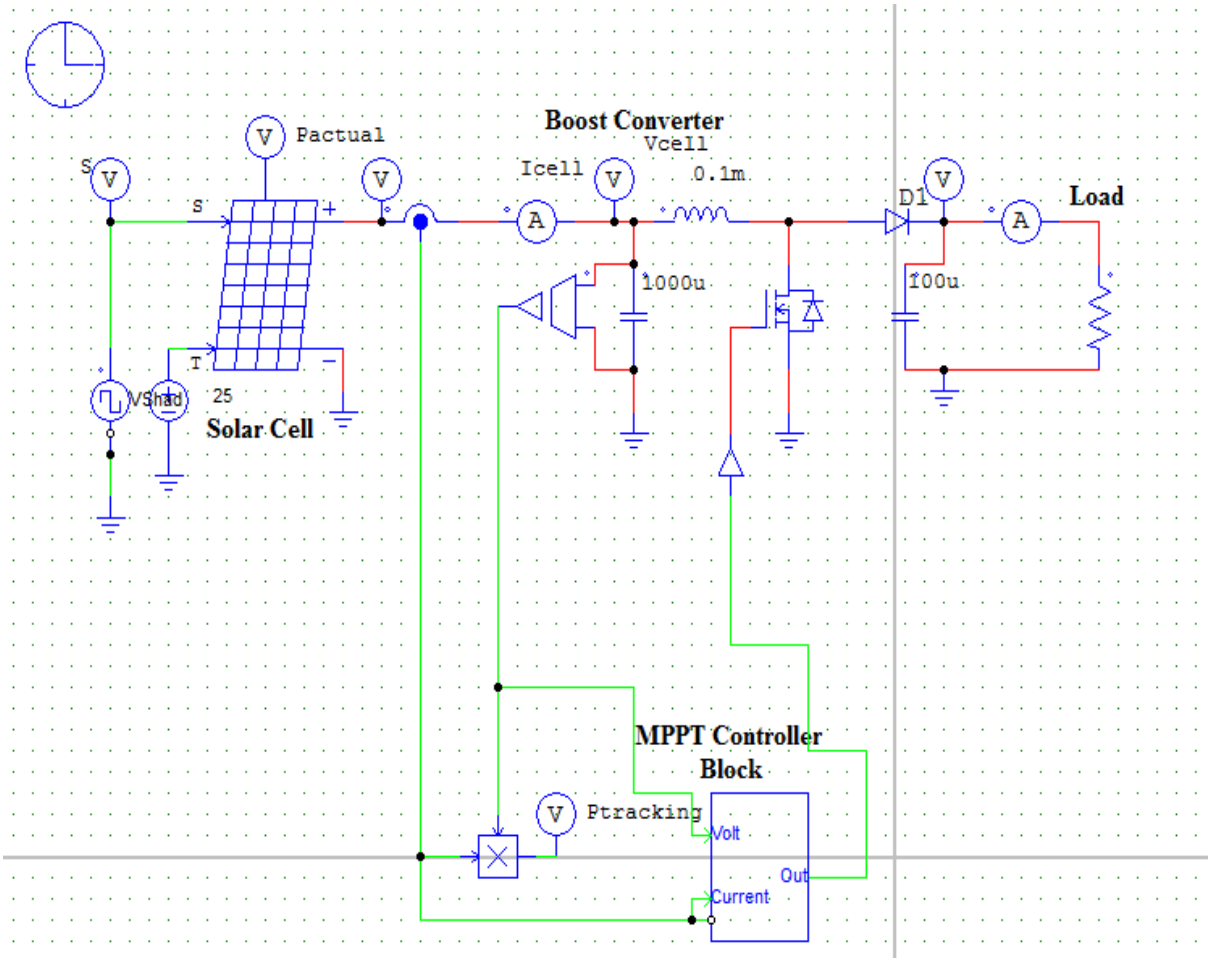

Figure 6.1: Boost converter circuit with the MPPT controller block

A more detailed schematic showing the complete circuit design including the C Block on which the codes implementing the proposed MPPT algorithm are implemented, and the gating circuit responsible for controlling the DC-DC converter is shown in Figure 6.2.

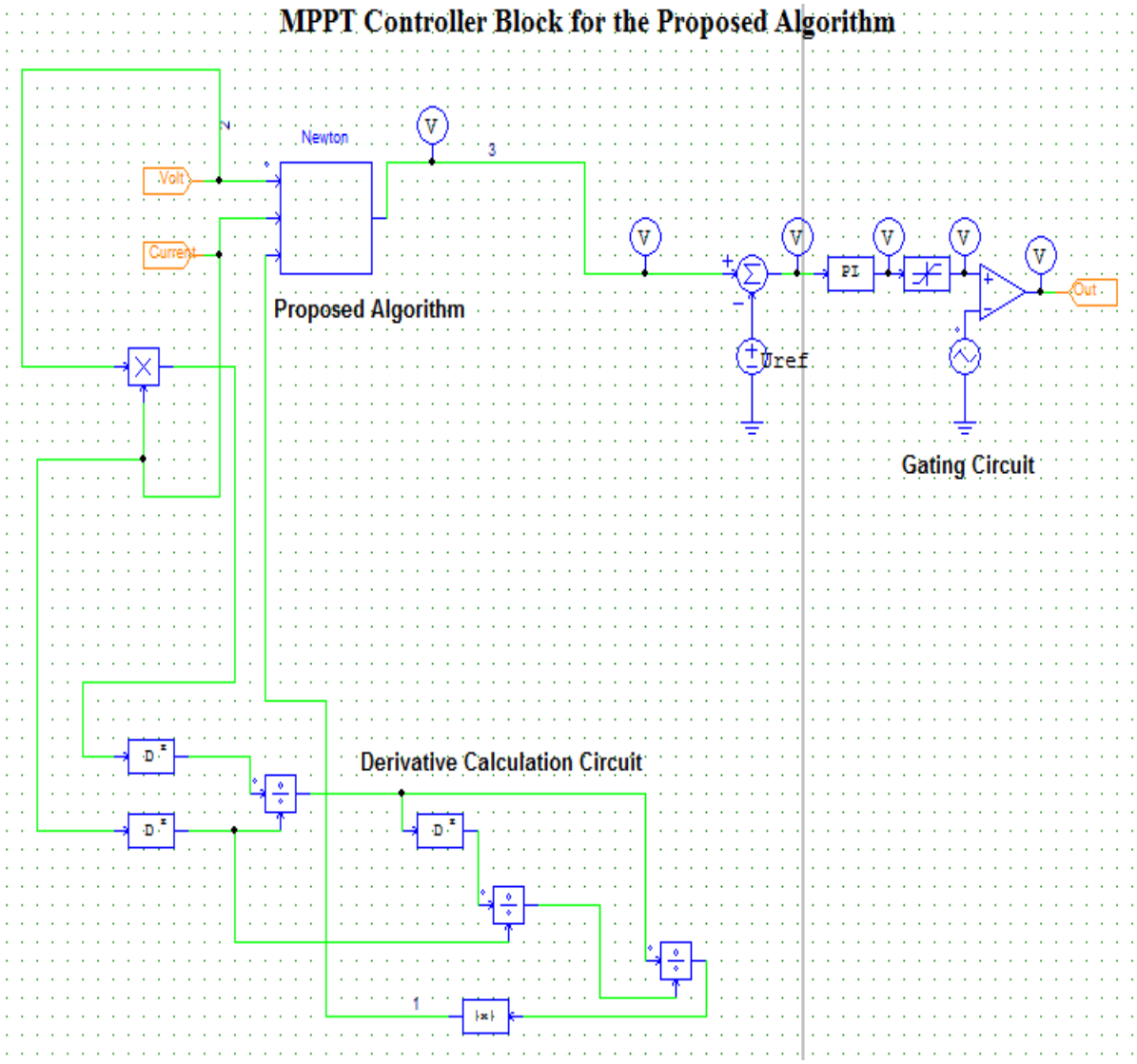

Figure 6.2: MPPT block diagram design circuit

Figure 6.3 shows the optimum power or the actual maximum power output of the solar cell versus the power output obtained by the tracking algorithm. As can be seen, the system accurately tracks the maximum power with a very small error of 0.063%, which is much better than all discussed MPPT algorithms.

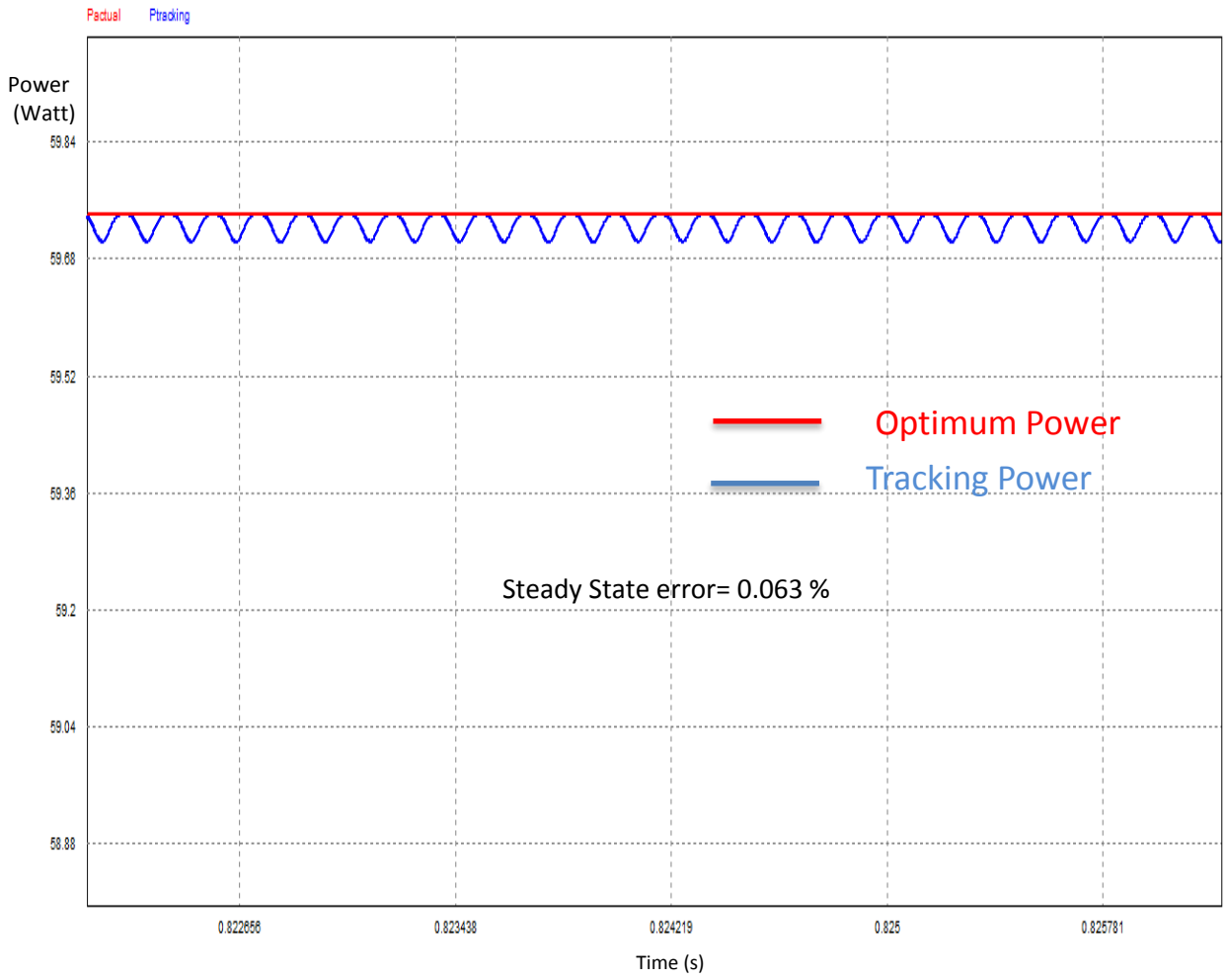

Figure 6.3: The optimum power versus power output using the proposed MPPT.

Figure 6.4 shows the delay between the tracking signal and the actual power if any shading or any changes in the power occurs. The time taken for the tracking is 1µs, which is very efficient and much better than the tracking time achieved by the incremental conductance algorithm.

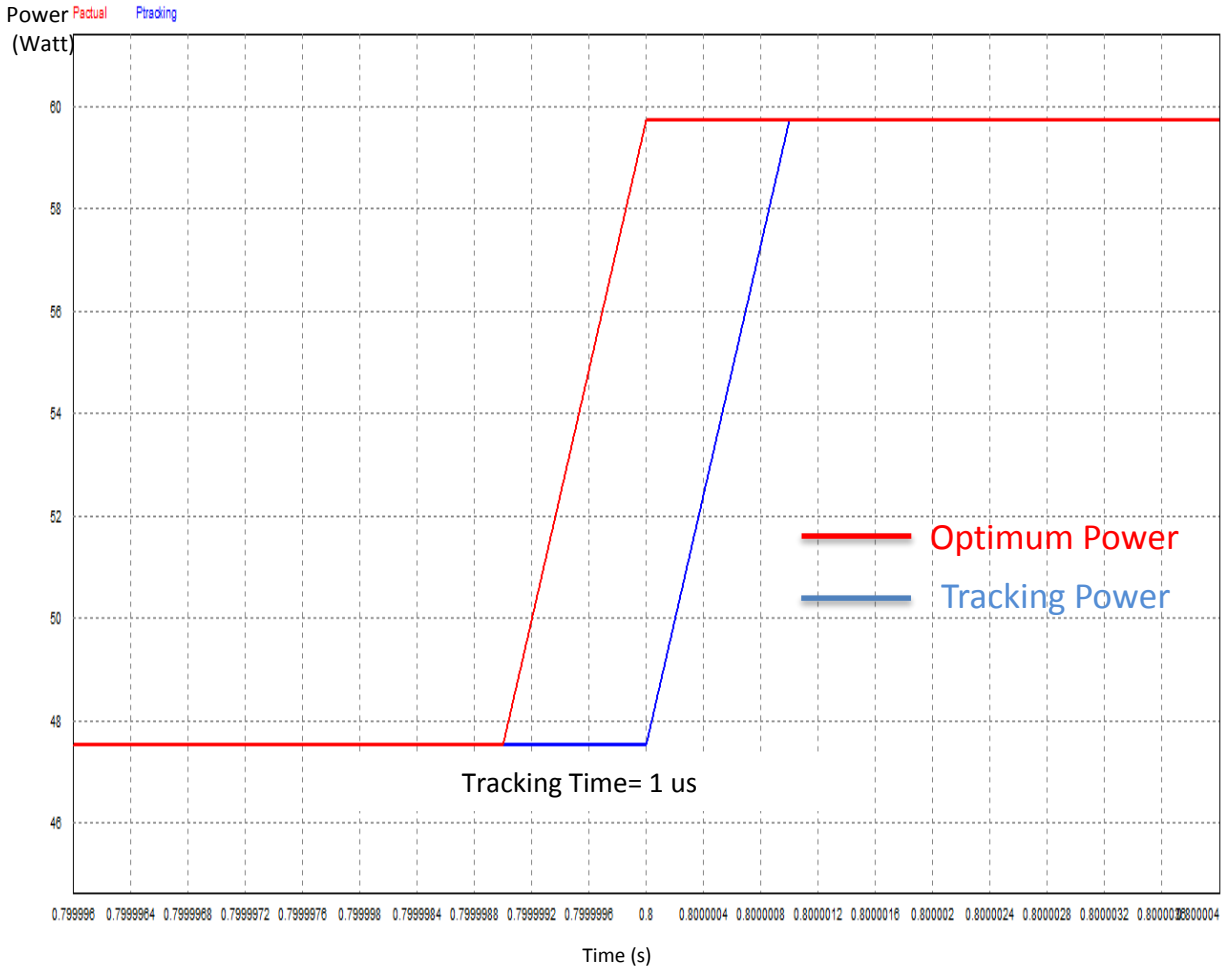

Figure 6.4: The MPPT tracking time for the proposed algorithm

In order to demonstrate the efficiency of this algorithm, we compare our results with those obtained using incremental conductance algorithm. Figure 6.5 shows a comparison between the proposed algorithm and the incremental conductance in tracking the maximum power point. It can be seen that the proposed algorithm gives very good results with very small error.

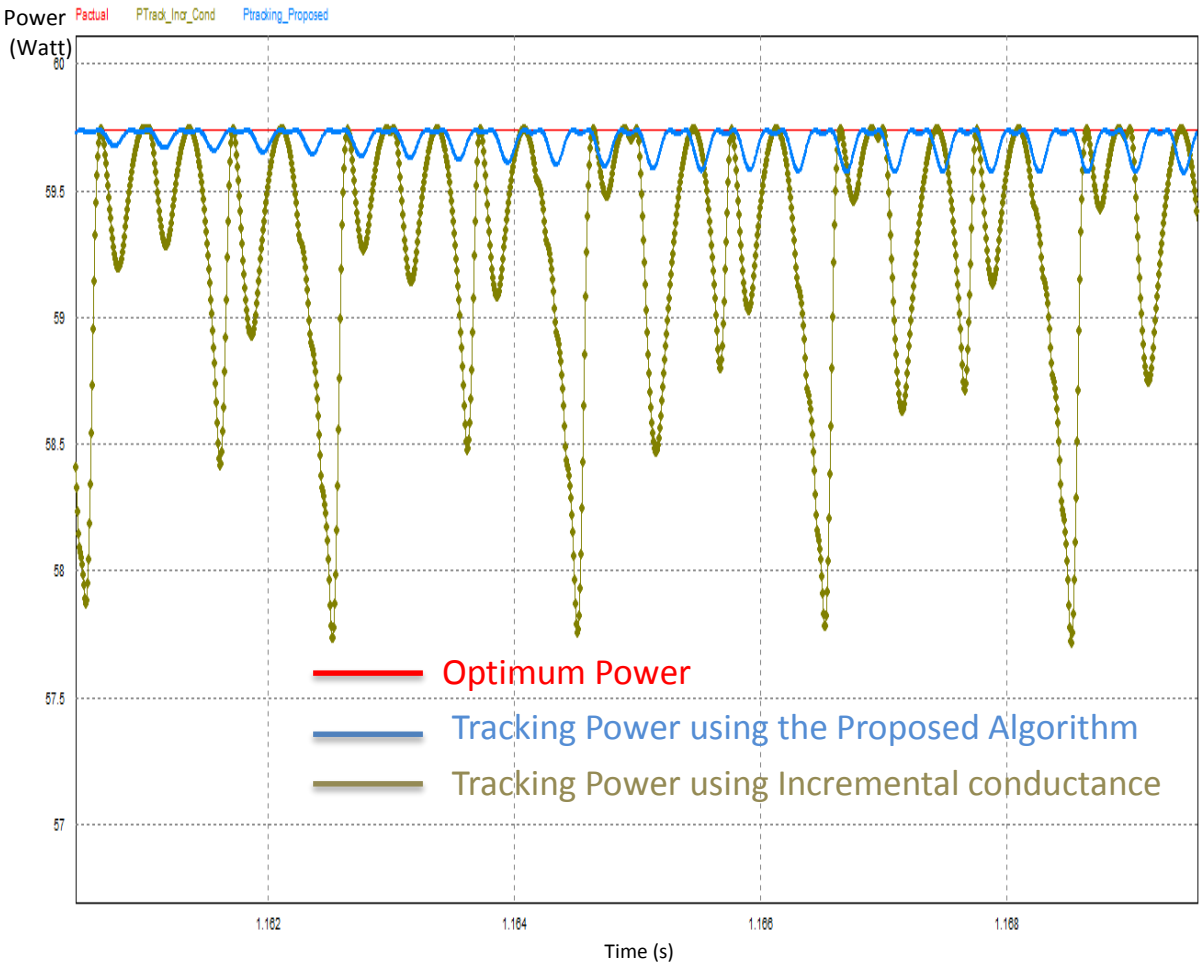

Figure 6.5: The optimum power versus power output using the proposed MPPT and incremental conductance algorithm

Sensitivity analysis

In order to check the stability of the system, we need to check the effect of the circuit components on the operation of tracking the maximum power. In the following section sensitivity analysis is carried out to show the stability of the algorithm under different effects, such as temperature, shading, and different DC-DC converter component values, such as boost converter inductor and capacitor, and also the effect of changing the load on tracking the maximum power.

Figure 6.6 shows the optimum power versus the output tracking power at resistive load and varying light intensity from 800 watt/m^2 and temperature =25 °C. The algorithm is able to track the maximum power point under these conditions for resistive load such as home lamps.

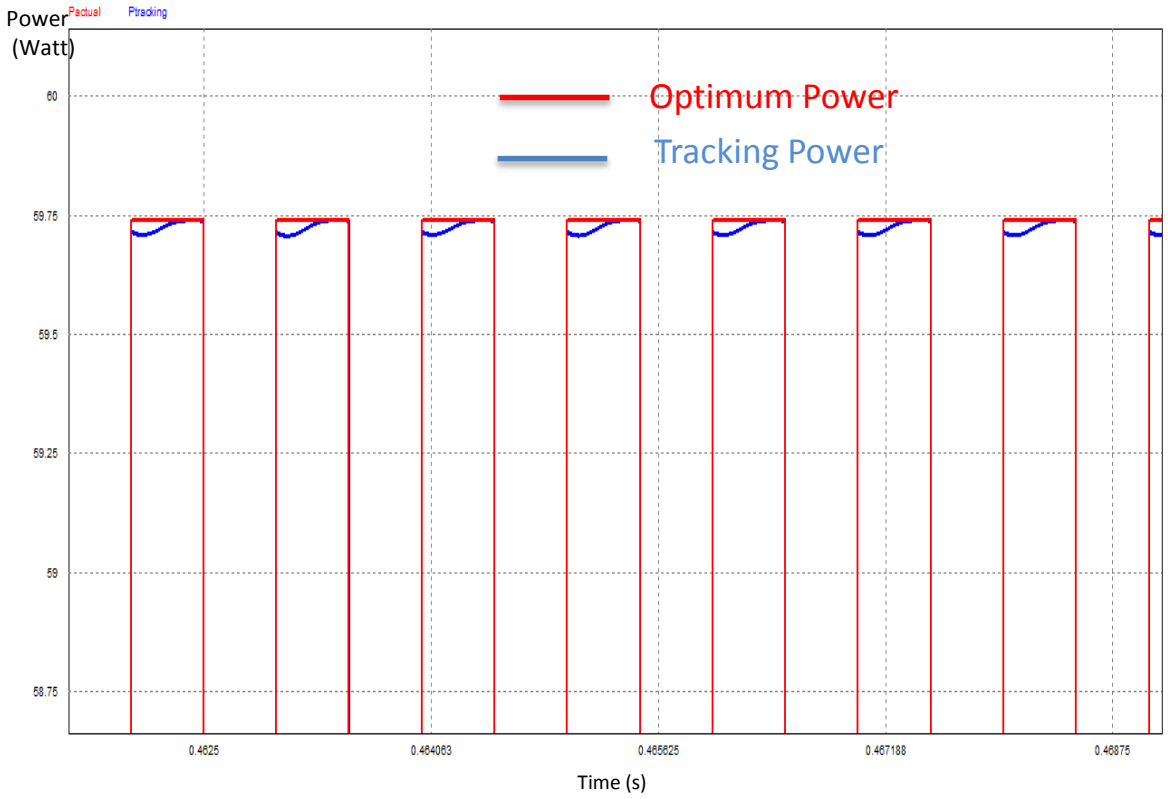

Figure 6.6: The optimum power versus the output tracking power at resistive load and varying light intensity from 800 watt/m^2 and temperature =25 °C

Figure 6.7 shows the optimum power versus the output tracking power at resistive load and light intensity =1000 watt/m^2 and varying temperature from 20 °C to 30 °C. We are using a 10 °C temperature range to check the system response on rapid changes in the temperature. And similarly if the system is able to track the changes within that range it will be also able to track the maximum power under different ranges of temperature. We found that the results are satisfactory under varying temperature.

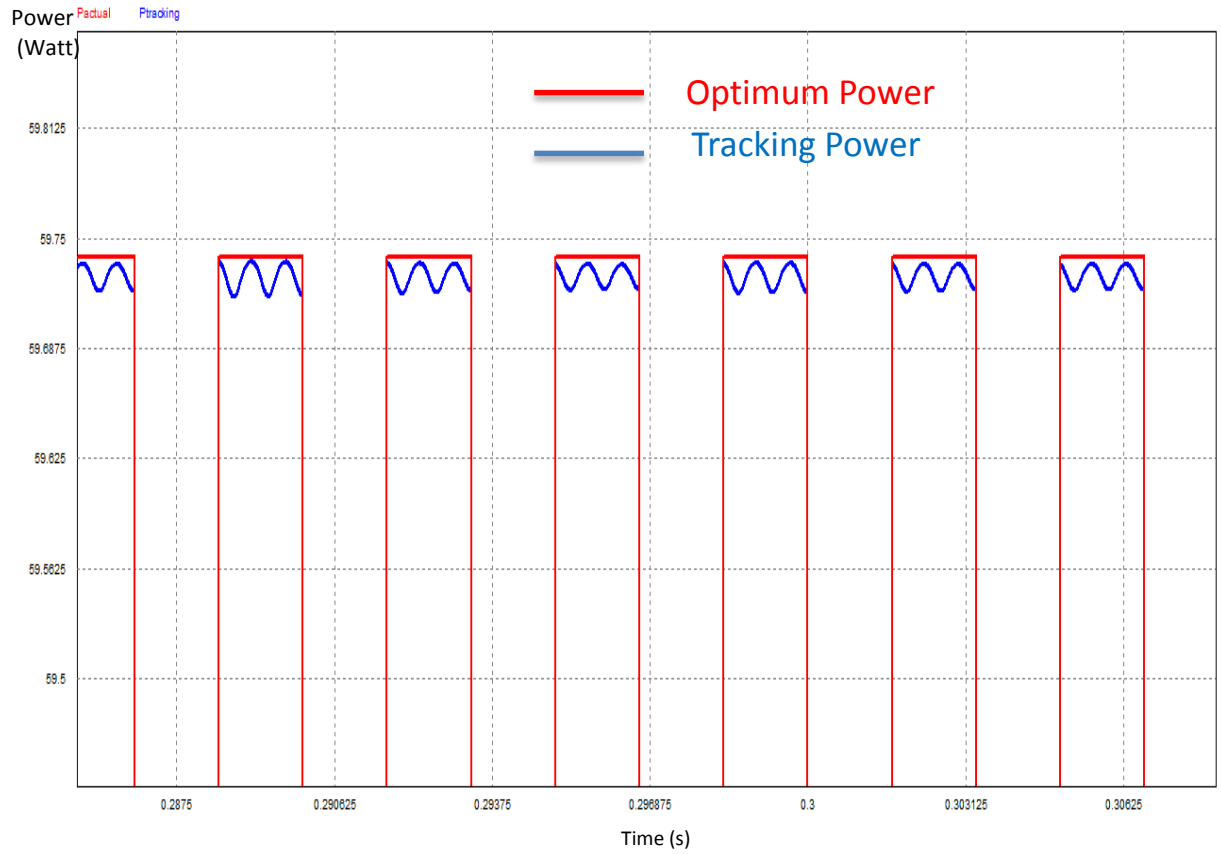

Figure 6.7: The optimum power versus the output tracking power at intensity =1000 watt/m^2 and varying temperature from 20 °C to 30 °C.

Figure 6.8 shows the optimum power versus the output tracking power at resistive inductive load such as a motor, and light intensity =1000 watt/m^2 and varying temperature from 20 °C to 30 °C. The system is giving good tracking with small errors.

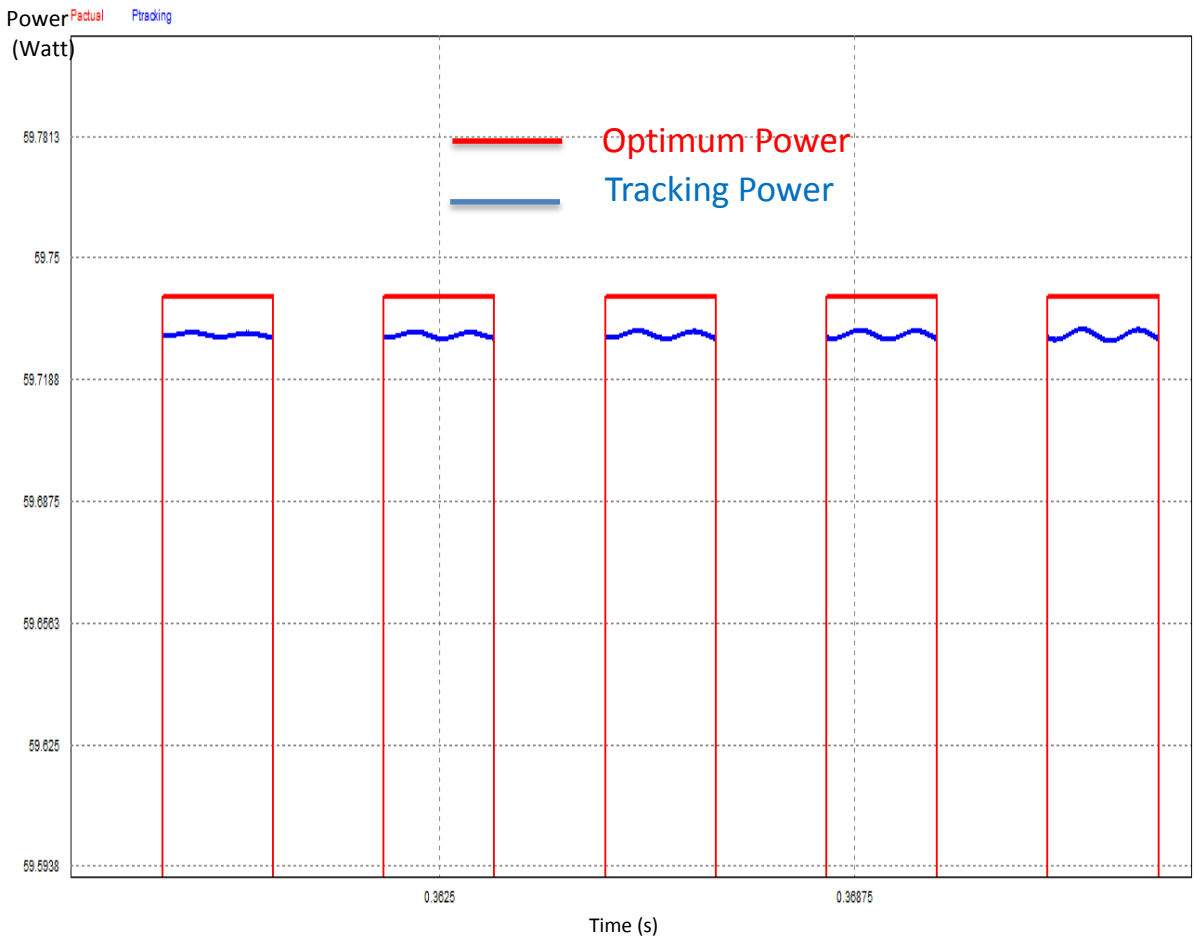

Figure 6.8: The optimum power versus the output tracking power at resistive inductive load and light intensity =1000 watt/m^2 and varying temperature from 20 °C to 30 °C

Figure 6.9 shows the optimum power versus the output tracking power at resistive capacitive load, which is equivalent to any electronic circuit such as telecommunication devices, and light intensity =1000 watt/m^2 and varying temperature from 20 °C to 30 °C, with good results.

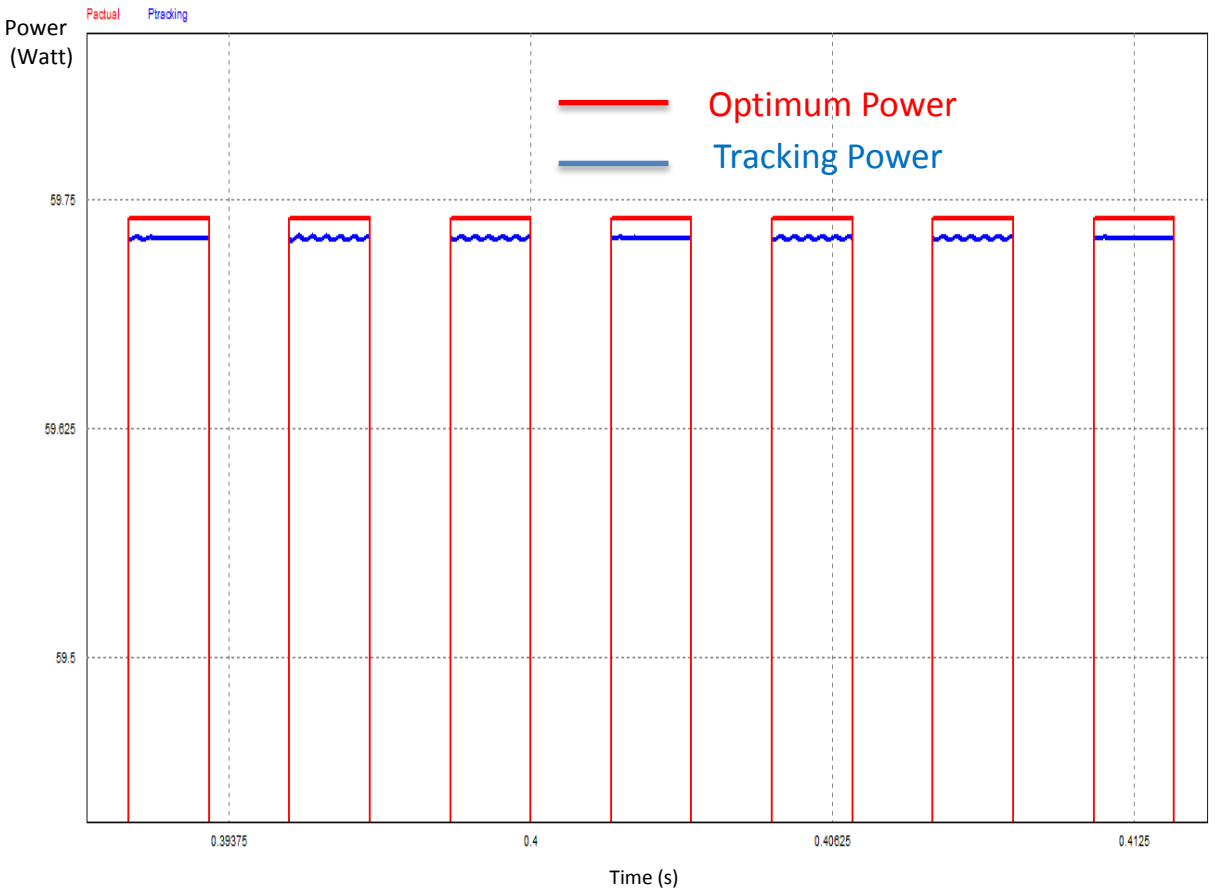

Figure 6.9: The optimum power versus the output tracking power at resistive capacitive load and light intensity =1000 watt/m^2 and varying temperature from 20 °C to 30 °C

Figure 6.10 shows the optimum power versus the output tracking power at resistive capacitive load and varying light intensity from 800 watt/m^2 to 1000 watt/m^2 and temperature 25 °C.

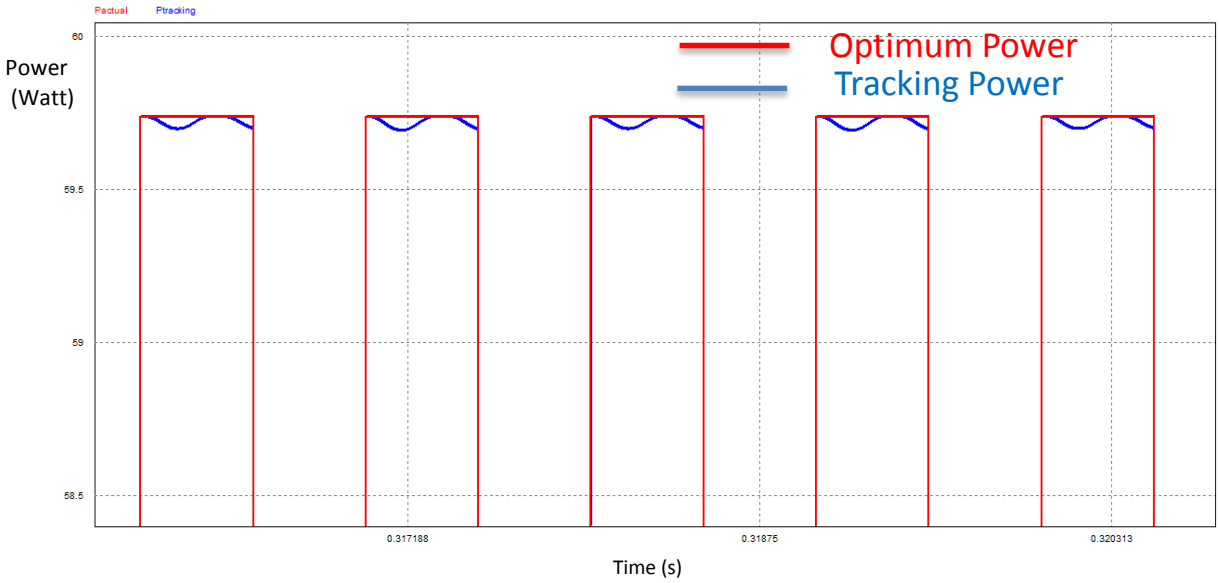

Figure 6.10: The optimum power versus the output tracking power at resistive capacitive load and varying light intensity from 800 watt/m^2 to 1000 watt/m^2 and temperature 25 °C

Figure 6.11 shows the optimum power versus the output tracking power at resistive inductive load and varying light intensity from 800 watt/m^2 to 1000 watt/m^2 and temperature 25 °C.

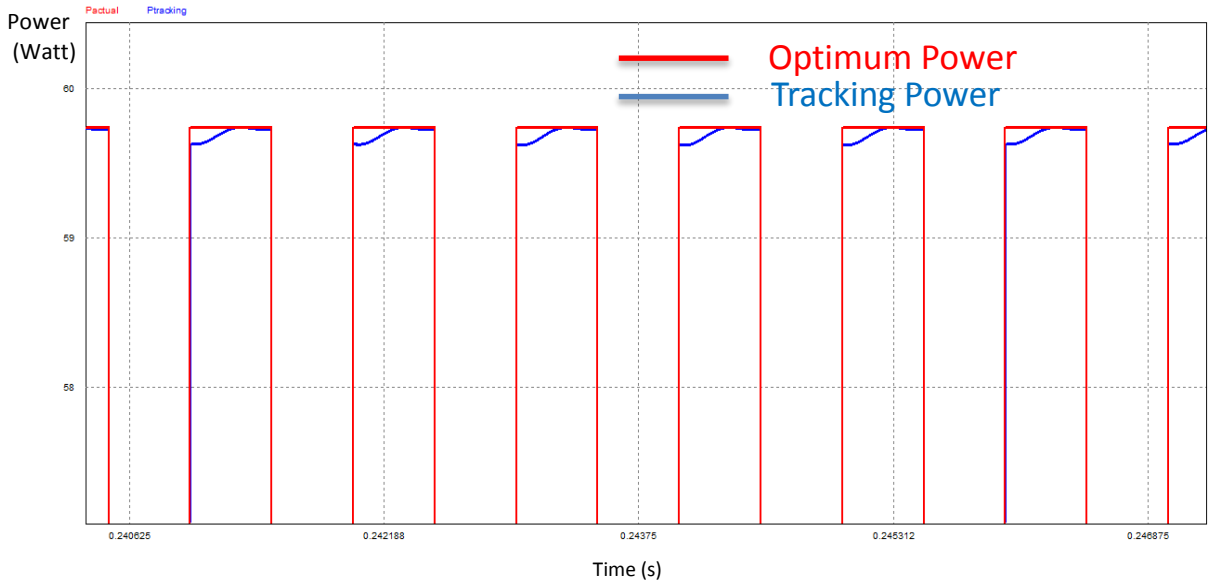

Figure 6.11: The optimum power versus the output tracking power at resistive inductive load and varying light intensity from 800 watt/m^2 to 1000 watt/m^2 and temperature 25 °C

Figure 6.12 shows the boost converter inductor current with light intensity =1000 watt/m^2 and temperature =25 °C.

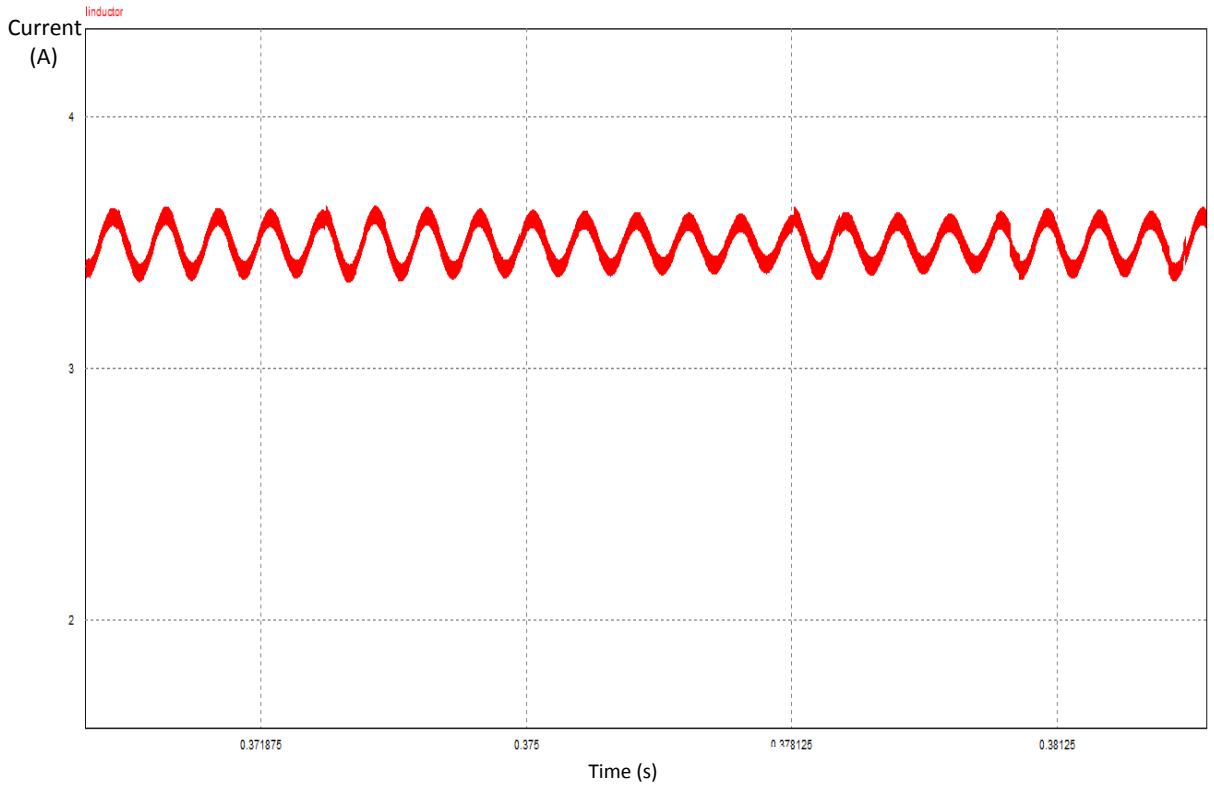

Figure 6.12: Boost converter inductor current with light intensity =1000 watt/m^2 and temperature =25 °C

Figure 6.13 shows the optimum power versus the output power parametric analysis on the boost converter inductor with light intensity=1000 watt/m^2 and temperature =25 °C.

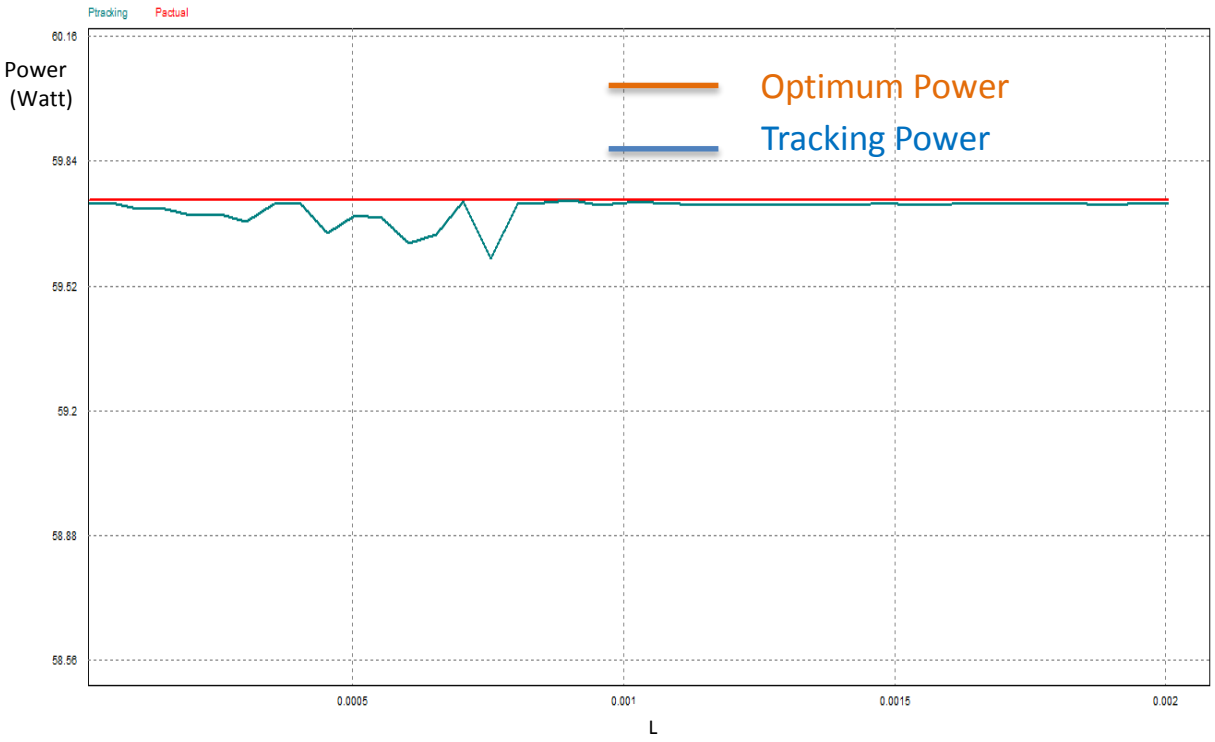

Figure 6.13: Optimum power versus the output power parametric analysis on the Boost converter inductor with light intensity=1000 watt/m^2 and temperature =25 °C

From the previous inductor parametric analysis we can see that inductor value affects the tracking error. Figure 6.14 shows the optimum power versus the output power parametric analysis on the boost converter capacitor with light intensity=1000 watt/m^2 and temperature =25 °C.

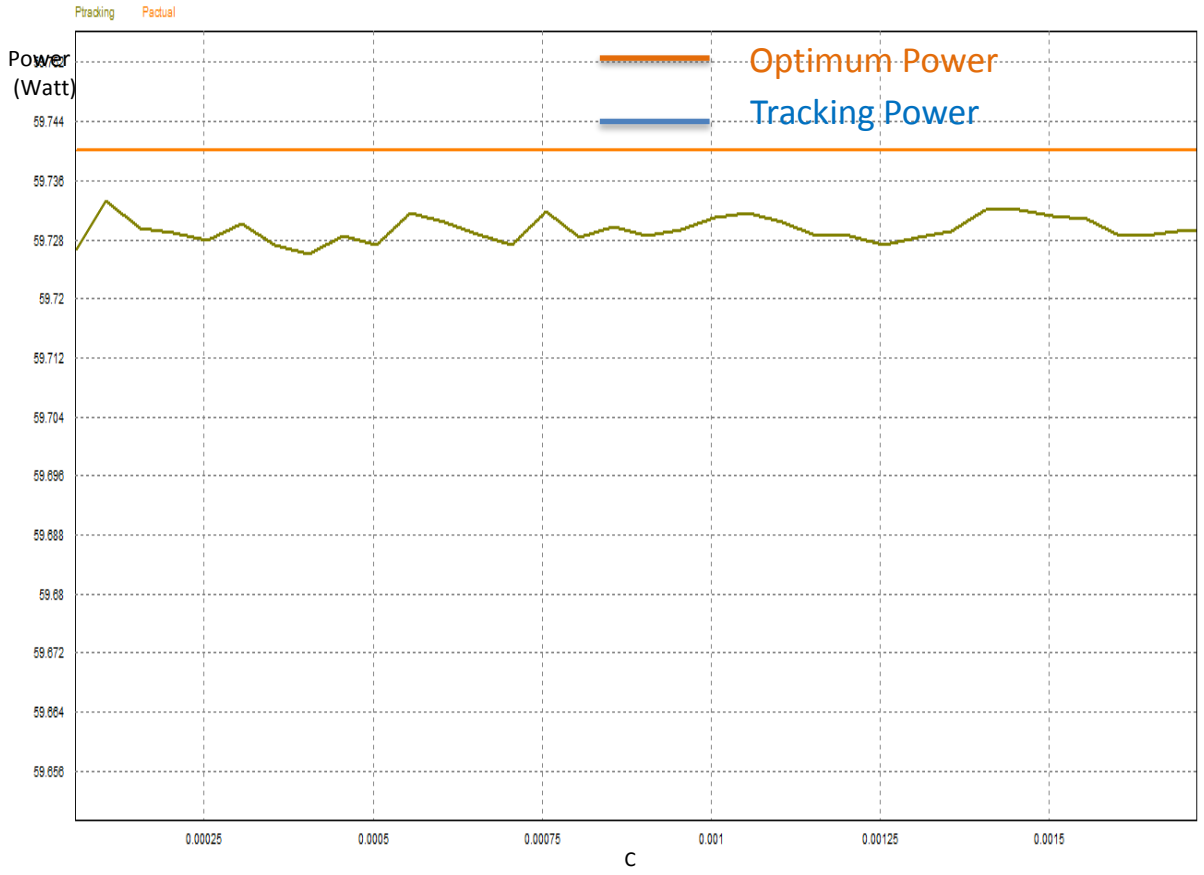

Figure 6.14: Optimum power versus the output power parametric analysis on the boost converter capacitor with light intensity=1000 watt/m^2 and temperature =25 °C

We can see from the capacitor parametric analysis that the capacitor value also affects the tracking error.

From the previous simulations we can conclude that the proposed system work efficiently under different environmental conditions and different loads.

6.2 Proposed DC-DC Converter Simulation Results

An implementation for the circuit has been done using PSIM software and the results are shown below. Figure 6.15 shows the waveform for different outputs, namely 42 volts, 24 volts and 200 volts. These outputs are typical values that are commonly used in important applications such as telecommunications and automotive applications.

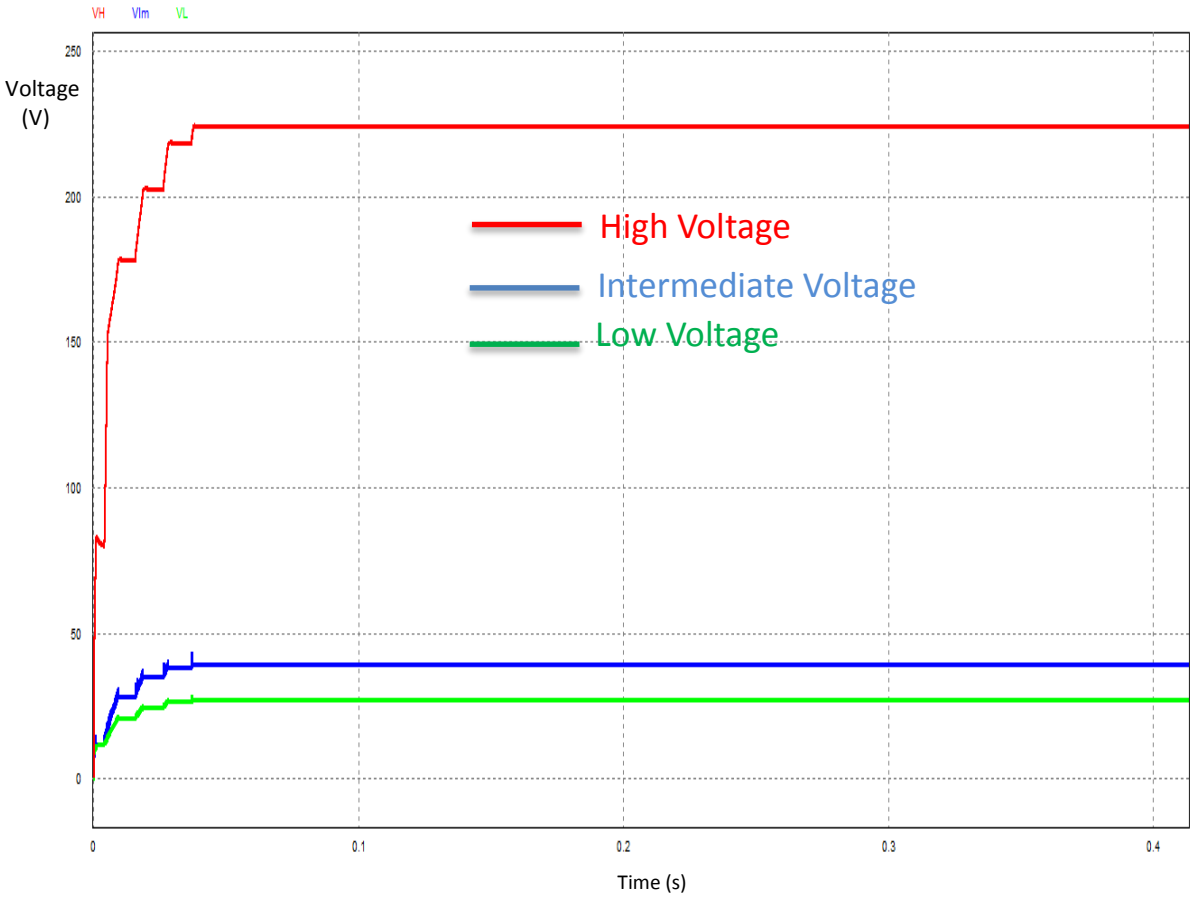

Figure 6.15: Output waveforms

Figure 6.16 shows some important characteristic waveforms for voltages and currents in the circuit, showing the stresses across some important components in the circuit.

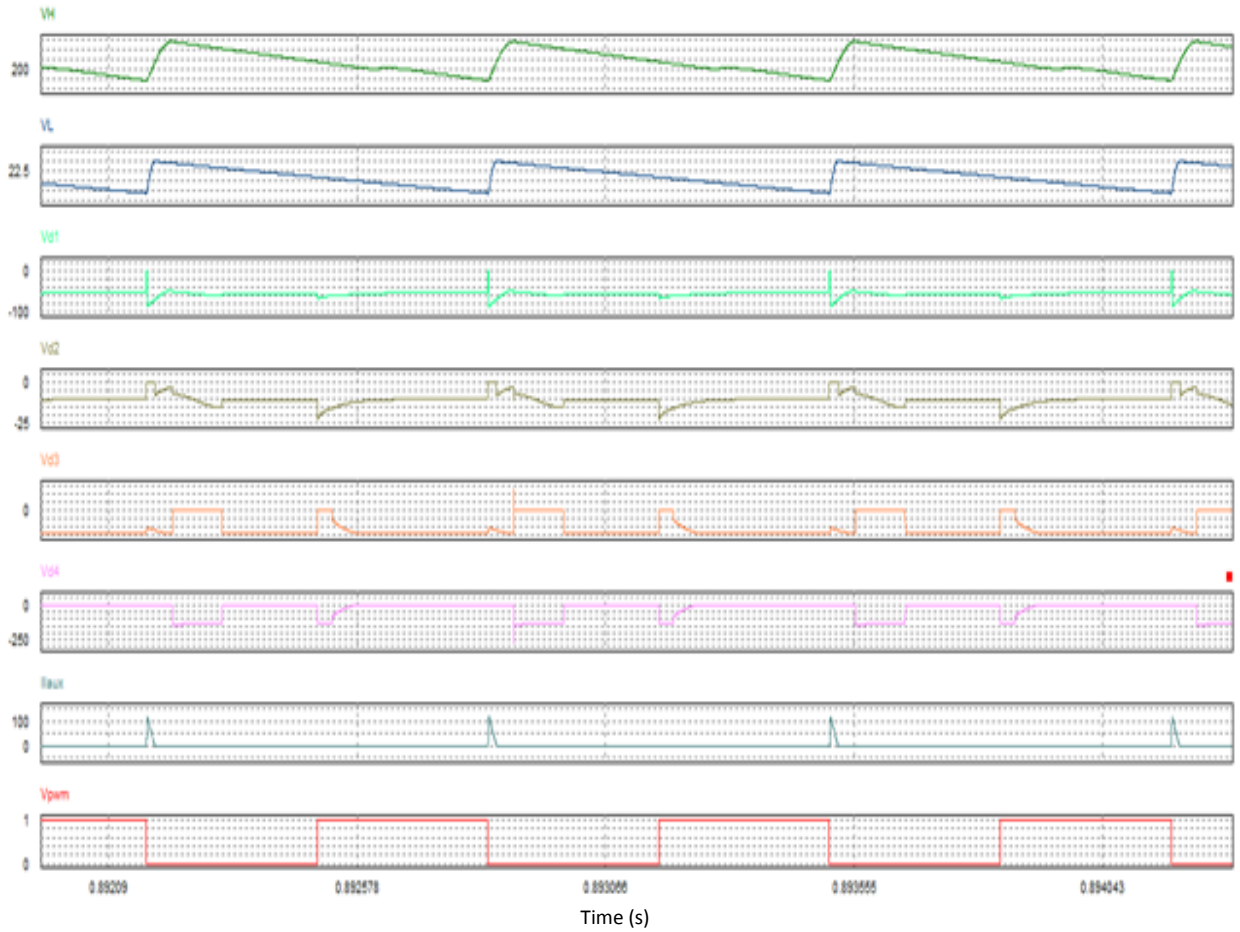

Figure 6.16: Characteristic waveforms.

Output waveforms for different loads

A closed loop circuit is implemented using PI controller and in the following section simulations using different loads are presented to show the system stability.

Resistive Loads

Figures 6.17 shows the output waveforms for a pure resistive connected load such as lamps showing a stable output voltage levels.

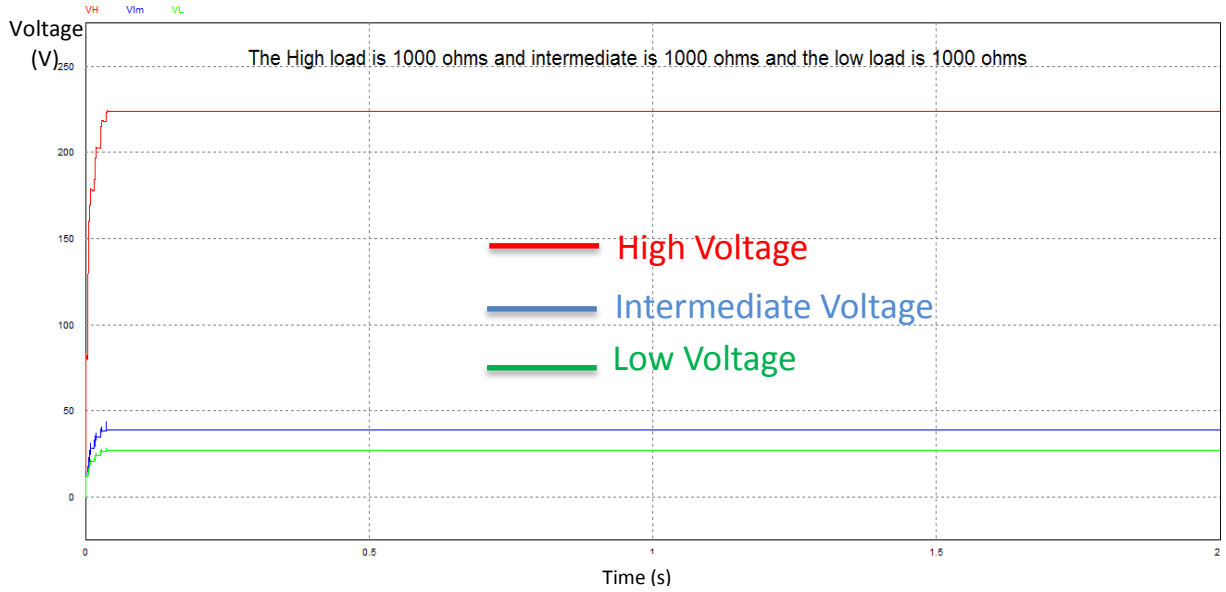

Figure 6.17: Output waveforms with resistive loads

Figures 6.18 shows the output waveforms for a different pure resistive connected load showing that the output is stable, verifying that control circuit is working well.

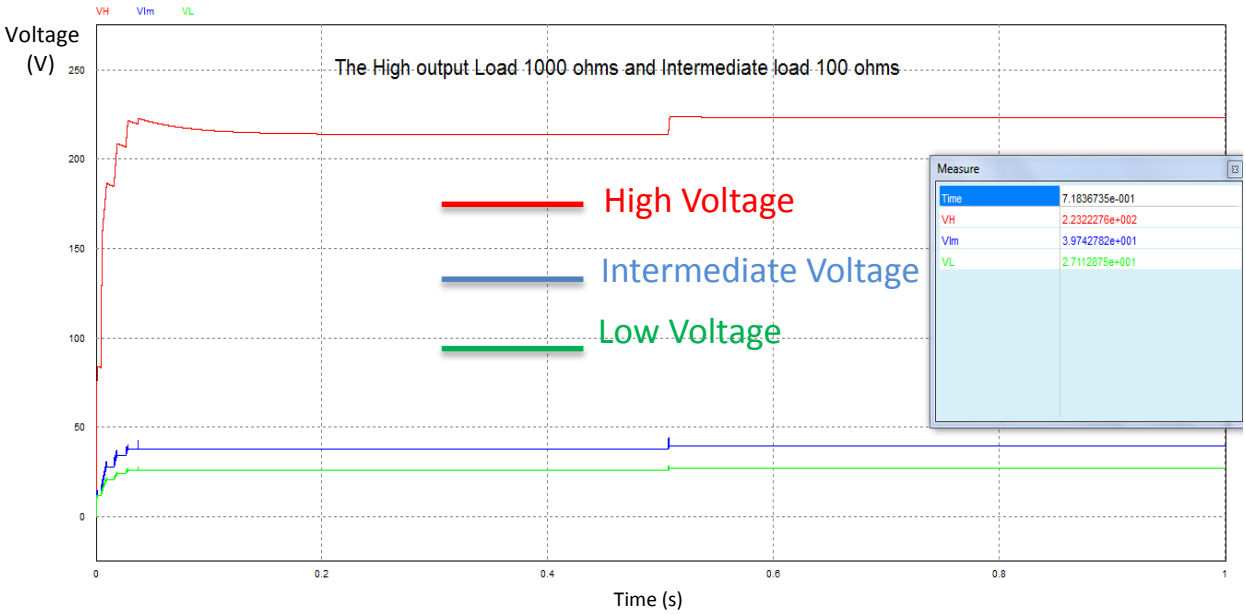

Figure 6.18: Output waveforms for different resistive loads

Resistive Capacitive Load

Figure 6.19 shows output waveforms for resistive capacitive such as electronic circuits used in telecommunication applications. It can be seen that we are getting a stable output voltages with a totally different load.

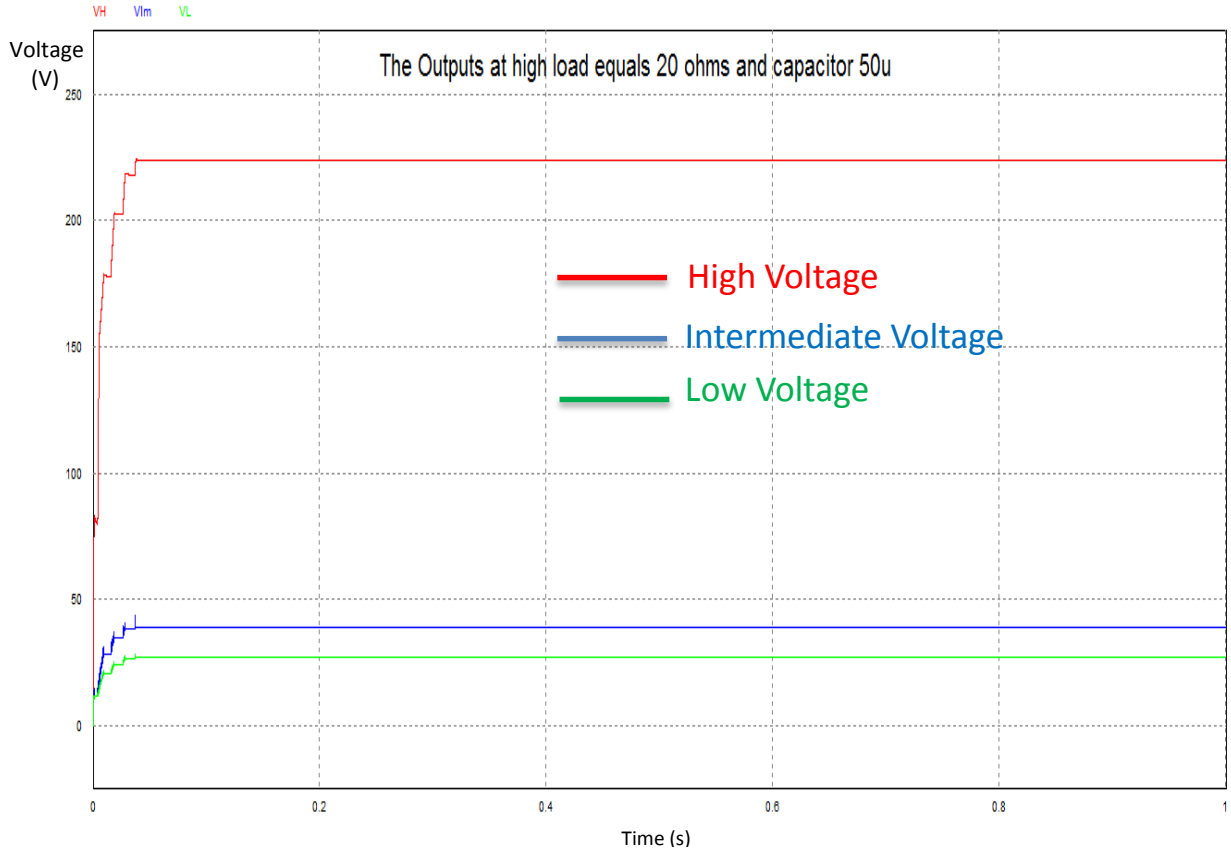

Figure 6.19: Output waveforms for a resistive capacitive Load

The previous simulations shows that the system is stable under different loads

Sensitivity Analysis

Some important sensitivity analysis, such as parametric analysis, has been done to see its effect on the circuit main output and the auxiliary output. As can be seen in Figure 6.20, the auxiliary inductor has a large effect on the auxiliary output.

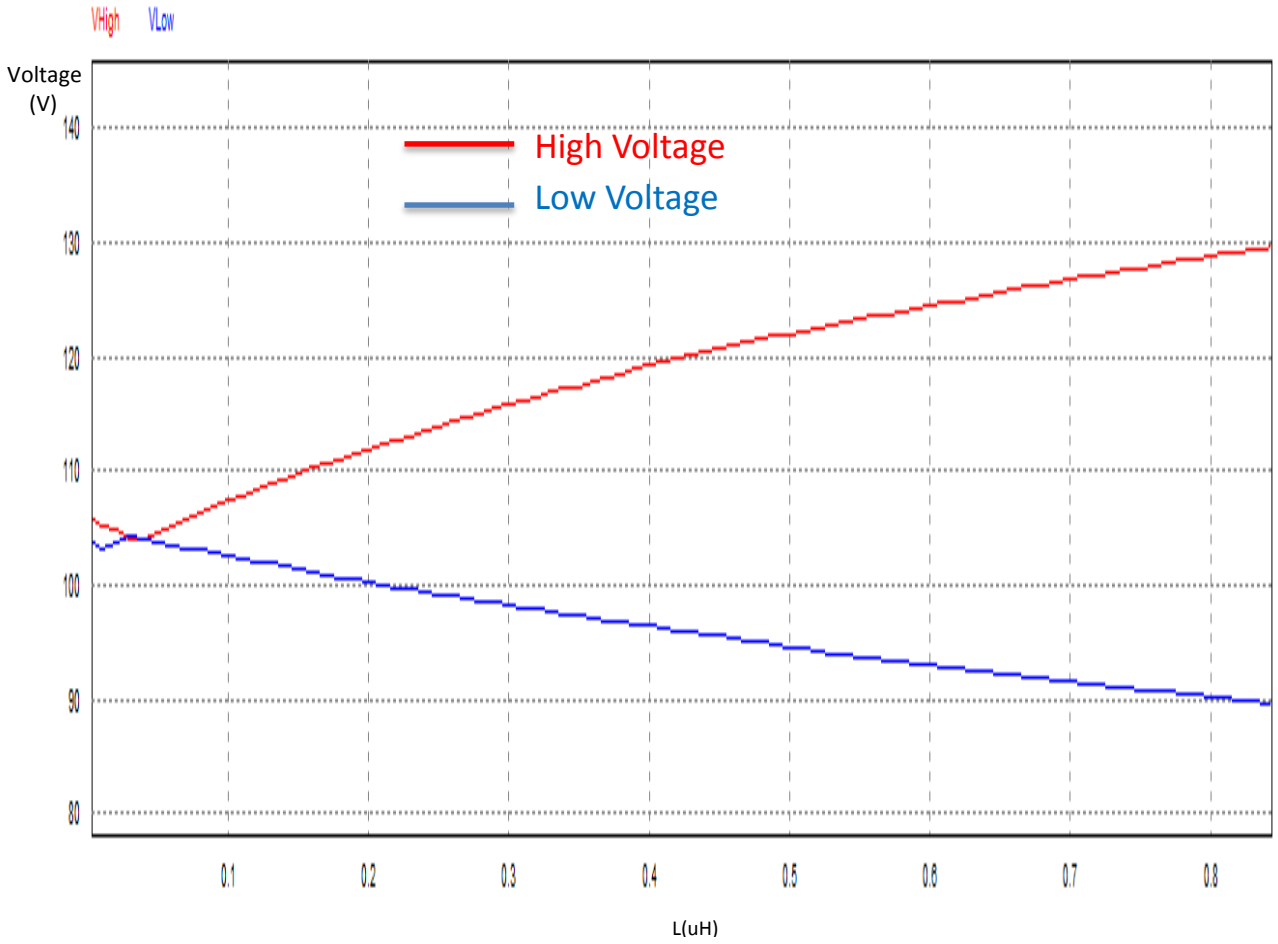

Figure 6.20: Auxiliary inductor parametric analysis

6.3 Proposed Application Solar Based Water Pump Simulation Results

In the following, simulation results for a system driving a motor from a solar panel using the proposed DC-DC converter and proposed MPPT algorithm are presented.

The input of the DC-DC converter is the solar panels with MPPT controller implemented. The three outputs are used as follows. The high output 200 volts is used to feed the motor, and the other outputs can be used for the control circuits needed for driving the motor.

Figure 6.21 shows the waveform of the rpm of the motor.

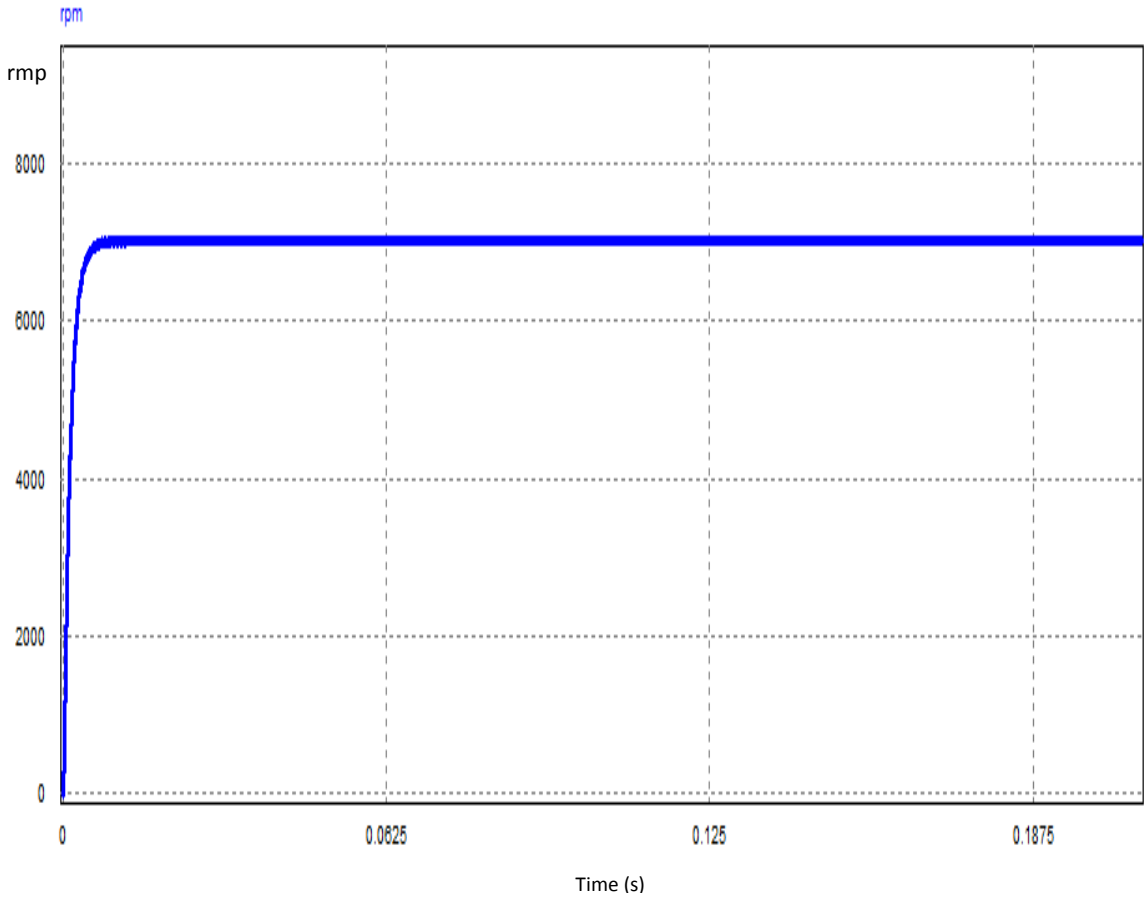

Figure 6.21: The motor number of rotations per minute

Figure 6.22 shows the three phase motor input currents

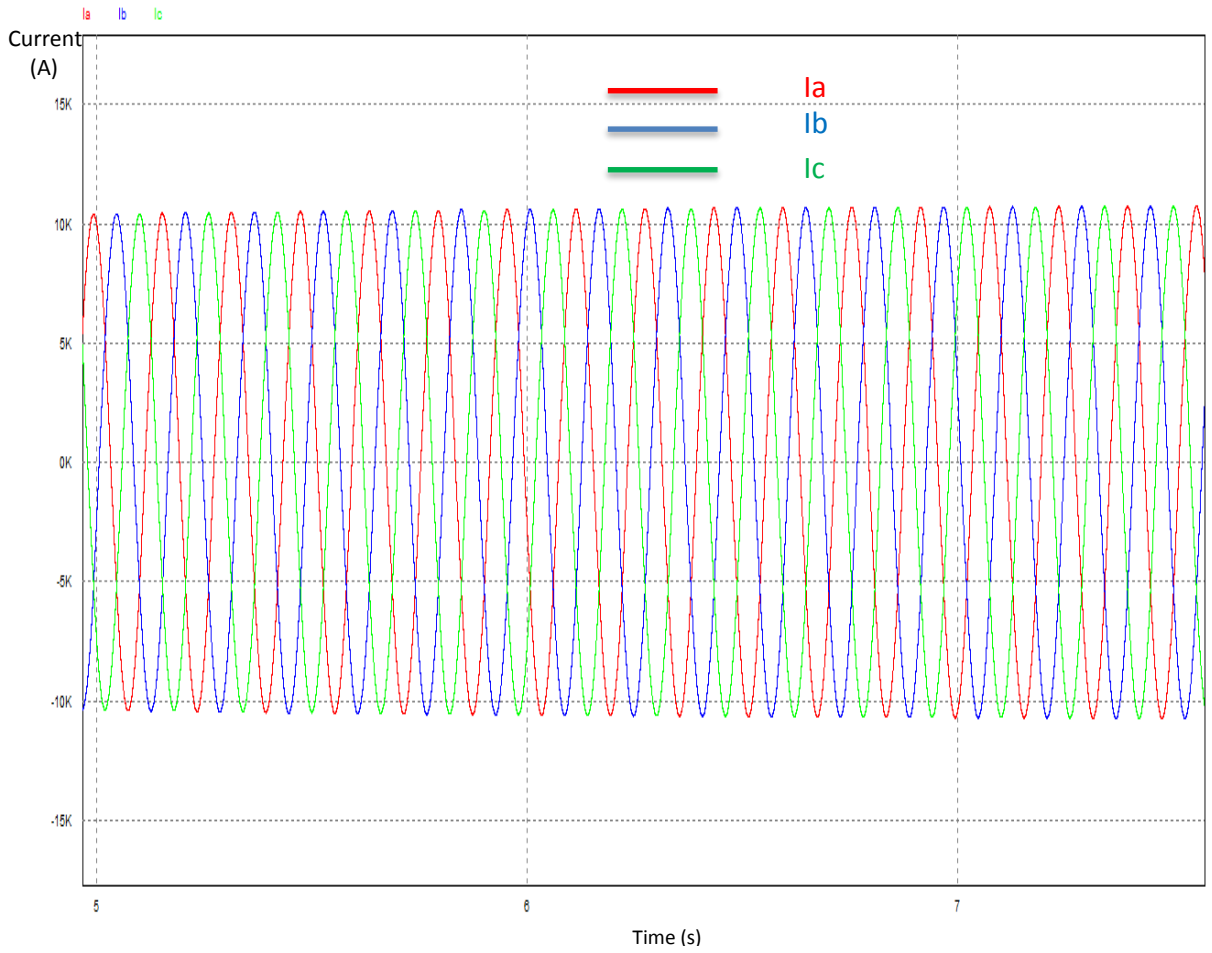

Figure 6.22: Three phase motor input currents

The three phase is the output of the AC-DC converter that is used to provide the motor with AC voltage from the DC voltage generated from the photovoltaic.

6.4 Experimental Results

A prototype of 10 watts with open circuit voltage 20 volts and short circuit current of 300 mA has been built to prove that the concept is working properly and to verify the simulation results. This stage is a very important step in the design. Measurements are done after designing some test cases and experimental results will be presented in this section some.

A typical circuit as shown in Figure 6.23 has been built. The algorithm is implemented in microcontroller PIC18F4553 and the component values are shown in Table 6.1.

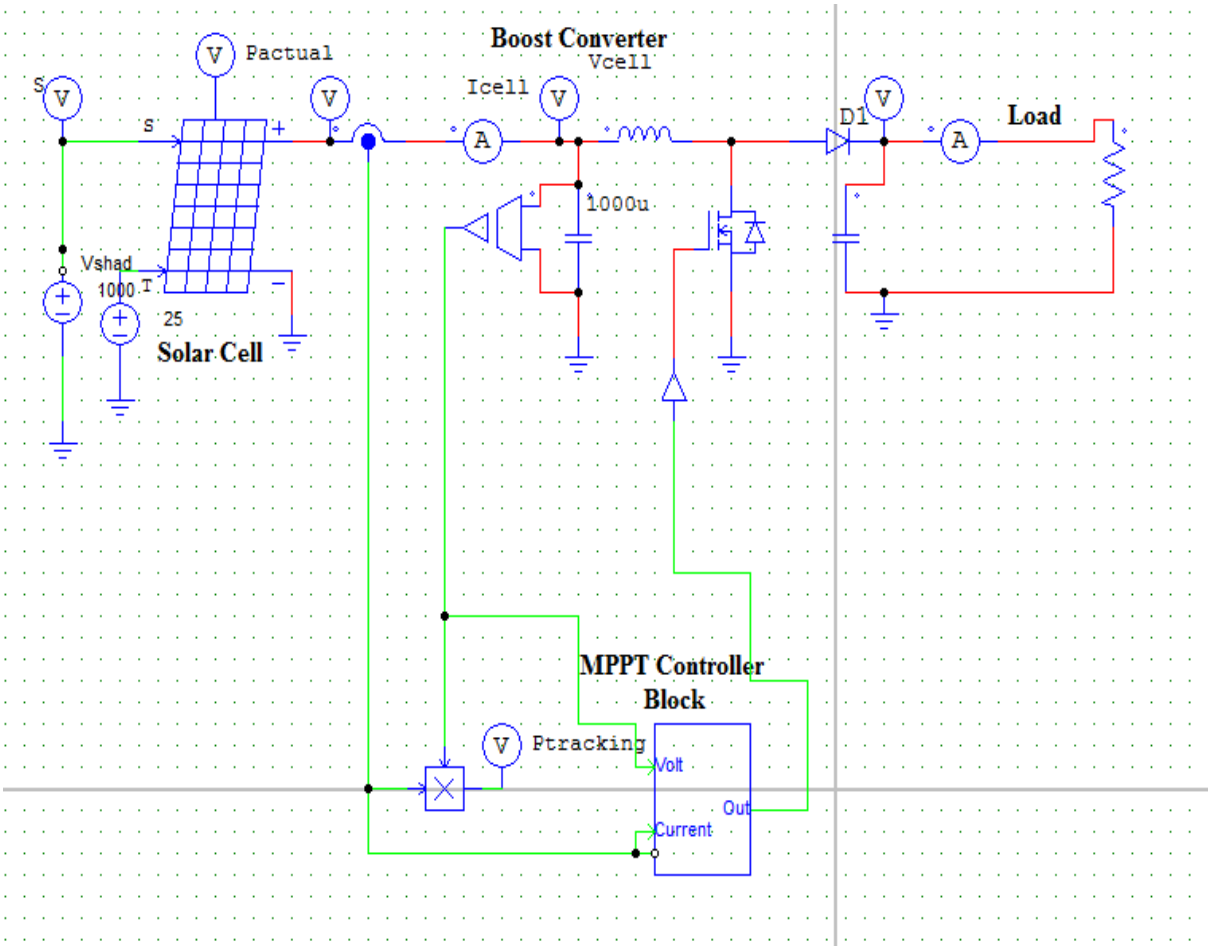

Figure 6.23: Implemented circuit

Table 6.1: Hardware parameters of the system under consideration

Parameter	Value
Open circuit Voltage	20V
Short circuit current	3mA
Input Power	10 Watt
Microcontroller	Switching frequency 100 KHz
Semiconductors	IRLZ44
Inductor	29uH,3A
Capacitor	270uF, 50V
Diode	Schottky Diode,5A,60V D0201AD

Figure 6.24 shows the pulse width modulation (PWM) signal generated by the microcontroller, which is the key point of applying our proposed algorithm on the circuit. This pulse width modulation signal is after reaching the point of maximum power or in other words in the steady state so we are having here a constant duty cycle.

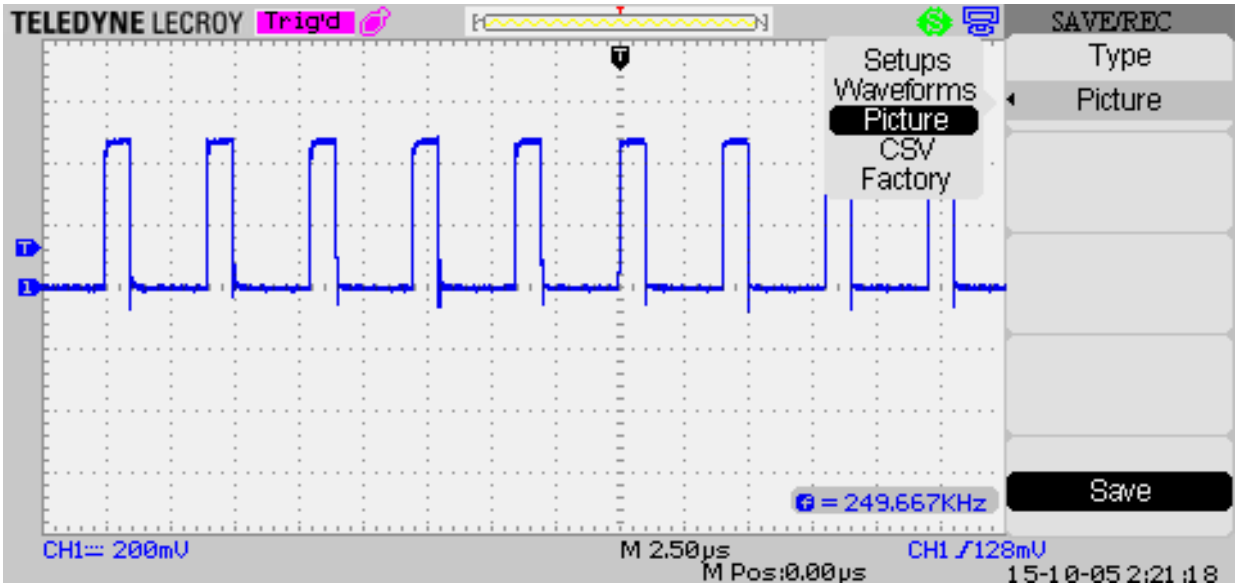

Figure 6.24: PWM switching control signal

It’s very important to check the performance of the controller under different loads. Figure 6.25 shows the output voltage on a pure resistive load connected versus the controlling PWM signal. The resistive load in this case is an array of lamps.

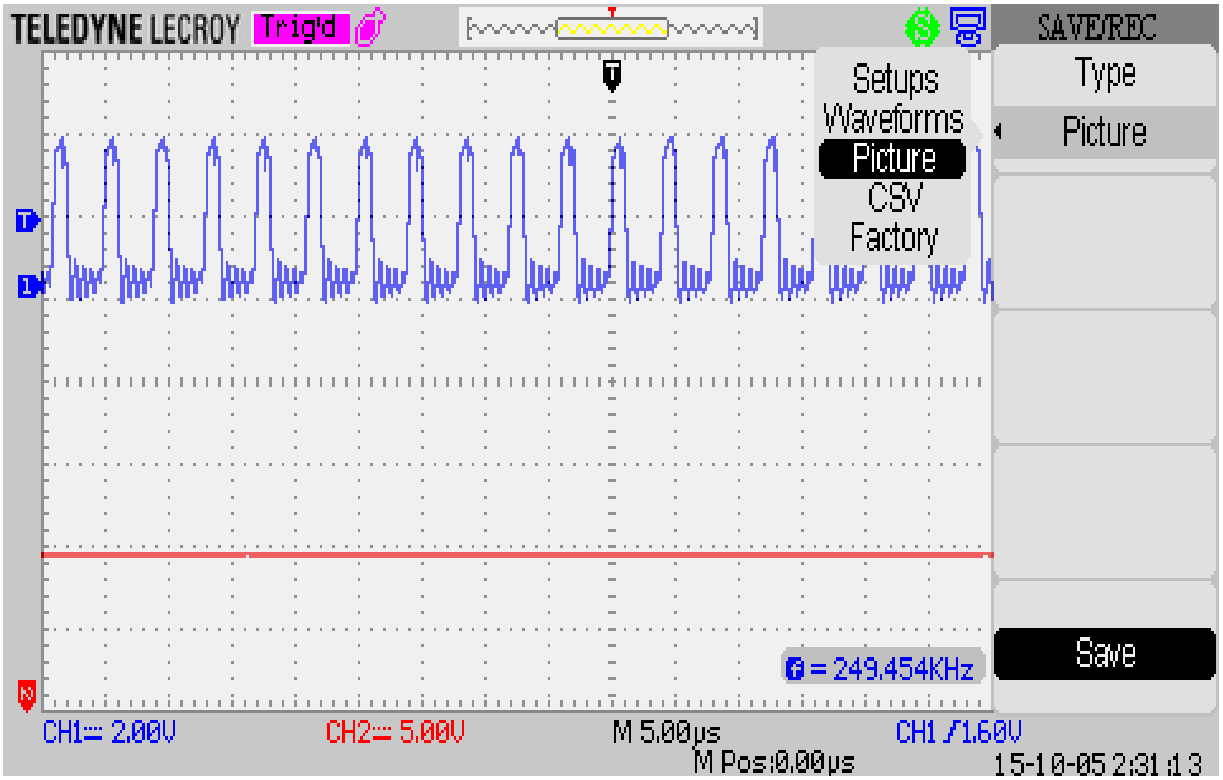

Figure 6.25: PWM switching signal versus the output volatge for a resitive load

Another load is connected to the controller such as small DC motor having the effect of adding resistive inductive load. Figure 6.26 shows the voltage output for a small brushless DC (BLDC) motor as a load versus the PWM control switching signal.

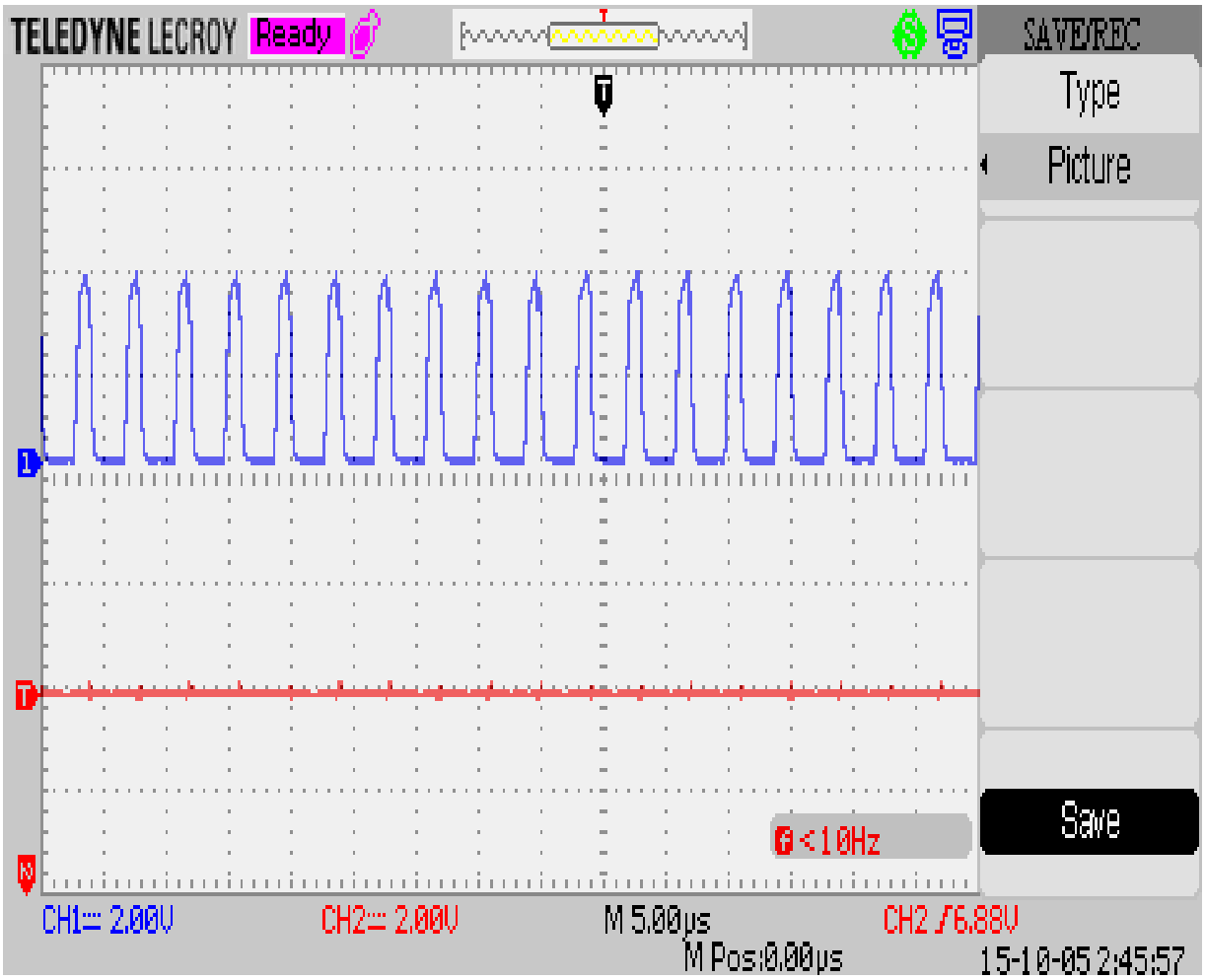

Figure 6.26: PWM signal versus the motor output voltage

It's important to check the voltage stress over other important components in the circuit such the CMOS switch. Figure 6.27 shows the voltage between the drain and source across the MOSFET switch used.

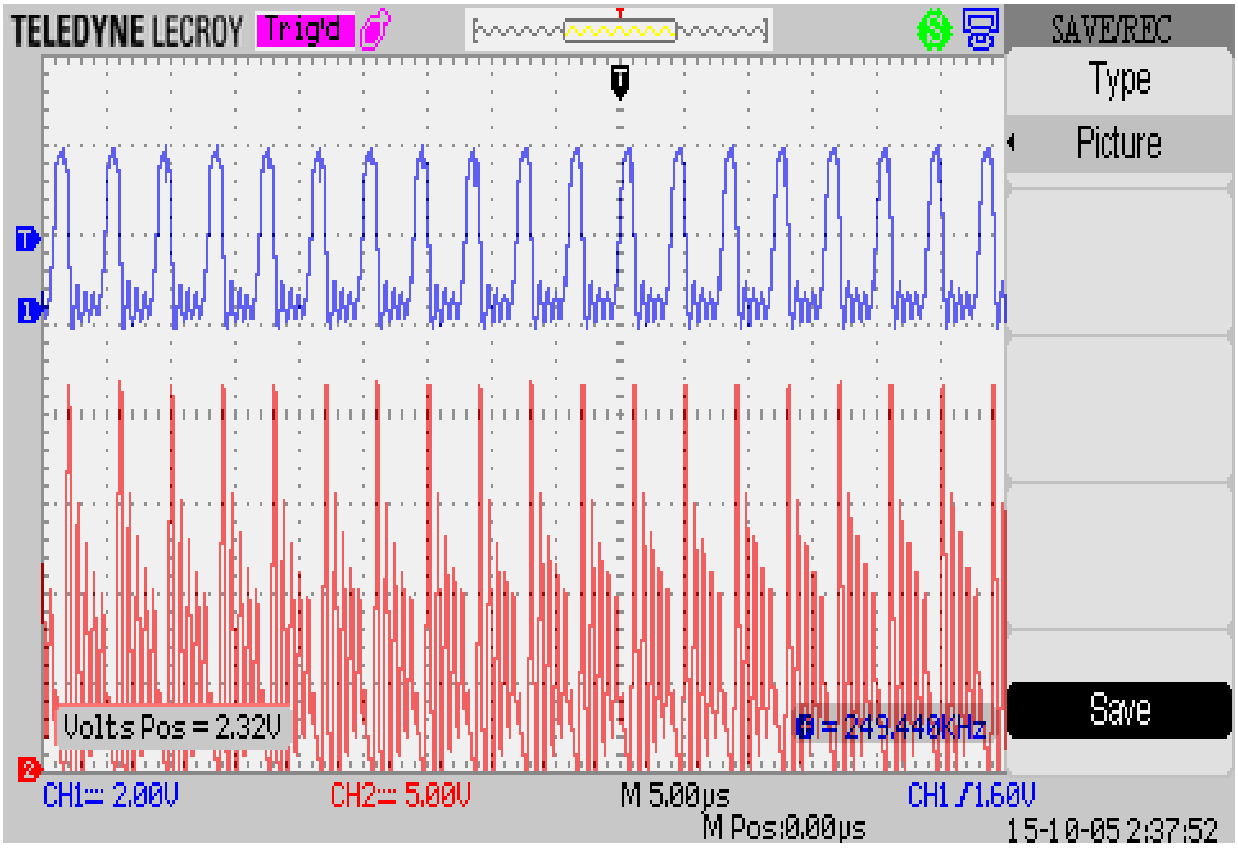

Figure 6.27: PWM signal versus the voltage across the switch Vds

In conclusion, measurements have been done using different connected loads, including pure resistive and a small BLDC motor. Experimental results have verified that the system is working efficiently with different loads.

Chapter 7: Conclusions and Recommendations

7.1 Conclusions

This thesis presents the proposed algorithm for the applied control method, a novel triple output DC-DC converter, and an application for the proposed system. The following points summarize the contributions made in this thesis.

- A novel algorithm based on EPP algorithm with predictive variable step size using Newton-Raphson method has been implemented and tested.
- The algorithm has been implemented in PSIM software. Comparison with other existing MPPT algorithms has been done. It has been shown that the combination of the Newton-Raphson method and EPP algorithm gives very good results with an error of 0.063 % and a tracking time 1μs, while the conventional incremental conductance gives an error of 1.2% and tracking time 10 μs.
- This algorithm is well suited for shading conditions, in which light intensity decreases. The system will adjust itself in a very short period of time to track the new operating point for maximum power, with very small error. This will increase the overall output power and consequently cut the total cost for the industry.
- A DC-DC converter has been developed. The new converter is efficient compared to other converters in the market and cost efficient as it uses only one power switch for different outputs. Three outputs are presented and can be efficiently used in telecommunications, automotive and other applications.
- Parametric analysis has been done for the purpose of reaching the appropriate design parameters.
- Prototyping phase is successfully achieved and tested. The new algorithm and circuit are built into a complete system for application in the solar based water pumps. Measurement results have verified the validity.

7.2 Recommendations

It is recommended to use a predictive adaptive step size as used in the proposed algorithm to efficiently track the maximum power with a very small error. When developing a control system using MPPT, it is recommended to develop and improve the important block diagrams used after the MPPT block to increase the efficiency of the entire system. As what has been done in this research by improving the DC-DC converter and may be improving other blocks such as the DC-AC converter**.** In addition, a future work is going to be integrating the system components and moving from the prototyping phase to product phase.

References

[1] Khaligh, Alireza and Onar, Omer C "Energy harvesting: solar, wind, and ocean energy conversion systems", 2010

[2] C. Honsberg and S. Bowden, "Fundementals of solar cells " [online].Available:" *http://pveducation.org/pvcdrom/solar-cell-operation/solar-cell-structure"*

[3] S. Hosseinil, A. Farakhor and S. Haghighian,"Novel Algorithm of MPPT for PV Array Based on Variable Step Newton-Raphson Method Through Model Predictive Control*", 13th International Conference on Control, Automation and Systems (Lccas 2013) in Kimdaejung Convention Center,Gwangju,* Korea, pp.1577-1582 ,2013.

[4] A. Montecucco , and A.Knox" Maximum Power Point Tracking Converter Based on the Open-Circuit Voltage Method for Thermoelectric Generators", *IEEE Transactions on Power Electronics* (Volume:30 , Issue: 2), 2014

[5] P. Barrade, S.Delalay, and A.Rufer" Direct Connection of Supercapacitors to Photovoltaic Panels With On–Off Maximum Power Point Tracking*", IEEE Transactions on Sustainable Energy* (Volume:3 , Issue: 2),2012

[6] Chih-Yu Yang, C.Hsieh, F.Feng, and K.Chen" Highly Efficient Analog Maximum Power Point Tracking (AMPPT) in a Photovoltaic System*", IEEE Transactions on Circuits and Systems I: Regular Papers* (Volume:59 , Issue: 7), 2012

[7] J. Raj and A. Jeyakumar" A Novel Maximum Power Point Tracking Technique for Photovoltaic Module Based on Power Plane Analysis of I – V Characteristics" *IEEE Transactions on Industrial Electronics,* (Volume:61 , Issue: 9),2014

[8] X.Li, Y. Li, and J.Seem" Maximum Power Point Tracking for Photovoltaic System Using Adaptive Extremum Seeking Control",*IEEE Transactions on Control Systems Technology* (Volume:21 , Issue: 6),2013.

[9] A.Latham,R.Podgurski, K.Odame and C.Sullivan" Analysis and Optimization of Maximum Power Point Tracking Algorithms in the Presence of Noise",*IEEE Transactions on Power Electronics* (Volume:28 , Issue: 7),2013.

[10] K. Lian, J. Jhang, and I. Tian" A Maximum Power Point Tracking Method Based on Perturb-and-Observe Combined With Particle Swarm Optimization", *IEEE Journal of Photovoltaics,* (Volume:4 , Issue: 2), 2014.

[11] Sachin Jain, and Vivek Agarwal, "A new algorithm for rapid tracking of approximate maximum power point in photovoltaic systems", *IEEE Power Electronics Letters* (Volume:2 , Issue: 1),2004.

[12] F.Zhang, K.Thanapalan, A. Procter, S.Carr, and J.Maddy" Adaptive Hybrid Maximum Power Point Tracking Method for a Photovoltaic System", *IEEE Transactions on Energy Conversion* (Volume:28 , Issue: 2),2013.

[13] K.Sundareswaran1, S.Peddapati1 and S. Palani" Application of random search method for maximum power point tracking in partially shaded photovoltaic systems", *IET Renewable Power Generation* (Volume:8 , Issue: 6),2014.

[14] Y.Liu, S.Huang, J.Huang, and W.Liang" A Particle Swarm Optimization-Based Maximum Power Point Tracking Algorithm for PV Systems Operating Under Partially Shaded Conditions", *IEEE Transactions on Energy Conversion* (Volume:27 , Issue: 4),2012.

[15] D.Trejo,E.Bárcenas, D.Delgado, and C.De Angelo" Voltage-Oriented Input–Output Linearization Controller as Maximum Power Point Tracking Technique for Photovoltaic Systems", *IEEE Transactions on Industrial Electronics* (Volume:62 , Issue: 6),2015.

[16] M. Veerachary, T. Senjyu and K. Uezato" Maximum power point tracking of coupled inductor interleaved boost converter supplied PV system", *IEE Proceedings - Electric Power Applications* (Volume:150 , Issue: 1),2003.

[17] TEsram, JKimball, PKrein, P, and P.Midya" Dynamic Maximum Power Point Tracking of Photovoltaic Arrays Using Ripple Correlation Control", *IEEE Transactions on Power Electronics* (Volume:21 , Issue: 5),2006.

[18] K.Lee and R.Kim" An Adaptive Maximum Power Point Tracking Scheme Based on a Variable Scaling Factor for Photovoltaic Systems", *IEEE Transactions on Energy Conversion,* (Volume:27 , Issue: 4),2012.

[19] W.Xiao, H. Zeineldin, and P.Zhang" Statistic and Parallel Testing Procedure for Evaluating Maximum Power Point Tracking Algorithms of Photovoltaic Power Systems", *IEEE Journal of Photovoltaics,* (Volume:3 , Issue: 3),2013.

[20] M.Veerachary, T.Senjyu , and K.Uezato" Neural-network-based maximum-power-point tracking of coupled-inductor interleaved-boost-converter-supplied PV system using fuzzy controller", *IEEE Transactions on Industrial Electronics* (Volume:50 , Issue: 4),2003.

[21] Y.Hong, S.Pham, T.Yoo, K.Chae,K.Baek,and Y.Kim" Efficient Maximum Power Point Tracking for a Distributed PV System under Rapidly Changing Environmental Conditions", *IEEE Transactions on Power Electronics* (Volume:30 , Issue: 8),2015.

[22] J.Qahouq and Y.Jiang" Distributed photovoltaic solar system architecture with single-power inductor single-power converter and single-sensor single maximum power point tracking controller", *IET Power Electronics* (Volume:7 , Issue: 10),2014.

[23] C.Wei, Z.Zhang, W.Qiao, and L.Qu" Reinforcement-Learning-Based Intelligent Maximum Power Point Tracking Control for Wind Energy Conversion Systems", *IEEE Transactions on Industrial Electronics* (Volume:62 , Issue: 10),2015.

[24] F.Pai, R.Chao, S.Ko, and T.Lee" Performance Evaluation of Parabolic Prediction to Maximum Power Point Tracking for PV Array", *IEEE Transactions on Sustainable Energy* (Volume:2 , Issue: 1),2010.

[25] L.Chen, C.Tsai, Y.Lin, and Y.Lai" A Biological Swarm Chasing Algorithm for Tracking the PV Maximum Power Point", *IEEE Transactions on Energy Conversion* (Volume:25 , Issue: 2),2010.

[26] B.Retnam1, A.Gounder,V.Goundend" Hybrid power electronic controller for combined operation of constant power and maximum power point tracking for single-phase grid-tied photovoltaic systems", *IET Power Electronics* (Volume:7 , Issue: 12),2014.

[27] R.Linus ,and P. Damodharan" Maximum power point tracking method using a modified perturb and observe algorithm for grid connected wind energy conversion systems", *IET Renewable Power Generation* (Volume:9 , Issue: 6),2015.

[28] W.Xiao, W.Dunford, P.Palmer,and A.Capel" Application of Centered Differentiation and Steepest Descent to Maximum Power Point Tracking", *IEEE Transactions on Industrial Electronics,* (Volume:54 , Issue: 5),2007.

[29] M.Veerachary, T.Senjyu and K.Uezato" Voltage-based maximum power point tracking control of PV system", *IEEE Transactions on Aerospace and Electronic Systems,* (Volume:38 , Issue: 1),2002.

[30] L.Zhang, W.Hurley, and W.Wolfle "A New Approach to Achieve Maximum Power Point Tracking for PV System With a Variable Inductor" *IEEE Transactions on Power Electronics,* (Volume:26 , Issue: 4),2011.

[31] S. Jiang, D.Cao, Y.Li and F.Peng" Grid-Connected Boost-Half-Bridge Photovoltaic Microinverter System Using Repetitive Current Control and Maximum Power Point Tracking", *IEEE Transactions on Power Electronics,* (Volume:27 , Issue: 11),2012.

[32] N.Kasa, T.lida and H.lwamoto" Maximum power point tracking with capacitor identifier for photovoltaic power system", *IEE Proceedings - Electric Power Applications,* (Volume:147 , Issue: 6),2000.

[33] H.Chung, K. Tse, S. Hui , C. Mok, and M. Ho" A novel maximum power point tracking technique for solar panels using a SEPIC or Cuk converter", *IEEE Transactions on Power Electronics,* (Volume:18 , Issue: 3),2003.

[34] Y. Jiang and J. Qahouq" Single-sensor multi-channel maximum power point tracking controller for photovoltaic solar systems",*IET Power Electronics* , (Volume:5 , Issue: 8),2012.

[35] M.Shadmand, R.Balog,and H.Abu-Rub" Model Predictive Control of PV Sources in a Smart DC Distribution System: Maximum Power Point Tracking and Droop Control" *IEEE Transactions on , Energy Conversion,* (Volume:29 , Issue: 4),2014.

[36] W. Xu, C.Mu, and J.Jin" Novel Linear Iteration Maximum Power Point Tracking Algorithm for Photovoltaic Power Generation", *IEEE Transactions on Applied Superconductivity*, (Volume:24 , Issue: 5),2014.

[37] T.Nguyen and K.Low" A Global Maximum Power Point Tracking Scheme Employing DIRECT Search Algorithm for Photovoltaic Systems", *IEEE Transactions on Industrial Electronics*, (Volume:57 , Issue: 10),2010.

[38] B.Subudhi, and R.Pradhan" A Comparative Study on Maximum Power Point Tracking Techniques for Photovoltaic Power Systems", *IEEE Transactions on Sustainable Energy*, (Volume:4 , Issue: 1),2012.

[39] M.Elgendy, B.Zahawi, and D.Atkinson" Assessment of the Incremental Conductance Maximum Power Point Tracking Algorithm", *IEEE Transactions on Sustainable Energy*, (Volume:4 , Issue: 1),2012.

[40] E.Koutroulis, K.Kalaitzakis, and N.Voulgaris" Development of a microcontroller-based, photovoltaic maximum power point tracking control system", *IEEE Transactions on Power Electronics*, (Volume:16 , Issue: 1),2001.

[41] A.Chikh, and A.Chandra" An Optimal Maximum Power Point Tracking Algorithm for PV Systems With Climatic Parameters Estimation", *IEEE Transactions on Sustainable Energy*, (Volume:6 , Issue: 2),2015.

[42] N.Femia, G.Petrone, G.Spagnuolo, and Massimo Vitelli" Optimization of perturb and observe maximum power point tracking method", *IEEE Transactions on Power Electronics* (Volume:20 , Issue: 4),2005.

[43] P.Manganiello, M.Ricco, G.Petrone, E.Monmasson, and G. Spagnuolo, "Optimization of Perturbative PV MPPT Methods Through Online System Identification",*IEEE Transactions on Industrial Electronics*, VOL. 61, NO.12,pp. 6812 – 6821, 2014.

[44] C. Liu, B. Wu and R. Cheung, "Advanced Algorithm for MPPT Control of Photovoltaic Systems", *Canadian Solar Buildings Conference Montreal*, 2004.

[45] K. Chen, S. Tian, Y. Cheng, and L. Bai, "An Improved MPPT Controller for Photovoltaic System under Partial Shading Condition", *IEEE Transactions on Sustainable Energy*, VOL. 5, NO. 3, pp.978-985, 2014.

[46] S. Kollimalla, and M. Mishra, "Variable Perturbation Size Adaptive P&O MPPT Algorithm for Sudden Changes in Irradiance", *IEEE Transactions on Sustainable Energy*, VOL. 5, NO. 3, pp.718-728, 2014.

[47] K. Tey and S. Mekhilef, "Modified Incremental Conductance Algorithm for Photovoltaic System under Partial Shading Conditions and Load Variation", *IEEE Transaction on Power Electronics* VOL. 61, NO. 10, pp.5384-5392, 2014.

[48] R. Khanna, Q. Zhang, W. E. Stanchina, G. F. Reed and Z. Mao," Maximum Power Point Tracking Using Model Reference Adaptive Control" *IEEE Transactions on Power Electronics*, VOL. 29, NO. , pp.5384 – 5392, 2014.

[49] W. Xu, C. Mu, and J. Jin," Novel Linear Iteration Maximum Power Point Tracking Algorithm for Photovoltaic Power Generation",*IEEE Transactions on Applied Superconductivity*, VOL. 24, NO. 5, 2014.

[50] M.Atiqi, M. Zainuri, M. Radzi, A.Soh, N.Abd Rahim," Development of adaptive perturb and observe-fuzzy control maximum power point tracking for photovoltaic boost dc–dc converter",*IET Renewable Power Generation*, pp. 183 – 194, 2013.

[51] H.Renaudineau, F.Donatantonio, J.Fontchastagner, G.Petrone, G. Spagnuolo, J.Martin, and S.Pierfederici," A PSO-Based Global MPPT Technique for Distributed PV Power Generation" *IEEE Transactions Industrial Electronics*, and Volume: 62, Issue: 2, pp. 1047-1058, 2014.

[52] K. Hussein, I. Muta, T. Hoshino M. Osakada "Maximum photovoltaic power tracking: an algorithm for rapidly changing atmospheric conditions*" IEEE Proceedings Generation, Transmission and Distribution*, 1995.

[53] N. Mohan, T. M. Undeland, and W. P. Robbins, Power Electronics: Converters Applications, and Design. New York: Wiley, 1995.

[54] M. Eid, M. Youssef and Y. Wang "A Novel Efficient EPP-Based Algorithm for MPPT PV Applications "*IEEE Proceedings of the International Conference of Energy and Telecommunications, INTELEC* October 2015 Japan.

[55] M. Eid, M. Youssef and Y. Wang "Single Input Triple Output DC-DC Converter for Automation Applications", *IEEE Proceedings of the International Conference of Energy and Telecommunications, INTELEC* October 2015 Japan.

[56] P. Patra, A. Patra, and N. Misra, "A single-inductor multiple-output switcher with simultaneous buck, boost and inverted outputs," *IEEE Transactions. Power Electron*, vol. 27, no. 4, pp. 1936–1951 , 2012

[57] A. Nami, F. Zare, A. Ghosh, and F. Blaabjerg, "Multiple-output DC–DC converters based on diode-clamped converters configuration: Topology and control strategy," *IET Power Electron*, vol. 3, no. 2, pp. 197–208, 2010

[58] S. D. Gamini Jayasinghe, D. Mahinda Vilathgamuwa, and U. K. Madawala, "Diode-clamped three-level inverter-based battery super capacitor direct integration scheme for renewable energy systems," *IEEE Transactions Power Electronics*, vol. 26, no. 6, pp. 3720–3729, 2011

[59] F. Gao, B. Blunier, M. G. Sim˜oes, and A. Miraoui, "PEM fuel cell stack modeling for real-time emulation in hardware-in-the-loop application",*IEEE Transactions Energy Converters*., vol. 26, no. 1, pp. 184–194, 2011

[60] Y. Chen, Y. Kang, S. Nie, and X. Pei, "The multiple-output DC–DC converter with shared ZCS lagging leg," *IEEE Transactions Power Electronics*, vol. 26, no. 8, pp. 2278–2294, 2011

[61] D. Christen, S. Tschannen, J. Biela," Highly Efficient and Compact DC-DC Converter for Ultra-Fast Charging of Electric Vehicles",*IEEE International Power Electronics and Motion Control Conference*, EPE-PEMC ECCE Europe, Novi Sad, Serbia, 2013

[62] O.Ray, A.Prasad J., and S.Mishra," A Multi-port DC-DC Converter topology with simultaneous Buck and Boost outputs "*IEEE Industrial Electronics (ISIE),*2013

[63] H. Keyhani, H. A. Toliyat," A ZVS Single Inductor Multi Input Multi Output DC-DC Converter with thaqe Step Up/Down Capability" *IEEE Energy Conversion Congress and Exposition (ECCE),* 2013

[64] R. J. Wai, , and K. H. Jheng," High-Efficiency Single-Input Multiple-Output DC–DC Converter",*IEEE Transactions on Power Electronics*, VOL. 28, NO. 2, 2013